UNIVERSIDADE FEDERAL DO RIO GRANDE DO SUL
INSTITUTO DE FÍSICA
DEPARTAMENTO DE ASTRONOMIA

The mysterious object around Mrk 1172*

Augusto Lassen

Masters dissertation presented to the graduate programme in Physics of the Federal University of Rio Grande do Sul supervised by Prof. Dr. Rogério Riffel and co-supervised by Prof. Dr. Ana Leonor Chies Santiago Santos

Porto Alegre, RS, Brasil
August, 2020

* Financed by CAPES and CNPq

"A pior das loucuras é, sem dúvida,
pretender ser sensato num mundo de loucos."
Erasmo de Roterdã (Elogio da loucura, 1511.)

Acknowledgments

Agradeço à minha família pelo apoio, manifestado de todas as formas possíveis. Em especial à minha mãe, que nutriu durante anos o desejo de prover educação de qualidade a seu filho.

Agradeço à minha namorada, Gabriella, que me fez ver que todos os obstáculos eram superáveis, mesmo quando eu mesmo não acreditava.

Aos meus amigos Fábio, Luan e Ramon, que alegraram os meus dias quando eu precisava de um sorriso e com quem eu sempre pude contar. Esse trabalho jamais teria acontecido sem vocês.

Agradeço ao professor Rogerio e à professora Ana, que nunca mediram esforços para me auxiliar, e me guiaram com muita sabedoria durante essa caminhada.

Gostaria de agradecer aos colaboradores Evelyn Johnston e Boris Häußler pela hospitalidade com a qual me receberam em Santiago, também pelos ensinamentos e ajuda e por toda atenção dedicada.

Agradeço também ao Gabriel, sempre disposto a me auxiliar quando necessário fosse.

Ao CNPq e à CAPES, pelo auxílio financeiro.

Agradeço àqueles que porventura esqueci de mencionar e contribuíram direta ou indiretamente para que esse trabalho pudesse ser concluído.

Resumo

Uma região nebular com fortes linhas de emissão foi encontrada próxima à galáxia elíptica e quiescente Mrk 1172. Estudos extensivos foram realizados com o intuito de determinar a natureza desse objeto, uma vez que, até onde sabemos, não existem estudos prévios sobre este objeto na literatura. Os dados utilizados nesse trabalho são provenientes do espectrógrafo *Multi Unit Spectroscopic Explorer* (MUSE), no *Very Large Telescope* (VLT) do *European Southern Observatory* (ESO), cobrindo o intervalo em comprimento de onda de 4650 – 9300 Å. Um estudo espacialmente resolvido das populações estelares dominantes em cada sistema (chamamos este objeto de BCD-UFRGS-01) revela que, enquanto Mrk 1172 é dominada por populações estelares velhas com $t \sim 10^{10}$ anos, BCD-UFRGS-01 apresenta duas populações estelares dominantes. A mais jovem delas, que possui menor contribuição (~ 40 %), é composta por estrelas jovens com idades $\sim 10^8$ anos, enquanto a outra possui idade da ordem de 10^9 anos. Determinamos a massa estelar de ambas, obtendo $\sim 2 \times 10^{11} M_\odot$ para Mrk 1172 e $\sim 4 \times 10^9 M_\odot$ para BCD-UFRGS-01. Calculamos também o limite inferior da massa do gás ionizado em BCD-UFRGS-01, obtendo $3.5 \times 10^6 M_\odot$. As abundâncias relativas dos ions associados às linhas de emissão presentes no espectro de BCD-UFRGS-01, i.e., N, S e O, também foram determinadas. Esse cálculo foi reproduzido para todos os spaxels de BCD-UFRGS-01, onde obtivemos uma média de $N(O^{++}) = 7.71$, $N(N^+) = 6.91$ e $N(S^+) = 6.56$, em unidades de $\log(\mathrm{X/H}) + 12$. Os valores de abundância de oxigênio ($\sim 1/15\, Z_\odot$) e massa estelar obtidos estão dentro do intervalo típico encontrado para *Blue Compact Dwarf Galaxies* (BCDGs). O espectro de BCD-UFRGS-01 apresenta linhas de emissão muito intensas, como [O III] λ5007 Å, H_α, [N II] λ6584 Å, and [SII] λ6717 Å. A partir da razão dessas linhas concluímos que o gás de BCD-UFRGS-01 é ionizado por estrelas jovens massivas. Medidas de SFR e $\sum$SFR resultam em $0.71\, M_\odot\,\mathrm{anos}^{-1}$ e $1.4 \times\ 10^{-2}\, M_\odot\,\mathrm{anos}^{-1}\,\mathrm{kpc}^{-2}$, respectivamente. Estudos da dinâmica deste objeto revelam também que o gás está rotando no sentido anti-horário em torno de um eixo maior de BCD-UFRGS-01 e seu movimento é compatível com o movimento de órbita circular no plano de um disco. Concluímos, portanto, que BCD-UFRGS-01 é uma galáxia anã discoidal e é uma forte candidata a se encaixar na categoria de *Blue Compact Dwarf Galaxy*.

Abstract

A nebular region with strong emission lines is found near the quiescent Early-Type Galaxy (ETG) Mrk 1172. Extensive studies are performed in order to determine the nature of this object, since to the best of our knowledge this object has not been analysed in detail before. The data used in this work is from the Multi Unit Spectroscopic Explorer (MUSE), at the Very Large Telescope (VLT) from the European Southern Observatory (ESO), covering the spectral range 4650 – 9300 Å. An analysis of the spatially resolved stellar populations of Mrk 1172 and its neighbour in projection (from now on we refer to the nebular region as BCD-UFRGS-01) reveals that while Mrk 1172 is dominated by old stellar populations with $t \sim 10^{10}$ yrs, BCD-UFRGS-01 presents two dominant stellar populations. The youngest of both, which has the lowest contribution (~ 40 %), is composed of young stars with $t \sim 10^{8}$ yrs, while the other has $t \sim 10^{9}$ yrs. We determined the stellar mass of both objects, obtaining $\sim 2 \times 10^{11}\, M_{\odot}$ for Mrk 1172 and $\sim 4 \times 10^{9}\, M_{\odot}$ for BCD-UFRGS-01. We also calculate a lower limit for the mass of the ionised gas in BCD-UFRGS-01, obtaining $3.5 \times 10^{6}\, M_{\odot}$. The relative abundances of the ions associated with the emission lines present in the spectrum of BCD-UFRGS-01, i.e., N, S and O, are also determined. This calculation was performed for all spaxels of BCD-UFRGS-01, where we have obtained the average values of $N(O^{++}) = 7.71$, $N(N^{+}) = 6.91$ and $N(S^{+}) = 6.56$, in units of $\log(\mathrm{X/H}) + 12$. The values obtained for Oxygen abundance ($\sim 1/15\, Z_{\odot}$) and stellar mass are within the typical range of values found for other Blue Compact Dwarf Galaxies (BCDGs). The spectrum of BCD-UFRGS-01 shows very intense emission lines, namely [O III] λ5007 Å, H_{α}, [N II] λ6584 Å, and [SII] λ6717 Å . From such emission line ratios we concluded that the gas within BCD-UFRGS-01 is ionised by young massive stars. Measurements of SFR and $\sum$SFR result in $0.71\, M_{\odot}\,\mathrm{yrs}^{-1}$ and $1.4\times 10^{-2}\, M_{\odot}\,\mathrm{yrs}^{-1}\,\mathrm{kpc}^{-2}$, respectively. Dynamical analysis of this galaxy reveals that the gas is rotating in the counter-clockwise direction along a major axis that crosses BCD-UFRGS-01 diagonally, and its motion is compatible with the motion of circular orbits in the plane of a disk. Thus, we conclude that BCD-UFRGS-01 is likely to be a dwarf disc galaxy that belongs to the Blue Compact Dwarf Galaxy Category.

Press Release: O misterioso colar de pérolas extragaláctico

Há menos de um século que o ser humano descobriu que a Via Láctea não é o Universo inteiro, senão uma em meio a centenas de bilhões de outras galáxias, cada uma com suas peculiaridades. Algumas, como a Via Láctea, são espirais, outras são elípticas. Algumas possuem formatos tão distintos que não é possível encaixá-las em uma categoria bem definida, sendo chamadas portanto de galáxias irregulares. Outro importante fator de diferenciação entre elas é o seu tamanho: observam-se galáxias muito grandes no Universo, no entanto o tipo mais abundante são as chamadas galáxias anãs.

Desde que o conhecimento da existência de inúmeras outras galáxias no Universo veio à tona, os astrônomos se desdobram sob a fundamental e complexa tarefa de compreender como o Universo evoluiu e formou as galáxias que observamos hoje. Nessa busca, as galáxias anãs desempenham um papel chave, não apenas por serem a classe mais abundante, mas também porque acreditamos hoje que a interação e consequente fusão dos sistemas menores leva à formação dos sistemas maiores. Se isto é verdade, é de se esperar também que as progenitoras das galáxias atuais, denominadas primitivas, encontram-se no Universo distante. Infelizmente, com a tecnologia e os instrumentos que possuímos hoje, encontrá-las e estudá-las com o detalhe necessário ainda não é possível. No entanto, diversas galáxias anãs relativamente próximas a nós compartilham propriedades importantes com essas galáxias, de forma que analisar os processos evolutivos nessas anãs permite estabelecer análogos com os processos que ocorreram nas galáxias primitivas, ampliando assim o nosso conhecimento sobre a evolução do Universo e a formação de galáxias.

Nesse trabalho descrevemos e caracterizamos um objeto misterioso próximo à galáxia Mrk 1172 (o maior objeto da Figura 1) que relembra um colar de pérolas, e que não possui relatos científicos prévios. A análise desse "colar de pérolas" indica que o seu tamanho e sua massa são da ordem de grandeza de uma galáxia anã. Além disso, analisamos também a abundância química dessa galáxia, isto é, determinamos a quantidade de átomos de Oxigênio, Nitrogênio e Enxofre em relação à quantidade de átomos de Hidrogênio no gás que circunda as pérolas do nosso colar de pérolas. Com esses resultados somos capazes de estimar a fração de elementos pesados (em astronomia, quaisquer elementos que sejam mais pesados que o Hélio são ditos elementos pesados), onde observamos que a metalicidade do colar de pérolas é muito baixa compatível com a faixa de valores de metalicidade encontrados em estudos

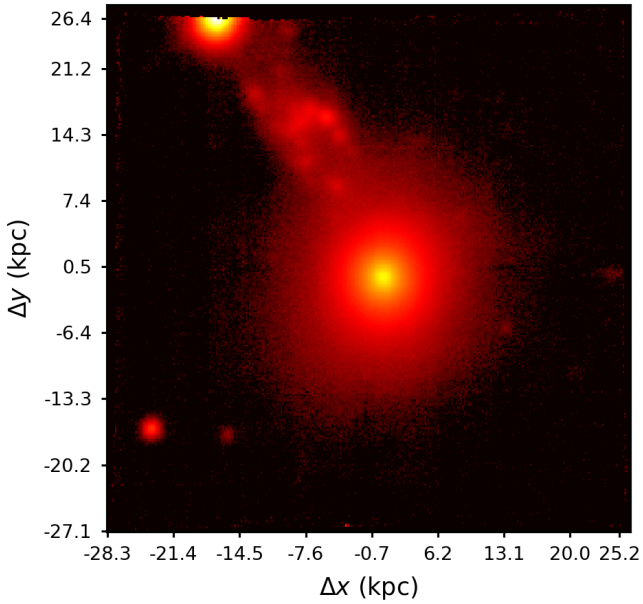

Figure 1: Campo de visão da galáxia Mrk 1172, situada no centro da imagem. A região nebulosa que aparece ao lado de Mrk 1172 é, na verdade, a galáxia anã BCD-UFRGS-01. O objeto brilhante no topo é uma estrela,a qual situa-se a uma distância diferente de ambas galáxias. Definindo a localização de Mrk 1172 como o centro, as legendas nos eixos x e y indicam o deslocamento em relação a esse centro ($1\,\mathrm{kpc} \sim 3{\times}10^{16}\,\mathrm{km}$).

científicos para as chamadas *Blue Compact Dwarf Galaxies* (BCDG, galáxias anãs azuis e compactas), uma classe de galáxias anãs que estão entre as menos metálicas no Universo. Essa é uma das características marcantes das galáxias primitivas, um dos aspectos que torna o estudo dessa classe de galáxias tão importante. Apesar do colar de pérolas apresentar outras propriedades compatíveis com as BCDGs, conforme analisado neste trabalho, determinar a verdadeira natureza e a classificação precisa desta galáxia requer estudos mais detalhados, uma vez que o sistema é complexo, e também por se tratar de uma galáxia sem análise prévia, o que faz com que existam muitas questões ainda necessitando de respostas.

Abbreviations

AGN: Active Galactic Nuclei
BCDG: Blue Compact Dwarf Galaxy
CDM: Cold Dark Matter
dI: Dwarf Irregular
DM: Dark Matter
EELR: Extended Emission Line Region
ESO: European Southern Observatory
ETG: Early-Type Galaxy
FOF: Friends-of-Friends
ICF: Ionisation Correction Factor
IMF: Initial Mass Function
ISM: Interestellar Medium
LINER: Low Ionisation Emission Line Region
LSB: Low Surface Brightness
MNRAS: Monthly Notices of the Royal Astronomical Society
MUSE: Multi Unit Spectroscopic Explorer
MW: Milky Way
MZR: Mass-Metallicity Relation
NIR: Near Infrared
NLR: Narrow Line Region
PSB: Peak Surface Brightness
SDSS: Sloan Digital Sky Survey
SED: Spectral Energy Distribution
SFR: Star Formation Rate
SMBH: Supermassive Black Hole
SSP: Simple Stellar Population

Contents

List of Figures

Chapter 1

Introduction

Historical records indicate that the study of astronomy was a recurrent practice even in the older known civilisations. Monuments like the Stonehenge and the Callanish stones, for example, show that astronomy was important to produce calendars to determine the cycle of time, using the most bright objects in the sky (Pearson, 2016, Higginbottom & Clay, 2016). While the solar and lunar cycles were dictating the concepts of time, many punctual bright sources were present in the sky and their fixed position in the sky led several civilisations to visualise independently positional configurations in the sky, the constellations, which became fundamental elements of each culture and religion.

The nature of these objects has remained a mystery for millennia, and their beauty together with their complexity inspired poets and philosophers throughout these years. Among the punctual objects in the sky such as stars and planets, there were also extended sources of lights, as noticed and reported by Ptolemy in 150 A.D. in books VII–VIII of his *Almagest* and by Abd al-Rahman al-Sufi in his *Book of fixed stars*, written around 964, where he describes the existence of a "cloud" where nowadays we know the Andromeda galaxy is located. These objects were called *nebula*, including at the epoch thousands of objects, from the closer galaxies to open clusters. In the first decades of 20th century, Edwin Hubble was dedicated to study these nebular objects, when he discovered in 1923 that the distance of the Andromeda galaxy is far greater than the dimensions of the Milky Way, thus indicating that our Galaxy is not the entire Universe but one galaxy among many others. Naturally questionings concerning the processes of galaxy formation and evolution arose and the subject attracted many astronomers since then.

1.1 Galaxy formation and evolution

Understanding how galaxies formed and evolved is fundamental to understand the evolution of the Universe in itself. However, the physics involved in these evolutionary processes are complex and challenging, and the progress in this topic frequently finds the edge of human knowledge as an obstacle. Since the discovery by Hubble (Hubble, 1925) that galaxies are common structures in the Universe, astronomers try to describe their properties such as morphologies, and look for clues in their stellar populations to better understand the processes that shape their formation and evolution.

In the 1930's it was already known that galaxies generally exhibit a spiral or elliptical morphology, as evidenced by the Hubble tuning fork diagram, but it took about thirty years for astronomers to build a scenario of galaxy formation that was convincing and coherent at the epoch. In 1962 Eggen, Lynden-Bell and Sandage published a seminal work in the topic of galaxy formation and evolution (Eggen et al., 1962), where they performed a kinematical analysis of 221 dwarf stars in the solar neighbourhood. In this work it was observed that the stars in the halo of the Milky Way (MW, now the component known to contain the older stars in the Galaxy), present a considerably high orbital eccentricity that could be caused by a free fall motion, and in this case they argued that the formation of the MW must have happened in a process of gravitational collapse. Considering this, the authors introduced a model of galaxy formation known as the **monolithic collapse scenario**, also known as Eggen-Lynden-Bell-Sandage model (ELS model). Since the gas is originally metal-poor, so were the first formed stars that followed the kinematical properties of the gas. These were the stars located in the bulge and in the globular clusters, therefore the older stars in the Galaxy. During contraction of the cloud, part of the energy was lost in the form of heat due to collisions (this process is called *dissipative collapse*). Due to conservation of angular momentum the rotational velocity was increased, and the collapse of the gas, before directed preferentially towards the center, now happened along the rotational axis. In this picture, the gas progressively flattens, and a disk is created. Since formed later, the stars formed from this flattened gas will be younger and also more metallic in comparison to their counterparts in the bulge (Chiappini, 2001). The scenario described above is illustrated in figure 1.1. Though fundamental in the historical point of view, several observations in the 1970's and 1980's indicated that the timescales of the collapse involved in the formation of MW in the ELS model are too short, as evidenced

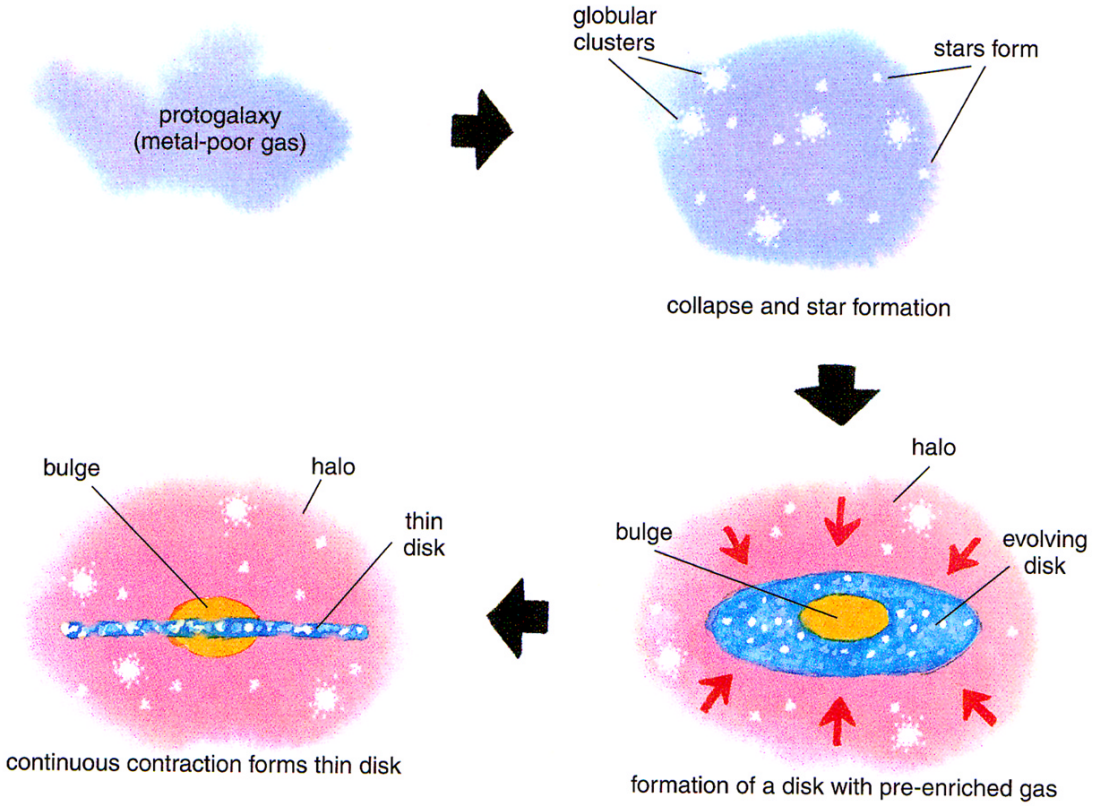

Figure 1.1: In four steps, an illustrative image of the formation of MW in the ELS model. The metal-poor protogalaxy collapses due to gravitational instabilities and the first stars are formed. Due to dissipative collapse the gas flattens and a disk is formed, where younger and metal enriched stars (in comparison to the stars in the bulge) are formed. The ELS model does not take into account the role of Dark Matter, which has proven to be one of the protagonists in the scenario of galaxy formation and evolution years later. Figure taken from Chiappini (2001).

by the ages and metallicities of some globular clusters (Searle & Zinn, 1978). An important aspect to mention is that the ELS model does not take into account the role of Dark Matter (DM) and minor/major mergers in the context of galaxy formation and evolution, and thus new models were proposed, as follows below.

One development important to be mentioned is the observation of rotation curves of spiral galaxies beginning in the 1970's (e.g., the canonical works of Rubin & Ford Jr, 1970, Sofue et al., 1999, Sofue & Rubin, 2001). Such studies indicated that the observed galaxies are embedded in dark matter halos, and many astronomers argued then that dark matter plays an important role in the process that govern galaxy formation (Mo et al., 2010). The seminal work of White & Rees (1978) and the advance in the understanding of Cold Dark Matter (CDM) and application in

models of galaxy formation (Efstathiou & Rees, 1988, Frenk et al., 1988) led to the construction of a **hierarchical scenario** (at the epoch an alternative galaxy formation model, now the most successful model), where dark matter is thought to play a fundamental role in the early steps of galaxy assembly.

In the hierarchical merging scenario the baryonic matter[1] does not have a crucial role such as in the monolithic scenario, since dark matter is dominant. Instead forming galaxies, **the first formed structures in the hierarchical scenario are low mass halos**, due to the collapse of dark matter condensations (Longair & Einasto, 2013, Harko, 2014). The baryonic matter is gravitationally bound to the potential wells of the halos, and starts to collapse, warming up to partially cool down later. Due to conservation of angular momentum the cold gas takes the shape of a disk (Mo et al., 2010).

Besides dark matter, galaxy mergers also play a fundamental role in the hierarchical scenario. When the ratio of the masses of the galaxies involved in the merging process is lower than $\sim 1/3$ it is called a *minor merger*, while for the case which the galaxies involved have similar masses ($\sim 1/1$) the process is called *major merger*. In the former the morphology of the larger galaxy remains unchanged in most of the cases, simply accreting the whole minor galaxy. In the case of a major merger the morphology of the systems can be harshly disrupted during the process. Stars located on structures that are destroyed during the interaction, like the disks of the interacting galaxies, for example, can acquire higher velocity dispersion, creating a spheroidal component typical of a bulge. If the gas is ejected amid the violent merger, this spheroidal component remains, and an elliptical galaxy can result from this process (Schneider, 2014). In the case of disk galaxies the picture seems to be more complex, since the presence of a thick disk is ubiquitous among edge-on disk galaxies (Mo et al., 2010). For more details of the thin and thick disk components of the disk galaxies and the theory of formation of both structures, see Yoachim & Dalcanton (2006), Bournaud et al. (2009).

One might think that from a hierarchical point of view the more massive halos are generally formed later than the less massive ones, i.e., minor systems merge to build up larger ones. Since the behaviour of baryons follows the behaviour of DM halos the same should be true for galaxies. However, this is in opposition to what is observed, i.e., the more massive ellipticals show the presence of older stellar populations in comparison to smaller systems, like dwarf galaxies for example (Cook

[1]The baryonic matter is the class of matter composed by baryons, and interacts with light, thus being also called luminous matter. The dark matter, on the other hand, does not interact with photons, and that is why it is called dark.

et al., 2009). This phenomena is referred as *archaeological downsizing* (Neistein et al., 2006, Fontanot et al., 2009, Bezanson et al., 2009, Oser, 2012). This is thought to happen due to successive minor mergers, which have proven to be a very efficient process in the sense of increasing the stellar mass of the larger system without drastically changing its structure (Li et al., 2007, Bezanson et al., 2009, Wang et al., 2020).

A **two phase scenario** for galaxy formation was proposed from the statistical behaviour that showed that stars in $z = 0$ galaxies are originated *in situ* and *ex situ*. Stars formed in situ are those formed within the galaxy, i.e., closer than $r/r_{\rm vir} \sim 10^{-1}$, while stars formed ex situ are formed outside the galaxy, at $r/r_{\rm vir} \sim 10^{0.5}$ and are accreted later on via merging processes (Pillepich et al., 2015, Rodriguez-Gomez et al., 2016). In the first of these two phases an early fast collapse happens with a series of violent major mergers that are responsible for effectively gathering mass and to reconfigure the potential wells (Lapi & Cavaliere, 2009). A simple spherical collapse model indicates that the inner density profile is established in this fast-accretion phase (Lu et al., 2006). The second phase is denoted by many minor mergers and mass accretion happens smoothly and slowly, where the mass accreted concentrates predominantly in the halo outskirts. As said before, this process barely affects the inner structure of the system, though its mass re scales upwards (Cook et al., 2009, Oser et al., 2010).

In the framework of the hierarchical scenario, the formation history of a dark matter halo can be described by a merger tree that traces all its progenitors. Thus, a galaxy should not be viewed as an object evolving in time, but as the ensemble of its progenitors at a given time (De Lucia & Blaizot, 2007, Mo et al., 2010). In figure 1.2 we present an example of a merger tree for the central galaxy of a DM halo with a mass of $8.9 \times 10^{14}\, M_{\odot}$ at $z = 0$, which is the largest circle placed on the top of the figure. The progenitors of this galaxy are shown below, i.e., going back in time, where they are colour coded with respect to their rest-frame $B - V$ colour. The larger the symbol, the more massive the galaxy is, and only progenitors that are more massive than $1 \times 10^{10} h^{-1}\, M_{\odot}$ have symbols. The branch at the left is the main branch, as detailed in De Lucia & Blaizot (2007), and the galaxies represented by circles are those which are connected to the main branch via a Friends-of-Friends (FOF) algorithm (for details of this algorithm, see Feng & Modi, 2017), while those that did not join the FOF group are represented by triangles.

As described above, galaxy interactions are very common processes with fundamental importance to the understanding of the physics behind the formation and

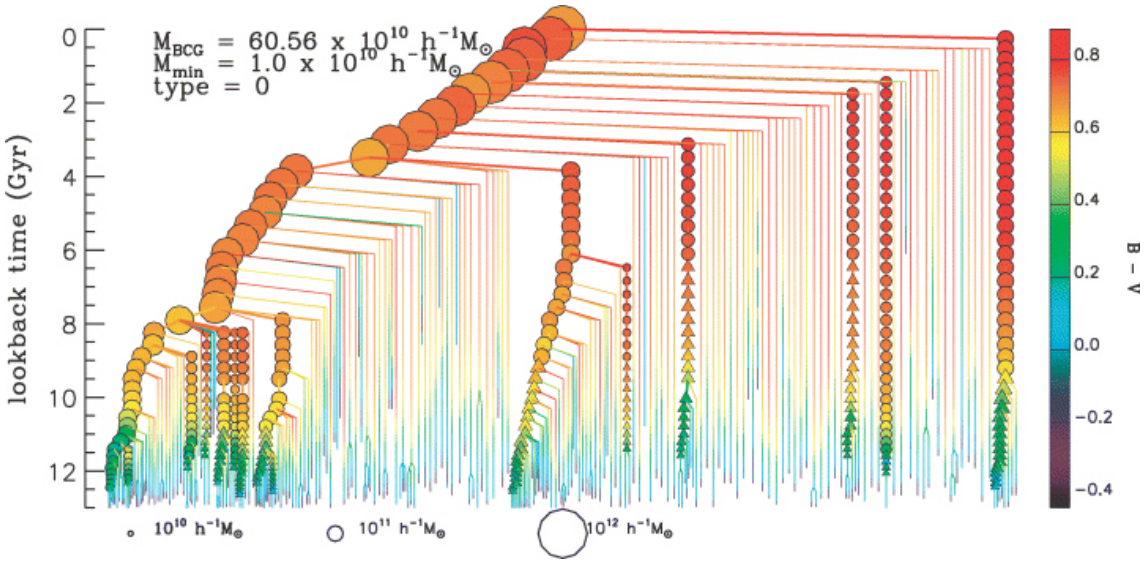

Figure 1.2: Merger tree for a central galaxy in a DM halo, represented by the largest circle in the top (i.e., at $z = 0$) of the figures. The size of the symbols scale with the stellar mass of each galaxy, and they are colour coded with respect to its rest-frame $B-V$ colour. Only galaxies more massive than $10^{10}h^{-1}\,M_\odot$ have symbols. Circles are for galaxies within the FOF group of the main branch, while triangles are for the galaxies that did not join the FOF group. Figure taken from De Lucia & Blaizot (2007).

evolution of galaxies. The violent interaction in a major merger affects the structure and the chemical abundance of the galaxies involved, and imprints on the evolutionary histories of each system can be found in the remaining gas and also in the stars formed previous to the merging process, since the environment where these were formed is very different in comparison to the older stars. **Studying the gas also offers the possibility to understand deeper the physical processes that happened in the interestellar medium (ISM) of the progenitor galaxies.**

The metallicity of the ISM is strongly sensitive to the processes involved in the baryonic cycle within galaxies (Anglés-Alcázar et al., 2017, Curti et al., 2020). The relation between the metallicity of the ISM and the stellar mass of a galaxy is called mass-metallicity relation (MZR). The first indication of the existence of such a relation was demonstrated in Lequeux et al. (1979) for dIs and BCDGs. In the work of Tremonti et al. (2004) this correlation was extended by using a sample of 54300 star-forming galaxies from SDSS in DR2. In Andrews & Martini (2013) $\sim$ 200000 star-forming galaxies were stacked in bins of stellar mass and SFR in order to enhance the signal of [O I] λ4363 and [O II] $\lambda\lambda$7320+7330 and estimate the metallicity from the electron temperature, which is more accurate than measuring the metallicity directly from strong emission lines. This work provides

a MZR that covers a wider range of stellar masses and metallicities than previous relations. This relation, which holds for a large range of masses ($10^7\,M_\odot$–$10^{12}\,M_\odot$) reveals that the most massive systems are the most chemically evolved stages of galaxy formation, and also that the stronger gravitational potential wells make larger galaxies more capable of maintaining their metal-rich content, since they are less affected, in that sense, by winds and outflows than minor galaxies (Somerville & Davé, 2015, Chisholm & Kingstone, 2015). In figure 1.3 we show the Andrews & Martini (2013) mass-metallicity relation, represented by a black solid line, which was obtained as described above. The circles represents the bins of stellar mass. The coloured lines represent calibrations made using the strong emission lines (McGaugh, 1991, Zaritsky et al., 1994, Denicoló et al., 2002, Kewley & Dopita, 2002, Kobulnicky & Kewley, 2004, Pettini & Pagel, 2004, Tremonti et al., 2004).

As shown in figure 1.3, the mass-metallicity relation is widely studied for high and intermediate redshifts, where most of the studies focus on massive star-forming galaxies (Erb et al., 2006, Kewley & Ellison, 2008), so that the low-metallicity and low-mass end of the MZR are not explored as well as its counterparts. In 1.3, for example, we observe that most of the empirical relations do not cover the regime of $\log(O/H) + 12$ $\log(O/H) + 12 \lessapprox 8.5$. Figure 1.4 presents the MZR at lower stellar mass (and consequently metallicity) end, for intermediate-z and local BCDGs ($z \sim 0.03$ to $z \sim 0.3$). Grey dots represent a sample of SDSS BCDGs, while the red circles are BCDGs from the Cosmic Evolution Survey (COSMOS), where the sample was analysed in Lian et al. (2016).

A large variety of structures can be formed and found close to galaxies, and they provide important information about the past of these galaxies, as it is in the case of giant ionised gas clouds (HII regions), which will be discussed in more detail in the next section.

1.2 The ionised interestellar medium

One of the most common structures of ionised gas in galaxies are the H II regions, which are composed mainly of ionised Hydrogen. Due to the self-gravitational well these regions often show spherical symmetry, with electronic temperatures of the order of $10^4\,\mathrm{K}$, while its electronic density span orders of magnitude, lying in the range of $10^2 \sim 10^3\,\mathrm{cm}^{-3}$, though H II regions with higher or lower electronic densities are not rare (Reynolds et al., 2001, Hunt & Hirashita, 2009).

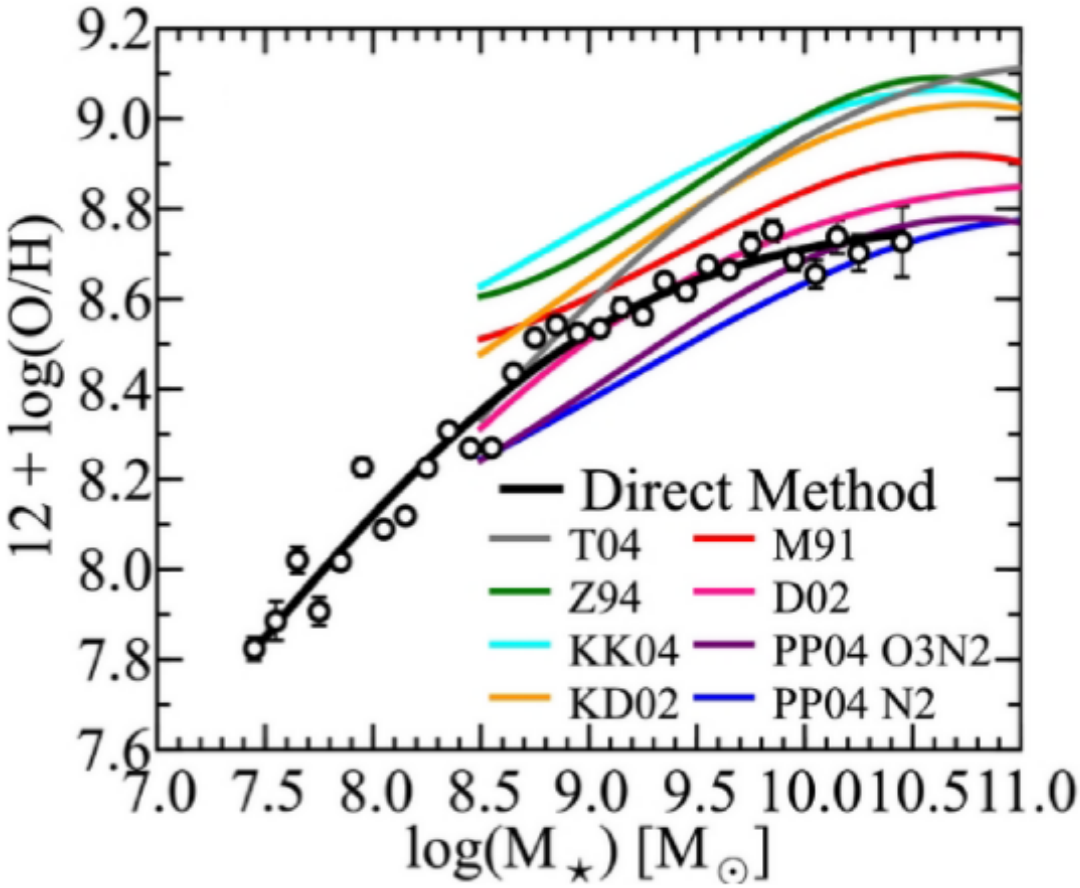

Figure 1.3: The mass-metallicity relation obtained in Andrews & Martini (2013) using the stacked spectra of $\sim$ 200000 star-forming galaxies to estimate the metallicity from the electronic temperature of H II regions within these galaxies. The relation is represented by the black solid line, where the circles are the bins of mass. Coloured lines represent calibrations made using the strong emission lines method (McGaugh, 1991, Zaritsky et al., 1994, Denicoló et al., 2002, Kewley & Dopita, 2002, Kobulnicky & Kewley, 2004, Pettini & Pagel, 2004, Tremonti et al., 2004).

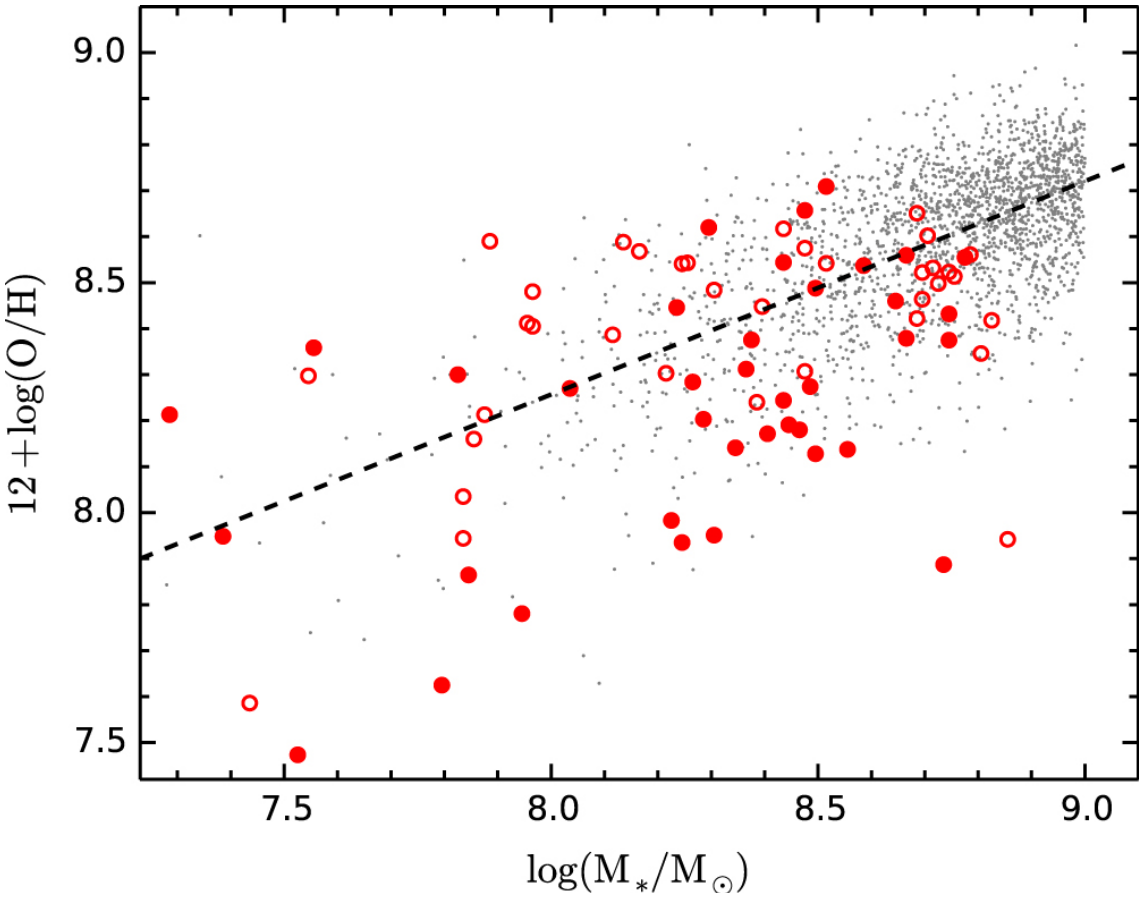

Figure 1.4: Low end of the mass-metallicity relation, including the Blue Compact Dwarf Galaxies. While the grey dots represent a sample of BCDGs in SDSS, the red circles are BCDGs from Cosmic Evolution Survey (COSMOS). Figure taken from Lian et al. (2016).

These regions are surrounded by young hot stars (in figure 1.5 we present examples of large H II regions.) of type O and B with effective temperatures in the order of 30 000 $\sim$ 50 000 K, responsible for the production of the photons that ionise the surrounding gas, presenting a variety of physical dimensions, like the Orion nebula (D $\sim$ 8 pc), or even smaller (Anderson et al., 2014), to hundreds of parsecs, such as 30 Doradus (D $\sim$ 200 pc), NGC 604 (D $\sim$ 460 pc), or NGC 5471 (D $\sim$ 1 kpc) as reported by Oey et al. (2003) and García-Benito et al. (2011). These latter ones are the prototypes of the extragalactic giant H II regions frequently found in the disks of spiral galaxies (Hodge & Kennicutt Jr, 1983, Dottori, 1987, Dottori & Copetti, 1989, Knapen, 1998). In some cases, the star formation is violent and extends over the whole galaxy (e.g. starburst and Blue Compact Dwarf Galaxies, Kehrig et al., 2008, Cairós et al., 2012).

Spectroscopically, these objects stand out due to their strong emission lines, specially in the optical wavelength range (4000 $\sim$ 7000 Å). These arise mainly due to the recombination of H and He, though there are other equally strong emission lines called *forbidden* lines[2]. The environment of the H II regions is perfect for these lines to arise, since it has a density that is sufficiently low (usually with electronic densities in the range of $10^2 \sim 10^3\,\mathrm{cm}^{-3}$) and exhibits a radiation field with energy enough to promote this process. Since such low density gas can not be reproduced in laboratories, these lines were observed by the first time in H II regions. Examples of forbidden lines usually found in H II regions are [O III] λ5007, [N II] λ6583 and [S II] λ6731. The square brackets enclosing the spectroscopic atomic notation indicate that the line is forbidden.

Though similar in the sense of being a gaseous region with the presence of strong emission lines in its spectrum, an H II region shall not be confused with an Extended Emission Line Region (EELR). The term EELR is usually associated to nebular regions found lying next quasars, though too distant to be considered as part of the Narrow-Line Region (NLR)[3] Since these regions are being ionised directly by

[2]These forbidden lines come from an atomic transition that violates the selection rules when considering the usual electric dipole approximation for the interaction between light and the bounded electron. This process is not strictly forbidden, since deeper approximations as the electric quadrupole, for example, changes the selection rules and allows this transitions to happen, though at much lower rate than the regular transitions. The mean lifetime of this state is of the order of hours, i.e., a long-lived state in comparison to the regular states with mean lifetime in the order of 10^{-9}s. It means that it would take hours for such an excited electron to decay back to its original level and emit a photon radiatively, what is extremely unlikely to happen in an environment with relatively high density, since the collisional de-excitement is almost certain within an hour. Even the best vacuum produced in laboratories today still is too dense to observe these lines, and this is why they were called forbidden.

[3]A gaseous region close to the central regions of a quasar and ionised by the radiation emitted

(a) 30 Doradus. Credits: Trappist/E. Jehin/ESO

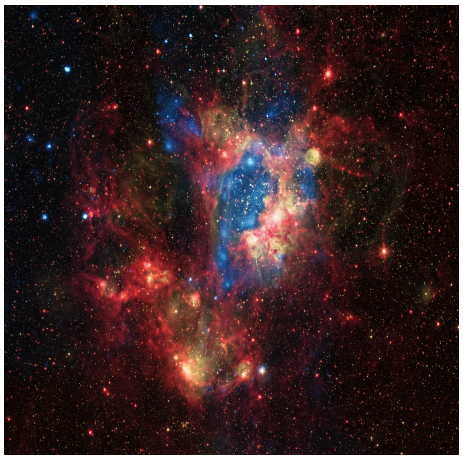

(b) N44. Credits: Optical: ESO, X-ray: NASA/CXC/U.Mich./S.Oey, IR: NASA/JPL

Figure 1.5: Examples of H II regions. 30 Doradus is located within the LMC with a distance of $\sim 49\,\mathrm{kpc}$ from us, where the picture shown is made from a composition of the filters B, V and R. The FoV of the image covers 20 arcmin. 30 Doradus is intrinsically the brightest star-forming region in the Local Group, with a stellar mass of $4.5 \times 10^5\,M_\odot$. N44 is also located within the LMC, and the picture shown displays a combination of images in the optical, IR and X-ray. It has a projected extension of $\sim 300\,\mathrm{pc}$ and an estimated stellar mass of $5 \times 10^5\,M_\odot$.

the Active Galactic Nuclei (AGN) it is thought that analysing the gas may reveal important information about the influence of the AGN activity into quenching or enhancing the star formation. In the former case, we call this process as *negative AGN feedback*, while the latter is called *positive AGN feedback* (Schawinski et al., 2007, Sijacki et al., 2007, Dubois et al., 2016, Gallagher et al., 2019). This hard radiation field can be ceased if the SMBH stops the mass accretion. Since the speed of light is finite the gas composing the EELR does not stop receiving this radiation immediately. Then, there is a window in time where the observed energetic level of the continuum needed to produce the emission lines seen in the spectrum of the EELR is not compatible with the radiation emitted by the faded quasar. Such an object is called a *quasar light echo*, and its existence was unknown until the serendipitous discovery of a faint nebula near IC 2497 by the citizen scientist Hanny Van Arkel during the visual inspection of data in the Galaxy Zoo project (Raddick et al., 2009, 2013). This peculiar object was named then as *Hanny's voorwerp* (voorwerp is the dutch word for object, Lintott et al., 2009, Józsa et al., 2009, Rampadarath et al., 2010, Schawinski et al., 2010). Similar objects found later are

by an Active Galactic Nuclei (AGN) due to the accretion of matter by the Supermassive Black Hole (SMBH, Ferrarese & Ford, 2005, Kormendy & Ho, 2013, Storchi-Bergmann, 2014).

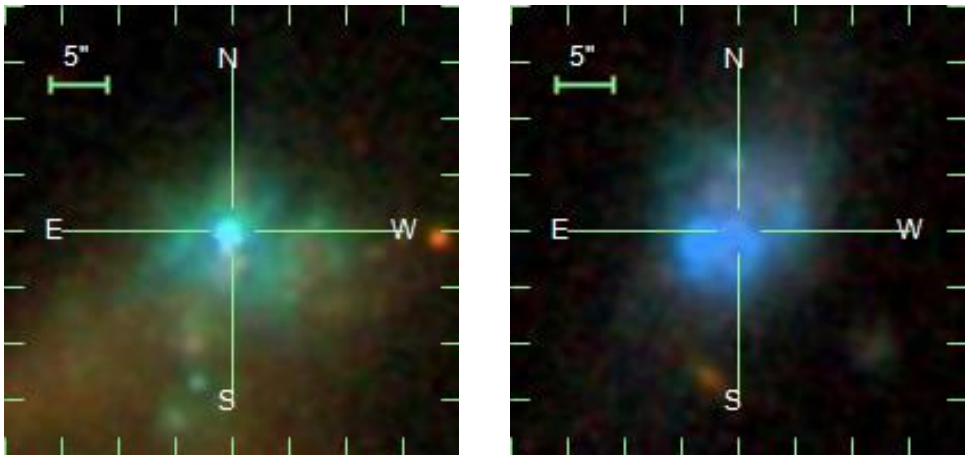

(a) II Zw 40. (b) Mrk 36.

Figure 1.6: Examples of H II galaxies, rich in gas, metal-poor and with irregular morphologies, these objects are actively forming stars. II Zw 40 is a widely studied Blue Compact Dwarf Galaxy, with $z = 0.00263$. Mrk 36 also a Blue Compact Dwarf Galaxy, has $z = 0.00215$. Figure taken from SDSS database.

called *voorwerpjes* (plural for voorwerp). These objects are large (the prototypical Hanny's voorwerp, for example, extends itself over a 11 x 16 kpc projected region (Sartori et al., 2018) and thought to be originated in the release of huge amounts of gas occurred in past merger events (Keel et al., 2012).

There are galaxies that have morphologies that resembles giant H II clouds, as II Zw 40 and Mrk 36, which are illustrated in figure 1.6, with images taken from SDSS (Zhao et al., 2013, Fernández et al., 2018). This is why these are referred sometimes as H II galaxies in the literature. These *H II galaxies and other low metallicity dwarf galaxies represent key objects in the process of improvement of the theory behind the hierarchical scenario of galaxy formation, since smaller low metallicity galaxies in the Early Universe (and today) are the minor pieces that shall merge to form the larger galaxies*. Thus, finding local Universe low metallicity analogues to these kind of objects is fundamental to study in detail and understand the physics behind such types of sources.

1.3 Dwarf irregular galaxies

Dwarf galaxies differ from larger galaxies in several aspects. Noticeable they are smaller in size, fainter and have lower mass content, usually orbiting as satellites of larger galaxies. These objects play a fundamental role in the hierarchical model of

galaxy formation and evolution, since it is thought that smaller objects go through successive mergers to form the observed galaxies, meaning that they have perhaps also been dwarfs in the past (Digby et al., 2019).

Although the most abundant galaxies in the Universe, the fraction of all stars that are located in dwarf galaxies is not equally significant (i.e., though the most abundant class of galaxies, these do not hold the highest fraction of stars when compared with massive galaxies), once the gas content varies from case to case (Mo et al., 2010). Numerous, dwarf galaxies are seen in a wide range of environments, providing important information about the formation of these systems and the impact of the environment on their evolution. Indeed, they present diverse observed structures, so that we have dwarfs with high gas and stellar content with active star formation, classified as Dwarf Irregulars (dI).

From the relatively high amount of gas present in the dwarf irregulars, a fair fraction of neutral gas is observed, i.e., the gas composed of the neutral atoms of Hydrogen and Helium[4] (H I and He I). Molecular gas can also be observed in some cases, i.e., the gas composed of H_2 (Riffel et al., 2010, Brum et al., 2019).

One of the most important feature in a dI is its metallicity[5], which can be estimated via several methods. In the case of gas-rich systems, such as dIs, metallicity can be traced from the Oxygen abundance in H II regions (Kunth & Östlin, 2000). Considering the optical wavelength range, Oxygen is the most reliable element, since it often presents stronger emission lines in comparison to other elements (i.e., N, S, Ne, He) and the most important stages of ionisation can all be observed (Kunth & Östlin, 2000). Dwarf irregulars are said to be metal-poor, presenting, in the Local Group, metallicities that varies from 1/3 $Z_\odot$ to 1/40 $Z_\odot$, some of them between the most metal-poor known systems, where $Z_\odot$ is the metallicity of the sun (Gil de Paz et al., 2003, Thuan & Izotov, 2005). dIs have, on average, a major axis of about 7 kpc with masses[6] of the order of 10^8–10^9 $M_\odot$(Hunter & Gallagher III, 1985).

Metallicity is an unique feature of these systems. Such metal-poor systems resemble the primitive galaxies in the Universe, which are located at high redshift, and due to the typical faintness of the dwarfs they can not be be observed directly with the instruments available today. The dwarf galaxies represent an unique class of extragalactic objects, since in the hierarchical scenario they are the minor pieces that assembly the larger galaxies via successive mergers. In the case of the primitive galaxies, which are the first formed galaxies, the processes of evolution and forma-

[4]Adopting the spectroscopic notation $X^0 \equiv X\ I$ and $X^+ = X\ II$

[5]The fraction of elements heavier than He

[6]This value corresponds to the mass measured using atomic Hydrogen, M_{H_I}

tion of such objects are still unclear, since the environmental conditions in the early Universe are far distinct than today. Understanding empirically the formation and evolution of primitive galaxies can improve several constraints in hierarchical theory, leading to a more refined scenario, and also provide deeper knowledge on star formation in different environmental conditions (Pritchet, 1994, Djorgovski, 1992). Fortunately, local metal-poor galaxies with high content of gas, such as the dI and specially the Blue Compact Dwarf Galaxies (BCDGs), represent nearby analogues to the primitive galaxies in the sense that we are able to explore the thermal balance of the ISM under the condition of low metallicities. This allows inferences on the evolutionary driving processes in primitive galaxies (Lebouteiller et al., 2017).

1.4 Blue Compact Dwarf Galaxies

Blue compact dwarf galaxies are also referred in the literature as H II galaxies, since spectroscopically they are indistinguishable from H II regions often found in the outskirts of spiral galaxies, being usually found in emission line surveys because of this feature. The Blue Compact Dwarf Galaxies (BCDGs) differ in many properties from the regular (galaxies that are not classified as dwarfs) galaxies and in many times differ from other known dwarf galaxies, even though the categories of dI and BCDGs often overlap, i.e., there are irregular BCDGs and dIs exhibiting H II regions. Such overlap happens mainly because the transition between one category to the other is gradual and the division criteria might be too arbitrary (Kunth & Östlin, 2000). In Gil de Paz et al. (2003), a criteria is proposed to segregate dIs from BCDGs: Since in dI the recent star formation is less active in comparison to BCDGs and thus the Peak Surface Brightness (PSB) of the former is fainter and redder than the latter, a criteria of $\mu_{B,\mathrm{peak}} - \mu_{R,\mathrm{peak}}$ can be used. Indeed, Gil de Paz et al. (2003) introduces a criteria where BCDGs are thought to follow a trend where $\mu_{B,\mathrm{peak}} - \mu_{R,\mathrm{peak}} \lesssim 1$. BCDGs stand out for its activity in forming stars, and the presence of a large quantity of young hot stars increasing the luminosity on the blue part of the spectrum, and this is why they are called blue.

The BCDGs are very faint in the optical, with absolute B magnitudes regularly ranging from -17 to -21 mag. To separate Blue Compact Galaxies (BCGs) from BCDGs, the main criteria used in the literature is to set as dwarfs the ones fainter than $M_B \approx -18$ mag (Kunth & Östlin, 2000, Janowiecki et al., 2017, Yin et al., 2018). These galaxies are relatively rich in gas, specially when compared with other dwarfs, also exhibiting clumpy knots where the recent star formation is taking place

and stars are formed at high rates, exhausting the available gas in timescales of ∼1 Gyr (Fanelli et al., 1988). Results in the literature show that the SFR in BCDGs span about 5 orders of magnitude. Using different methods for samples of BCDGs, such as SFR(60 μm), SFR(1.4 Ghz) and SFR($L_{H\alpha}$), the median SFR in these galaxies seems to lie in the range of $0.1 - 10\, M_{\odot}\, yr^{-1}$ (Hopkins et al., 2002, Zhao et al., 2011). Similarly as in the case of the dIs, the class of BCDGs include galaxies with the lowest measured Oxigen abundance, as first shown by Searle & Sargent (1972) for the cases of I Zw18 and II Zw40 and confirmed for several other galaxies in many posterior investigations, establishing the BCDGs among the least chemical evolved objects in the Universe, thus said to be metal-poor. Indeed, Oxygen abundance measurements reveal that the BCDGs usually lies in the range of metallicity of $1/2\ Z_{\odot} \sim 1/50 Z_{\odot}$ (Gil de Paz et al., 2003).

The low metallicity measured in these galaxies and the presence of young stars made many researchers argue that the BCDGs could be even more similar to the primeval galaxies located at high redshift, in the sense that the observed episode of SF could actually be the first of these systems (Searle & Sargent, 1972, Kunth et al., 1988). The idea behind this argument is the fact that in the process of evolution of the massive stars, elements like H and He are converted into metallic elements via nuclear fusion in the interior of the stars. In this scenario, when these massive stars die, these heavier formed atoms are thrown back to the original environment, a process that happens successively, making the gas within the H II regions to be more metal-rich.

However, extensive photometric analysis in the optical (Loose & Thuan, 1986, Papaderos et al., 1996) and in the NIR (Noeske et al., 2005) revealed that almost all BCDGs present a low surface brightness (LSB) stellar host with near-exponential profiles (Amorin et al., 2007). The LSB component appears as an extended envelope underlying the $t \leq 500$ Myr stellar population found in the SF regions, with ages in the order of 1 Gyr. The existence of these older stellar populations indicates that it is unlikely that these objects are actually experiencing their first starburst episode. Regarding the compactness, the initial criteria was to set an upper limit of 1 kpc in the optical for the BCDGs (Thuan & Martin, 1981). Due to the existence of the LSB component, it is more accurate to associate the compactness with the components within the galaxy with higher surface brightness (μ). An useful criteria for this situation was introduced in Zwicky (1970), where compact is said to be a galaxy or any part of a galaxy with $\mu < 20$ mag arcsec^{-2}. This criteria of compactness shows one of the subtle difference between dIs and BCDGs, as mentioned before.

When comparing the PSB measured in the Low-Surface Brightness components of a sample of both classes of galaxies, a trend is observed, where dIs present higher values of μ_B in comparison to BCDGs. The physical reason for this is that the recent star formation in BCDGs is more intense than in dIs, adding up the luminosity in the blue part of the spectrum (Gil de Paz et al., 2003). Another characteristic of BCDGs that often appears in the literature as a criteria to determine an object as a BCDG is the luminosity associated with Hα emission line, i.e., $L(\mathrm{H}\alpha)$. The upper limit of $L(\mathrm{H}\alpha) = 10^{41}\,\mathrm{erg\,s^{-1}}$ is used, for example (Gallego et al., 1997, Kong et al., 2002, Shi et al., 2005).

1.5 Motivation

During the visual inspection of data from the Multi Unit Spectroscopic Explorer (MUSE) we serendipitously found a nebular region near the quiescent Early-Type Galaxy (ETG) Mrk 1172. This object has photometric data available on the GALEX catalogue (as GALEX J020536.7-081424) in the NUV and FUV wavelength range and photometrical properties in the optical on SDSS. However, no spectrum was found for this object in the literature, neither studies exploring its relation with Mrk 1172.

This faint nebular region presents irregular shape (see figure 1.7), occupying a projected area of approximately $14 \times 14\,\mathrm{kpc}$. The inspection of its spectrum in the optical revealed the presence of strong emission lines, specially Hα and [O III] λ5007, indicating that the gas is ionised and is likely to be actively forming stars. From the strong emission lines we estimate the redshift of this object and its distance, comparing with the values found in the literature for Mrk 1172. Based on its mass, metallicity and star formation properties derived later in the dissertation we refer to this object as BCD-UFRGS-01 from now on. *In this work our efforts focus on the characterisation of BCD-UFRGS-01 with respect to its* ***physical*** *and* ***chemical properties***, in order to shed some light about its nature, thus, adding one extra piece to help solve the puzzle of galaxy evolution and inferring, if possible, how it is interacting with Mrk 1172.

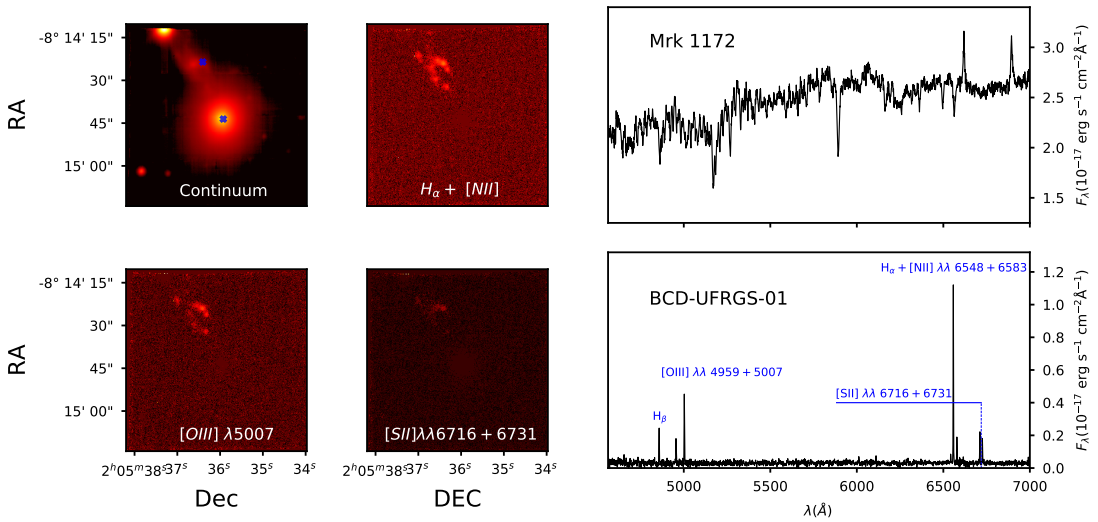

Figure 1.7: The MUSE Field of View (FoV) continuum centered in Mrk 1172 (top left), Hα+[N II]$\lambda\lambda$6550+6585 (top central), [O III]λ5007 (bottom left) and [S II]$\lambda\lambda$6716+6731 (bottom central) wavelength ranges. The wavelength windows used to subtract the continuum from the flux of each emission lines are presented in section 2. The spectrum of Mrk 1172 highest-SNR spaxel is presented in top right panel, while in bottom right panel we present the spectrum for the highest-SNR spaxel for BCD-UFRGS-01. The location of these spaxels within the FoV is indicated in blue in the top left panel.

Chapter 2

Methods

In this chapter we briefly describe the physics underlying the techniques applied in our analysis and the motivations that led us to apply each one of them.

2.1 Stellar population synthesis

We briefly debate the importance of the gas in the context of galaxy formation and evolution. Besides being able to dictate the morphology of a galaxy, when the gas collapses it begins forming stars, which are the responsible for the greater fraction of emitted light in a galaxy, disregarding the case of galaxies hosting an AGN. The evolution of stars is nowadays reasonably well understood, and assuming spherical symmetry and hydrodynamical equilibrium, a very accurate model for the birth, interior chemical processes and death of a star can be build using their mass, Initial Mass Function (IMF) and also the birth rate (Mo et al., 2010).

Roughly speaking, a galaxy is composed of dust, gas, stars and dark matter. Then, the evolution of the luminous matter within a galaxy is directly connected to the formation and evolution of its stars, and these should hold imprints on the galaxy star formation history. It would be amazing to study in detail each star to completely trace when they were formed and under which conditions, but they are numerous and the majority of the galaxies are too distant for them to be individually resolved. However, we know that tens to hundreds of stars are formed in the collapse of a single cloud, sharing the same initial environmental conditions and age (the timescale between the birth one star and other is negligible in comparison to time they will live), and then we call this set of stars a stellar population, in the case of the mentioned approximation, we can call them Simple Stellar Populations (SSPs).

Recovering the stellar content of a galaxy from its observed integrated light is not an easy task, as corroborated by the number of works on this topic and the constant improvement in the techniques seen in the past half century (e.g., Wood, 1966, Bica, 1988, Fernandes et al., 2001, Cid Fernandes et al., 2005, Conroy et al., 2009, Vazdekis et al., 2015).

In order to determine the main properties of the dominant stellar population of a galaxy, a stellar population synthesis technique was developed, where the spectra of individual stars is combined and synthesized to match the observed integrated spectrum of the galaxy. The spectrum of individual stars to be used can be obtained via two main approaches. In the empirical approach, a sample of nearby stars with measured bolometric magnitudes ($M_{\rm bol}$), effective temperatures ($T_{\rm eff}$) and metallicities (Z) is used to extrapolate/interpolate these spectra and create a model spectrum for a wide rage of stars. The empirical method has a limitation lying in the fact that the spectrum of these individual stars can be obtained with the necessary quality only for the stars in the solar neighborhood, meaning that the range of abundances and metallicities available in the empirical set is considerably restricted, and the extrapolation for stars formed in different environments is not very reliable (Mo et al., 2010). The second approach is theoretical and models of stellar atmospheres are build in order to produce spectra of stars in a wider range in comparison to the empirical approach. A detailed discussion of how this is done can be found in Mihalas (1978), Kurucz (1992), Coelho (2014), Barbuy et al. (2018). The limitations in this model are related to our current knowledge about the life cycle of stars instead of data availability, though the libraries of stellar evolutionary tracks are constantly being improved (Lejeune et al., 1997, Westera et al., 2002, Maraston & Strömbäck, 2011, Vazdekis et al., 2012).

Using the knowledge of stellar evolution (e.g., isochrones tracks and/or fuel consumption theorem, Maraston, 2005, Bressan et al., 2012) together with a stellar library allows the production of evolutionary population synthesis models (EPS), which are a set of simple stellar population models (SSPs). To disentagle the star formation history of a galaxy, one can fit a mixture of SSPs models to the underlying galaxy spectrum. In this work we used STARLIGHT code (Cid Fernandes et al., 2005), which uses a base of SSPs with a variety of ages and metallicities, and performs a linear combination between the elements in the base to produce synthetic spectra that are compared with the observed spectrum in order to determine the combination that minimizes the χ^2 associated with the fit. Considering O_λ as the observed flux and M_λ as the model flux vector given by the linear combination of

the elements in the base, the χ^2 of the fit is calculated using:

$$\chi^2 = \sum_{\lambda} \Big[(O_\lambda - M_\lambda) w_\lambda \Big]^2 \tag{2.1}$$

where w_λ is a weighting factor with wavelength dependency that can be set by the user. There are regions in the spectrum that the user may wish to ignore in the fitting process, like emission lines or spurious data, for example. In this case, the user can set $w_\lambda = 0$ for these regions in the spectrum.

To determine M_λ, STARLIGHT uses the equation:

$$M_\lambda = M_{\lambda_0} \Big[\sum_{j=1}^{N_\star} x_j \; b_{j,\lambda} \; r_\lambda \Big] \otimes G(v_\star, \sigma_\star) \tag{2.2}$$

where the index j covers all the $N_\star$ elements in the base, x_j is the j-th element of the population vector, $b_{j,\lambda}$ is the j-th element in the base and $r_\lambda = 10^{-0.4(A_\lambda - A_{\lambda_0})}$ is the term for reddening correction (reddening will be discussed further). The term inside the brackets is convoluted with a Gaussian with center determined by the stellar velocity ($v_\star$) and dispersion ($\sigma_\star$, i.e., $G(v_\star, \sigma_\star)$) and then multiplied by the model flux vector evaluated at $\lambda = \lambda_0$, ideally a featureless region in the original spectrum to be set by the user before the fit.

2.2 Interestellar extinction

When studying an H II region we are usually interested in the properties of the gas, to be obtained from the emission lines presented in its spectrum. However, such regions must not be considered as a pure volume of gas, since dust particles are present, located among the gas, absorbing and scattering the stellar continuum radiation. Thus, these dust particles affect the spectrum and consequently the emission lines, meaning that this effect must not be neglected in order to obtain the correct properties.

The amounts of dust can absorb the radiation, reducing the flux emitted by the source in the perspective of the observer, and this phenomena receives the name of extinction. The scattering of the photons has the result of reducing the energy of the incident photon, and thus the light is said to suffer an effect of reddening. The intensity of the light emitted by the source is called intrinsic intensity (I_{λ_0}), and relates with the observed intensity (I_λ) via the equation (Osterbrock & Ferland,

2006):

$$I_\lambda = I_{\lambda_0}\ \mathrm{e}^{-\tau_\lambda} \tag{2.3}$$

where τ_λ is the optical depth, which quantifies the transparency of the environment along the line-of-sight of the observer. The mean free path of a photon depends on its wavelength, since photons with considerably different energies will interact differently with the matter, and this is why τ_λ has a wavelength dependency. The optical depth is given by:

$$\tau_\lambda = C f(\lambda) \tag{2.4}$$

where C is a constant and $f(\lambda)$ is a function that holds the wavelength dependency of the optical depth. Combining equations 2.3 and 2.4 gives:

$$I_\lambda = I_{\lambda_0}\ \mathrm{e}^{-Cf(\lambda)} \tag{2.5}$$

Since C and $f(\lambda)$ are yet undetermined, the expression above cannot be solely determined. To proceed we must consider the ratio of this generic expression with its evaluation on a specific wavelength window. The typical sizes of the dust grains in H II regions make the interaction with photons more intense in the optical and Near Ultraviolet (NUV), and then the wavelength corresponding to Hβ (4861.33 Å) is very convenient to proceed with the analysis[1] (Osterbrock & Ferland, 2006):

$$\frac{I_\lambda}{I_{H\beta}} = \frac{I_{\lambda_0}}{I_{H\beta_0}}\ \frac{\mathrm{e}^{-Cf(\lambda)}}{\mathrm{e}^{-Cf(H_\beta)}} = \frac{I_{\lambda_0}}{I_{H\beta_0}}\ 10^{-0.434\ C\left[f(\lambda)-f(H\beta)\right]} \tag{2.6}$$

Considering the extinction at a given wavelength λ_1 in units of magnitude (A_{λ_1}) as $A_{\lambda_1} = 2.5\ \log\ (I_{\lambda_1}/I_{\lambda_0})$ we can use this definition in equation 2.6 to obtain that A_{λ_1} can be expressed as:

$$A_{\lambda_1} = -2.5\ C' f(\lambda_1) \tag{2.7}$$

where $C' \equiv 0.434C$. We have also that the excess of color $E(B-V) \equiv A_B - A_V$, where A_B and A_V are the extinction in the B and V bands, respectively. Adopting the ratio of total to selective extinction R[2] as $R = 3.1$, which represents the so called standard reddening law (since it is the most used), we get that $E(B-V) \approx 0.77C'$ (Osterbrock & Ferland, 2006). Then, we have:

[1] A conversion of the logarithmic base was applied: $\mathrm{e}^x = 10^y \Rightarrow y = 0.434\ x$

[2] $R \equiv \frac{A_V}{E(B-V)}$

$$A_\lambda = -2.5 \log\Big(\frac{I_\lambda}{I_{\lambda_0}}\Big) \tag{2.8}$$

Finally, using the relation between A_V and A_λ, we obtain $A_V f(\lambda) \approx 2.387 \log(I_\lambda/I_{\lambda_0})$. To determine the interestellar extinction the H I Balmer lines are often used. Usually Hα and Hβ are used, since they are strong lines in an emission spectrum, but also because they are able to provide accurate measurements even with poor temperature estimates. The assumed extinction curve gives $f(\mathrm{H}\alpha) = 0.818$ and $f(\mathrm{H}\beta) = 1.164$. Then, assuming the case B of recombination, an intrinsic Hα/Hβ intensity ratio of 2.87 and temperature of 10^4 K, we have (Nascimento et al., 2019):

$$A_V = 7.23 \times \log\left[\frac{F(\mathrm{H}_\alpha)}{F(\mathrm{H}\beta)}\right] - 3.31 \tag{2.9}$$

where $F(\mathrm{H}\alpha)$ and $F(\mathrm{H}\beta)$ are the observed fluxes. The reddening law used in this work is known as CCM law and was introduced in Cardelli et al. (1989).

The effect of dust has proven to be highly variable along the line of sight of the observer, and this is not only because the dust within the H II region, but specially because of the diffuse extragalactic background, dust and molecular emission from the ISM originated from within and beyond MW. To correct these effects a 2D dust reddening map based on thermal emission is made (see Schlegel et al., 1998) in order to correct this effects in Galactic and also in extragalactic scales. In this work we use both CCM law and the so called Schlegel dust maps in order to estimate the reddening effect in the observed system.

Since STARLIGHT only corrects the extinction of the underlying stellar population, the extinction effects of the fluxes of the free emission line gas (i.e., after subtracting the synthetic stellar population) are corrected as described above.

2.3 Emission Line Diagnostic Diagrams

As mentioned, when emission lines are seen in a spectrum, they indicate the excitation of the gas. However the excitation mechanism requires a deeper analysis than the simple visualisation of spectra, once different mechanisms can produce the same emission lines. In most cases the ionisation mechanism is one of the following: photoionisation by O and B stars, photoionisation by a power-law continuum source or heating due to shock waves.

O and B stars are blue and massive stars, with masses up to $20\,M_\odot$. Their

effective temperatures exceed 10 000 K, emitting photons with energy enough to ionise the surrounding interestellar gas. The gas can also be ionised by a power law continuum[3], a characteristic of the broad-band spectral energy distribution (SED) of a quasar, which emits energetic photons that are able to ionise the surrounding gas. The ionisation of the gas due to shocks has proven to be an important mechanism in systems around jets and high-velocity outflows originated in radio-loud AGNs. These shocks convert part of the kinetic energy in the colliding gas clouds into thermal energy, which is then converted into ionizing radiation (Laor, 1998, Keel et al., 2019). Galaxies presenting emission line spectra also might be a Low-Ionisation Nuclear Emission Line Region (LINER), an object that differs from the more common Seyfert galaxies (Singh et al., 2013). While studies in the past decades favoured a scenario that suggests that the ionisation is due to low-luminosity AGNs, inconsistencies were found in this hypothesis(Halpern & Steiner, 1983, Cid Fernandes et al., 2011). The most likely scenario points that ionisation in these galaxies is due to evolved stars (post-AGBs, Singh et al., 2013).

As mentioned before, all these excitation mechanisms provide photons or thermal radiation sufficiently energetic to produce the main emission lines in the optical. However, the intensity ratio of these lines is not equal for each case and therefore can be used to determine the source of ionisation. Baldwin et al. (1981) proposed diagnostic diagrams using the intensity line ratios of Hα, Hβ, [O III] λ5007, [N II] λ6583, [S II] λ6716 and [S II] λ6731. In figure 2.1 we present an example of both diagrams known as BPT diagrams (Kewley et al., 2006). The limitation lines, i.e., the lines separating each region in the diagram were obtained by extensive empirical studies in the past decades (Veilleux & Osterbrock, 1987, Kewley et al., 2001, Kauffmann et al., 2003, Osterbrock & Ferland, 2006, Kewley et al., 2006, 2013a,b).

2.4 Electron temperature and density determinations

It is known that in low density regimes the intensity of the auroral transition ^{1}s $\rightarrow^2$ d is considerably smaller than for the nebular-type transition of ^{2}d $\rightarrow^3$ p (Allen, 1987, Gordon & Sorochenko, 2009). It is also known that the intensities of

[3] $F_\nu \propto \nu^{-\alpha}$, where α is the power law index

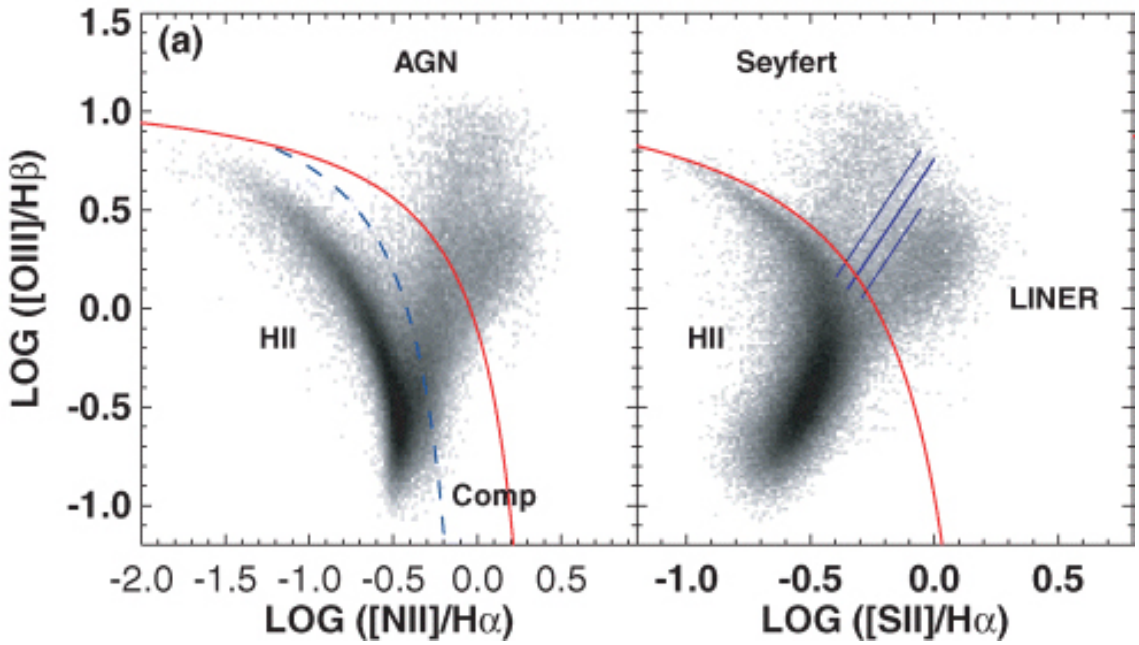

Figure 2.1: In the right panel, the diagram using [N II] and Hα emission line ratios, with the limitation lines that define the photoionisation mechanism of the observed gas. The same for left panel, but now using the emission line ratios of [S II] and Hα. Figure taken from Kewley et al. (2006).

forbidden lines are sensitive to ambient temperature and density through collisions, and then can be used to estimate physical conditions of their environments (Pilyugin et al., 2010, Aller, 2012, Boselli, 2012). In theory, the intensity ratio of the nebular and auroral transition of any element is sufficient to estimate the electronic temperature (T_e) of the photoionized gas, as long as these lines are not too distant in the wavelength direction. However, with the exception of [O III], [N II] and [S II], other intensity ratios are often weak and difficult to measure. Therefore the most popular choice used to determine T_e is [O III](λ4959 + λ5007)/[O III] λ4363 (Aller, 2012, Kewley et al., 2019). The emission line [O III]λ4363 is highly sensitive to temperature gradients, but turns out to be very faint and thus rarely observed in systems with high-metallicity [4] (Stasińska, 2005, Kewley & Ellison, 2008, Kewley et al., 2019). In figure 2.2 we present the the curves for the temperature dependency of the line ratios of the most used ions (Osterbrock & Ferland, 2006, Pradhan & Nahar, 2011).

The emission lines excited collisionally can also be used to determine the electronic density (n_e) of the photoionized gas. Most of the studies of electron densities in ionized gaseous regions in the optical use the emission lines of S[II] $\lambda\lambda$6716,6731

[4]Here considering a high-metallicity gas as $Z \gtrsim Z_{\odot}$

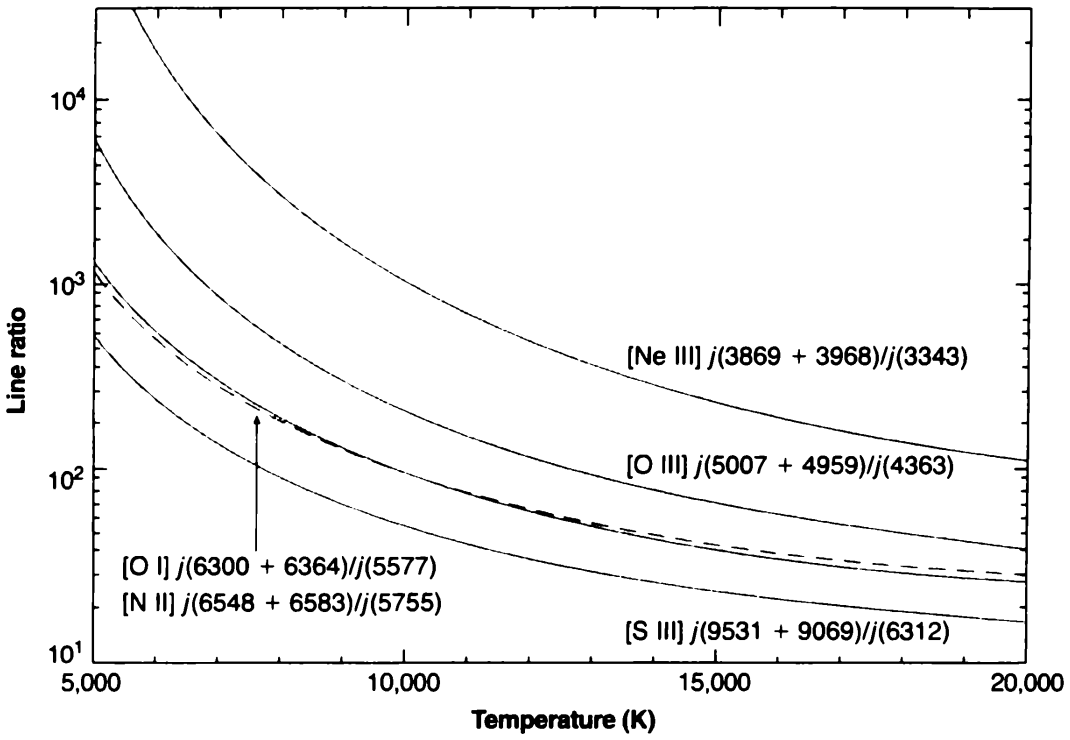

Figure 2.2: Line ratio dependency with electronic temperature for a set of emission lines sensitive to temperature. The ratios shown are considering the low-density limit of $n_e = 1\,\mathrm{cm}^{-3}$. Figure taken from (Osterbrock & Ferland, 2006).

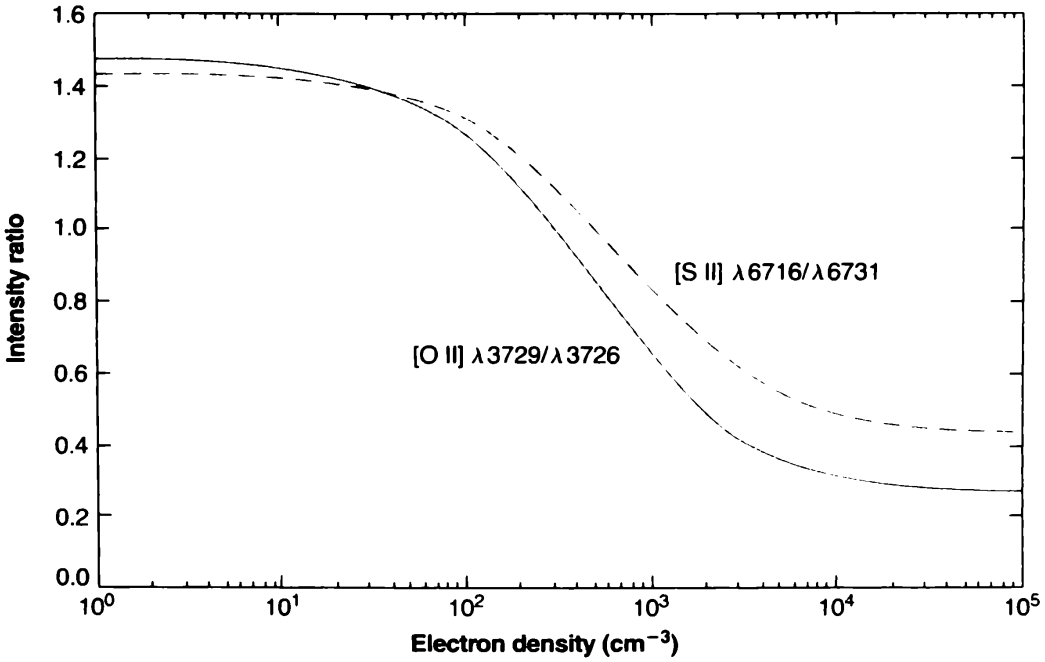

Figure 2.3: Line ratio dependency with electronic density assuming $T_e = 10^4\,\mathrm{K}$ for the most sensitive emission lines in the optical. The asymptotic behaviour of the curves indicates the values of density for which these lines saturate. Figure taken from Osterbrock & Ferland (2006).

and O[II] $\lambda\lambda$3726,3729. These are strong emission lines, thus often observed and accessible in a wide range of redshifts (Kakkad et al., 2018). Both lines are close in wavelength direction and have nearly the same excitation energy and then their relative flux depends only on the electronic density (Osterbrock & Ferland, 2006). The emission lines of O[II] $\lambda\lambda$3726,3729 are separated only by 3 Å, and often the spectrographs used do not have the spectral resolution necessary to resolve both lines. S[II] $\lambda\lambda$6716,6731 is more used than O[II] doublet, being sensitive to electronic densities in the range of $50 \sim 2000\,\mathrm{cm}^{-3}$, while the latter is more sensitive for systems with lower densities (Osterbrock & Ferland, 2006, Kakkad et al., 2018). The electronic density dependency for both doublets can be visualized in figure 2.3 (Ryden & Pogge, 2015), where the asymptotic behaviour of the functions indicate the density limits for which each doublet saturates. Examples of H II regions and galaxies that exceed the limit of S[II] doublet line ratio of ≈ 1.4 can be found in Wang et al. (2004).

2.5 Chemical Abundances

The chemical abundances of the ions in an ionised nebula can be derived from the relative strengths of each emission line. For an emission line excited collisionally, its intensity is given by the expression (Osterbrock & Ferland, 2006) :

$$I_{\lambda_{l,m}} = \frac{1}{4\pi} \int N(X^i) n_e h(\nu_m - \nu_l)\ q_{l,m}(T_e)\ b dS \tag{2.10}$$

where $N(X^i)$ is the abundance of element X, and i is the degree of ionisation of the element. The term $h(\nu_m - \nu_l)$ is the energy difference between atomic levels m and l, $q_{l,m}(T_e)$ is the collisional excitation rate, which depends on the electronic temperature of the gas T_e, and b is a factor that measures the deviation of the system from the thermodynamical equilibrium ($b = 1$ for an equilibrium state). The differential element dS is related to the path travelled by light in the observer line-of-sight. Considering n_e and $N(X^i)$ constant along the observer line-of-sight, we integrate the argument in equation 2.10 to obtain a new expression, dependent on S. To eliminate this dependency we can divide $I_{\lambda_{l,m}}$ by $I_{\mathrm{H}\beta}$ and express the relative abundance in function of both intensities (Osterbrock & Ferland, 2006):

$$\frac{N(X^i)}{N(H^+)} = \frac{I_{l,m}}{I_{H\beta}}\ \frac{h(\nu_m - \nu_l)\ q_{l,m}(T_e) b}{j_{H\beta}} \tag{2.11}$$

Assuming a value for T_e and n_e, and assuming the gas to be at an equilibrium state, the relative abundance can be determined from the intensity ratio of an emission line, since the other other parameters are already determined by the mentioned assumption. The relative abundance can be expressed as (Osterbrock & Ferland, 2006):

$$\frac{N(X^i)}{N(H^+)} = \sum_i \frac{N(X^i)}{N(H^+)} \tag{2.12}$$

Equation 2.12 means that the total relative abundance of an ion is given by the sum of the relative abundances of all the possible ionisation levels of atom X. However, these lines span a wide wavelength range in the spectrum and in many times are too faint to be detected, or are simply unavailable. Thus, in most cases equation 2.12 cannot be directly applied since the summation is incomplete. To correct this, an Ionisation Correction Factor (ICF) is used, and equation 2.12 is rewritten as (Luridiana et al., 2015):

$$\frac{N(X^i)}{N(H^+)} = \sum_{\bar{i}} \frac{N(X^{\bar{i}})}{N(H^+)} \times \text{ICF} \tag{2.13}$$

where now the index $\bar{i}$ covers the subset of available emission lines. The determination of the ICF for a given element can be done via photoionization models or via empirical observations done with comparisons between the ionisation potentials of different ions. The expressions for ICF are usually associated to Planetary Nebulae (PNe) or H II regions. The available emission lines in the spectrum of BCD-UFRGS-01 are those concerning the ions of O,N and S. We calculated their relative abundances using PYNEB (Luridiana et al., 2015), where the models for ICF for these in elements in H II regions are described in details in Izotov et al. (2006).

2.6 Star Formation Rate

Since the baryonic content of galaxies is essentially gas and stars, which are linked to each other via gravitational instabilities and strong radiative cooling, it is essential to study how this process is driven in a galaxy in order to better understand its evolutionary processes (Davé et al., 2011). It is known, for example, that environmental impact on SFR is stronger than that on morphology (Wetzel et al., 2012). Thus, SFR holds information about the environment in which a galaxy was formed and consequently how it evolved. As mentioned before, nebular emission lines provide a sensitive and direct probe of the young and massive stars. Evolutionary synthesis models indicate that only stars with masses $> 10 M_\odot$ and lifetimes of < 20 Myr contribute significantly for the integrated flux that is measured (Kennicutt Jr, 1998). Therefore, an estimate of the SFR based on these nebular emission lines is an "instantaneous" probe of a galaxy SFR.

Assuming solar abundances and a Salpeter IMF, calibrations computed using case B of recombination at $T_e = 10^4$ K (Kennicutt Jr, 1998, and references therein) yields to the relation:

$$\text{SFR}(M_\odot \text{ yr}^{-1}) = 7.9 \times 10^{-42} L(H\alpha) \text{ (erg s}^{-1}) \tag{2.14}$$

where the luminosity $L(\text{H}\alpha)$ is the luminosity associated with flux of Hα emission line, obtained using the equation:

$$L(\text{H}\alpha) = 4\pi F(\text{H}\alpha)\ d^2 \tag{2.15}$$

where d is the distance of the galaxy, which can be obtained in literature or calculated using $d = z(c/H_0)$, where z is the redshift, c is the speed of light and H_0 is the Hubble constant. Since the SFR is a measurement of the gas, and not of the stars, the flux $F(\mathrm{H}\alpha)$ in equation 2.15 must be obtained from a pure emission line spectrum, i.e., the stellar contribution must be subtracted from the gas contribution. It is also important to note that the extinction is a large source of uncertainty for the SFR measurement and thus a correction given by equation 2.5 must be applied to $F(\mathrm{H}\alpha)$ in order to obtain more accurate and reliable estimates of SFR.

Chapter 3

Results and Discussion

In this chapter we present the most recent draft version of a scientific article that is being written about the subject of this dissertation, which we intend to submit to Monthly Notices of the Royal Astronomical Society (MNRAS) when the analysis is ready. Besides the content explored in detail in the last two chapters of this dissertation, this article also contains the results obtained and a discussion related to these results

MNRAS **000**, 1–12 (2020) Preprint 19 October 2020 Compiled using MNRAS LATEX style file v3.0

The blue compact dwarf candidate galaxy next in projection to Mrk 1172

Augusto Lassen[1⋆], Rogerio Riffel[1], Ana L. Chies-Santos[1], Evelyn Johnston[2], Boris Häußler[3], Gabriel Azevedo[1], Daniel Ruschel-Dutra[4]

[1] *Departamento de Astronomia, Universidade Federal do Rio Grande do Sul, Av. Bento Gonçalves 9500, Porto Alegre, RS, Brazil*
[2] *Institute of Astrophysics, Pontificia Universidad Católica de Chile, Av. Vicuña Mackenna 4860, 7820436 Macul, Santiago, Chile*
[3] *European Southern Observatory, Alonso de Córdova 3107, Vitacura, Santiago, Chile*
[4] *Departamento de Física, Universidade Federal de Santa Catarina, P.O. Box 476, 88040-900, Florianópolis, SC, Brazil*

Accepted XXX. Received YYY; in original form ZZZ

ABSTRACT

We serendipitously discovered a nebular emission region with projected extension of 14×14 kpc near the quiescent ETG Mrk 1172, which we name BCD-UFRGS-01. In this work we aim to explore and describe BCD-UFRGS-01 in order to understand its nature. Using data from MUSE we perform a spatially resolved stellar population synthesis and from the strong emission lines in BCD-UFRGS-01 spectra we estimate its SFR, Oxygen abundance, spatially resolved kinematics and a lower limit for the ionised gas mass. From the stellar content, we estimate the stellar mass for both Mrk 1172 and BCD-UFRGS-01. BCD-UFRGS-01 presents two dominant stellar populations ($t_1 \sim 10^8$ yrs and $t_2 \sim 10^9$ yrs), while Mrk 1172 is dominated by an old stellar population ($t_3 \sim 10^{12}$ yrs). BCD-UFRGS-01 is metal-poor ($Z \sim 1/15\, Z_\odot$) and is actively forming stars ($0.71\ M_\odot\,\mathrm{yr}^{-1}$). It has a stellar mass of $4.06 \times 10^9\ M_\odot$ and an ionised gas mass higher than $3.5 \times 10^6\ M_\odot$. BCD-UFRGS-01 is rotating in the counter-clockwise direction, and the motion of the gas is well described by a gas in circular orbit around the plane of a disk. We conclude that BCD-UFRGS-01 is most likely to be a blue compact dwarf galaxy, although further analysis is necessary to better understand its nature.

Key words: galaxies: dwarf – H II regions – ISM: abundances

1 INTRODUCTION

The conditions at which stars formed within primeval galaxies in the early Universe were very different from the conditions on which stars form in the Local Universe (Kepley et al. 2016). Finding metal deficient dwarf galaxies that can be studied locally are invaluable as they have the potential to serve as laboratories where one can test a variety of properties of the almost metal-free gas of the young Universe. One such star forming laboratory can be found in Blue Compact Dwarf Galaxies (De Paz et al. 2003; Papaderos et al. 2008; Lebouteiller et al. 2017). This group of extragalactic small star forming galaxies are of low metallicity ($12 + \log(\mathrm{O/H}) \lesssim 7.6$). They are also blue in the optical, fainter than $M_B \approx -18$, and even more faint in the continuum, with the emitted light coming mainly from the strong emission lines originated in the ionised gas in H II regions, usually tracing the starburst regions (Van Zee et al. 1998; Remy-Ruyer et al. 2013). Despite the strength of these emission lines with respect to the continuum in the spectrum of BCDGs, such objects are said to be low-H luminosity, presenting H_α luminosities lower than $5 \times 10^7 L_\odot$ (Gallego et al. 1997; Shi et al. 2005).

BCDGs present optical linear sizes ~ 1 kpc (Bekki 2008; Meurer et al. 1996). The criteria used in the literature to determine if a certain object is compact or not follows the definition introduced in Zwicky (1970), where compact is said to be any galaxy or any part of the galaxy with surface brightness lower than 20 mag arcsec^{-2}. Initially the concept of compact was followed by a physical size upper limit, introduced by Thuan & Martin (1981) as 1 kpc, but the development of the CCD imaging observations revealed the extended structures correspondent to the LSB component in the BCDGs, meaning that the compactness is more strictly related to this parameter rather than physical size. Several BCDGs are thought to be experiencing their first episode of star formation (Thuan & Izotov 2005; Wu et al. 2006). However, studies in the optical(Loose & Thuan 1986; Papaderos et al. 1996) and in the near-infrared (Noeske et al. 2005) revealed that all BCDGs are likely to present a Low-

⋆ augusto.lassen@ufrgs.br

Surface Brightness (LSB) stellar host, and extended envelope underlying the star forming (SF) regions that shows elliptical isophotes and red colours, indicative of an older stellar population than the ≤ 500 Myr found in the SF regions. The age of this stellar population is ∼ 1 Gyr and is therefore the witness of the former events of SF (Bergvall & Östlin 2002; Cairós et al. 2003; Amorin et al. 2007). In many cases the visual aspect of BCDGs in the optical resemble a compact H II region within a larger irregular galaxy, for example, II Zw 40, I Zw 18 (Sargent & Searle 1970) and II Zw 70 (Oconnell et al. 1978; Thuan & Martin 1981). Adopting $\log(O/H) + 12 = 8.91$ for the solar Oxygen abundance, BCGs usually lie in the low-metallicity range of 1/3 to 1/50 $Z_\odot$ (Kunth & Östlin 2000; Izotov & Thuan 1999).

In this paper we report the serendipitous discovery of an extended nebular region near the massive (estimated stellar mass of the order of 10^{11} $M_\odot$) Early-Type Galaxy (ETG) Mrk 1172 that resembles in many properties the criteria used to classify an object as a BCDG, and, to the best of our knowledge, has no previous report in the literature. In section 2 we introduce the data and the adopted analysis methodologies, in section 3 we briefly describe the techniques used and present the results obtained, in section 4 we promote a discussion based on the results from the previous section, which is summarised in the last section. Throughout this paper, we adopt $H_0 = 69.32$ km s^{-1} Mpc^{-1} (Hinshaw et al. 2013).

2 DATA

In the present work, we present the Mrk 1172 Field of View (FoV) (J020536.18-081443.23) from Program-ID 099.B-0411(A) (PI: Johnston) that can be downloaded from the ESO Science Archive Facility. The data were obtained using UT4-Yepun telescope in the Wide Field Mode (WFM) of the Multi Unit Spectroscopic Explorer (MUSE), which covers the spectral range of 4650 – 9300 Å with a FoV of 1x1 arcmin^2, pixel resolution of 0.2 arcsec per spaxel and seeing of ∼ 1.4 Å(Bacon et al. 2010). Mrk 1172 was observed in 2018, two different nights (August 11th and October 2nd), where the total exposure time reached was 1.6hrs.

2.1 Data Reduction

In each night a standard star was observed for flux and telluric calibrations, sky flats were taken within a week from these observations and an internal lamp flat was taken immediately before or after each set of observations. This flat field image was used to correct for the time and temperature dependent variations in the background flux level of each CCD. Additional bias, flat field and arc images were observed the morning after each set of observations.

The data were reduced using the ESO MUSE pipeline (Weilbacher et al. 2012) in the ESO Recipe Execution Tool (EsoRex) environment (ESO CPL Development Team 2015). First we created a master bias and flat field images with a wavelength solution for each detector, each night separately. The flux calibration solution obtained from the standard star observations in both nights and the sky flats exposures are provided to the science frames, as part of the post-processing steps, which creates the reduced pixel, a table containing individual information corrected by the mentioned effects on each pixel. We combined them to generate a single aligned image and generate the final data cube. It is known that the sky-subtraction method used in this data reduction process recurrently leaves behind significant residuals that may contaminate the spectra of faint sources or in regions in the NIR, populated by strong sky emission lines, thus we applied the Zurich Atmosphere Purge (ZAP) (Soto et al. 2016) in the final data cube, in order to improve the correction of these issues.

2.2 Data specifications

During the inspection of the data cube for Mrk 1172, we have serendipitously found an extended nebular region (we will call this object as BCD-UFRGS-01 throughout this paper) near the ETG with similar redshift ($z = 0.04025 \pm 0.00003$) that was never reported in the literature to the best of our knowledge. Despite its irregular shape, we can estimate the projected extension of BCD-UFRGS-01 using a square box of ∼ 14 × 14 kpc that contains this region. However, it is noticeable from the FoV of MUSE shown in figure 1 that BCD-UFRGS-01 is near the edge, so we inspected images of Mrk 1172 in larger fields of view (***) to confirm that BCD-UFRGS-01 does not extend further than the observed. In figure 1 we show the MUSE FoV for the system in the continuum in H_α,[O III]λ5007 and [S II] λ6716 + [S II] λ6731 wavelength ranges. The spectra presented in this figure is from the spaxels with highest SNR. To produce the images that show the emission in each emission line wavelength range, we averaged the flux within the correspondent range and subtracted the continuum, evaluated as the mean flux within the following windows:

- H_α + [N II]: 6525–6535 Å, 6590–6600 Å
- [O III] λ5007: 4990–5000 Å, 5015–5044 Å
- [S II] : 6650-6700 Å, 6800–6900 Å

3 ANALYSIS

3.1 Stellar population fitting

A spatially resolved stellar population synthesis analysis is essential to reveal information regarding the formation, evolution and current state of the observed systems. With such technique we can obtain the star-formation history (SFH) of both Mrk 1172 and BCD-UFRGS-01, besides the possibility of removing the stellar contribution from the gas, allowing several properties to be estimated, like the extinction, star formation rate (SFR) and other that shall be discussed further, which can be illustrated via 2D maps (Cid Fernandes et al. 2013; Mallmann et al. 2018; Nascimento et al. 2019).

To perform the stellar population synthesis we used MEGACUBE module, which was developed to work as front-end for STARLIGHT code, operating in three main modules (Mallmann et al. 2018; Cid Fernandes et al. 2005). Since STARLIGHT is designed to operate with ASCII-format files, the spectra of each spaxel needs to be extracted from the original *fits* files, applying several pre-processing corrections,

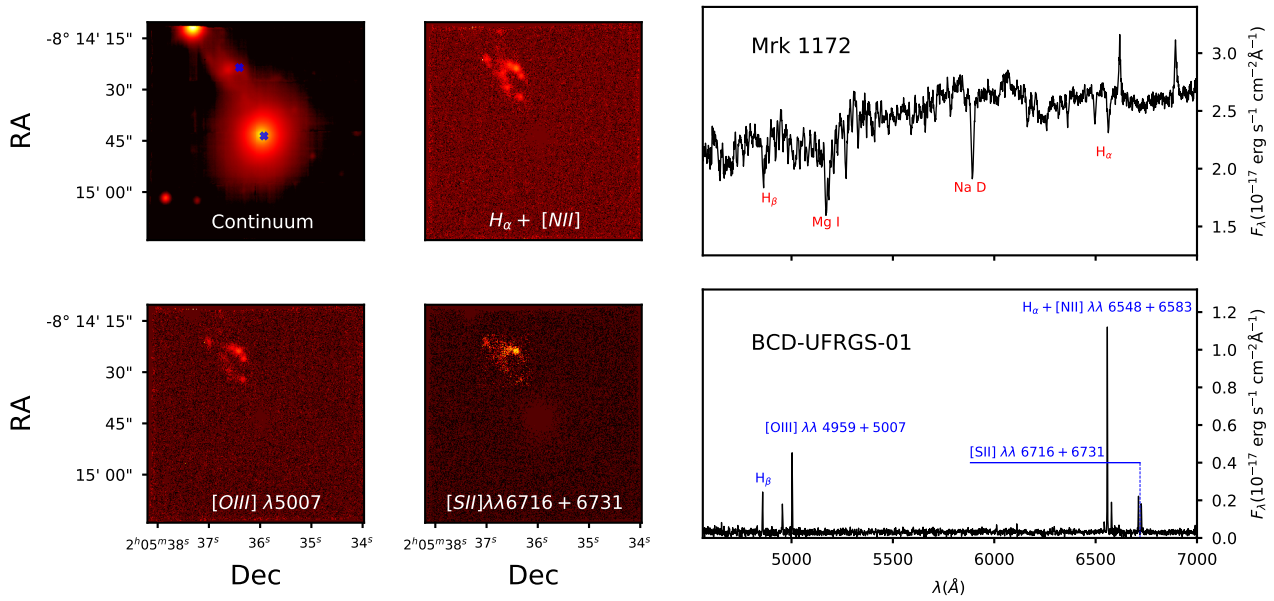

Figure 1. The MUSE FoV continuum centered in Mrk 1172 (top left), H$_\alpha$+[N II]$\lambda\lambda$6550+6585 (top central), [O III]λ5007 (bottom left) and [S II]$\lambda\lambda$6716+6731 (bottom central) wavelength ranges. The wavelength windows used to subtract the continuum from the flux of each emission lines are presented in section 2. The spectrum of Mrk 1172 highest-SNR spaxel is presented in top right panel, while in bottom right panel we present the spectrum for the highest-SNR spaxel for BCD-UFRGS-01. The location of these spaxels within the FoV is indicated in blue in the top left panel.

i.e., rest-frame spectrum shifting and galactic extinction correction. We used the dust maps from Schlegel et al. (1998) and the CCM reddening extinction law (using R_v = 3.1, Cardelli et al. 1989; O'Donnell 1994). Many spaxels, specially from the region corresponding to BCD-UFRGS-01 location, tend to present noisy spectra. In order to increase the SNR of the individual spaxels, we have binned the original data cube two by two along the spatial direction.

Since the spatial coverage of MUSE is high, many spaxels within the FoV are from empty regions in the sky, or even from objects we do not desire to analyse or want to analyse separately, therefore the creation of a 2D boolean mask that flags valid and invalid spaxels is very useful. However, to create the mask we must adopt a reliable criteria to separate valid spaxels from the invalid ones. In this work we adopted the following criteria:

- The flux vector of the individual spaxel must present 5 % or lower of non-positive numbers within the array in order to avoid the noisy spaxels, specially from the edge. The non-positive values in the valid spaxels are replaced by applying an interpolation with neighbouring valid values.
- The maximum of the flux must be at least 1.5 times higher than the maximum of the standard deviation for that flux vector. In this way only spaxels with high SNR and/or strong emission lines are set as valid.

The values used to create the criteria were obtained after several tests, by comparing the final 2D mask with the image of continuum plus H$_\alpha$ emission, as shown in figure 2. Finally, we must perform two more interpolations in the unmasked spectra, in order to match the spectral resolution with the SSPs in the base that are used in the synthesis and to have the recommended $\Delta\lambda$ = 1 Å. For the spaxel meeting the above criteria and with the corrections applied we performed the stellar population synthesis. As base set we used the Granada-Miles simple stellar population (SSPs) computed with the PADOVA200 isochrones and Salpeter initial mass function (Vazdekis et al. 2010; Cid Fernandes et al. 2014). We adopted 21 ages (1 Myr, 5.6 Myr, 10 Myr, 14 Myr, 20 Myr, 31 Myr, 56 Myr, 100 Myr, 200 Myr, 316 Myr, 398 Myr, 501 Myr, 638 Myr, 708 Myr, 794 Myr, 891 Myr, 1 Gyr, 2 Gyr, 5 Gyr, 8.91 Gyr and 12.6 Gyr) and 4 metallicities (0.19 $Z_\odot$, 0.39 $Z_\odot$, 1.0 $Z_\odot$, 1.7 $Z_\odot$). The fit was performed in the 4800-6900 Å spectral range with normalization point at λ_0 = 5600 Å.

With the stellar population synthesis done, we inspect the result for individual spaxels in Mrk 1172 and BCD-UFRGS-01. The location of the highest SNR spaxels are marked in blue in figure 1 and in red in figure 2. In figure 3 we can see the results for Mrk 1172 in the top panel and for BCD-UFRGS-01 in the lower panel. We present the observed spectra in black with the best-fit synthetic spectrum in red, and below we show the residual spectra and the regions masked by the sigma clipping method from STARLIGHT for both cases. In the right panel we show the histograms of the contribution weighted by luminosity of each stellar population with its respective ages. Mrk 1172 has dominant old stellar populations, despite the presence of a young stellar population with $\sim 10^7$ yr, while BCD-UFRGS-01 is predominantly young, presenting two dominant stellar populations with ages between 10^8 and 10^9 yr, most likely to be associated with the LSB component that is typically observed in the case of BCDGs.

We now assess the mean age weighted by luminosity (<

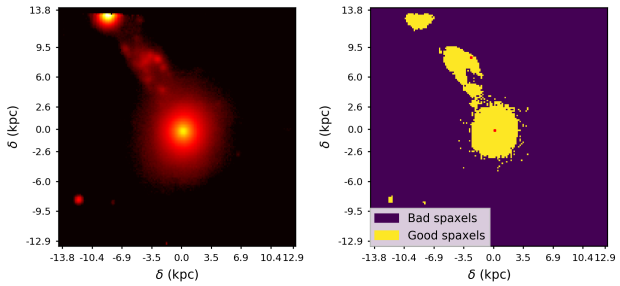

Figure 2. Comparison between Mrk 1172 FoV in continuum plus H_α emission (right panel) with a binary map (left panel), where the yellow regions represent the spaxels used in the synthesis, while the purple spaxels are discarded. The yellow regions in upper and lower left are field galaxies/stars that shall be masked manually. The scale measures the offset, in kpc, from the reference spaxel. In red, the highest-SNR spaxels for Mrk 1172 and BCD-UFRGS-01.

t_L >) for each spaxel and build a map with the age gradient for the dominant stellar populations using the equation:

$$< t_L >= \sum_j a_j \log t_j \quad (1)$$

where t_j is the age of the j-th element on the basis, and a_j is a renormalization factor that takes into account the fact that the total contribution of the SSPs used to reproduce the spectrum is not necessarily 100 % (Cid Fernandes et al. 2005). The resulting map can be seen in figure 4, where we can see that BCD-UFRGS-01 is dominated by young and intermediate stellar populations, while Mrk 1172 is dominated by old stellar populations. This figure shows the spatial distribution of the information given by the histogram in figure 3. Figure 4 shows that BCD-UFRGS-01 dominant stellar population is considerably younger than the dominant stellar population of Mrk 1172.

3.2 Emission Line Fluxes

Having the underlying fitted spectrum of each spaxel, we subtract it from our observed data, resulting in a pure emission line spectrum. However no sings of emission lines were detected in locations corresponding to Mrk 1172. For BCD-UFRGS-01, on the other hand, strong emission lines are clearly detected. We measure the fluxes using the IFSCUBE[1] tool, by fitting gaussian profiles to the emission emission lines for the spectra of each spaxel in the specified regions. We fitted each emission line using a single gaussian profile, where the constraints used are detailed below.

3.2.1 Single gaussian fitting

We did not used a polynomial function to fit the continuum of the spectra of BCD-UFRGS-01. It can be seen in figure 3 that the synthetic spectrum given by the result of the stellar population synthesis is more representative for the continuum than a low-order polynomial would in accuracy and in physical meaning. As input for the flux, we have provided the same spectrum we provided for the stellar population synthesis step, i.e., a rest-frame spectrum, resampled in $\Delta\lambda = 1$ Å and corrected for galactic reddening. We also provide the 2D mask, and the extension of the data cube containing the variance of each spaxel. As first constraint, we assume the presence of three different kinematic groups, i.e., two emission lines belonging to the same kinematic group shall have the same values on velocity and on the σ parameter of the modeled gaussian. From the stronger emission lines found in the spectrum of BCD-UFRGS-01 we use four different kinematic groups containing the lines respective to transitions in the atoms of H,O,N and S. We used specific constraints, such as the known doublet ratio [N II] λ6583 = 3.06 × [N II] λ6548 and established the lower and upper limit for the Sulfur doublet ratio, related to the asymptotic limits of the intensity ratio *vs.* electron density curve (Osterbrock & Ferland 2006).

An example of the outcomes of this fitting procedure is shown in figure 5, where we present the spectral regions containing the fitted emission lines. The observed spectrum is shown as a solid black line, the stellar continuum obtained via stellar population synthesis is shown in the solid blue lines and the best-fit model is shown by the dashed yellow line.

Besides fluxes, IFSCUBE also provides us the gas kinematic parameters (gas velocity and velocity dispersion). In the next sections we analyze these quantities.

3.2.2 Gas excitation

Emission line ratios allow us to determine the nature of the ionization source of the H II region within BCD-UFRGS-01, where we use the traditional diagnostic diagram in its spatially resolved version (for a similar analysis see Nascimento et al. (2019)), as shown in figure 6 (Baldwin et al. 1981).

In figure 6 we can visualise the spatially resolved diagnostic diagrams for BCD-UFRGS-01. In the right top panel in figure 6 the solid blue line separating H II from the transition region, as well as the solid red line separating Seyfert and LINER regions were obtained from Kauffmann et al. (2003), and the solid green line separating transition region from the hard-source photoionized region was obtained from Kewley et al. (2001). The dots are the position of a single spaxel in the diagnostic diagram. In this second diagram, the solid magenta line is from Kewley et al. (2001), while the solid red line is from Kauffmann et al. (2003). Both diagrams indicate that the gas seems to be ionised by young massive stars rather than by an AGN. Ionisation by shocks are investigated using the fast radiative shock models from Allen et al. (2008), adopting solar metallicity, $n_e = 1.0$ cm^{-3} and varying the values of magnetic field. In any of these cases the curve of emission line ratio vs. shock velocity was able to approach the low observed value of [N II]/$H_\beta \sim 0.56$, indicating that shock ionisation is unlikely in BCD-UFRGS-01.

[1] `https://ifscube.readthedocs.io/en/latest/intro.html`

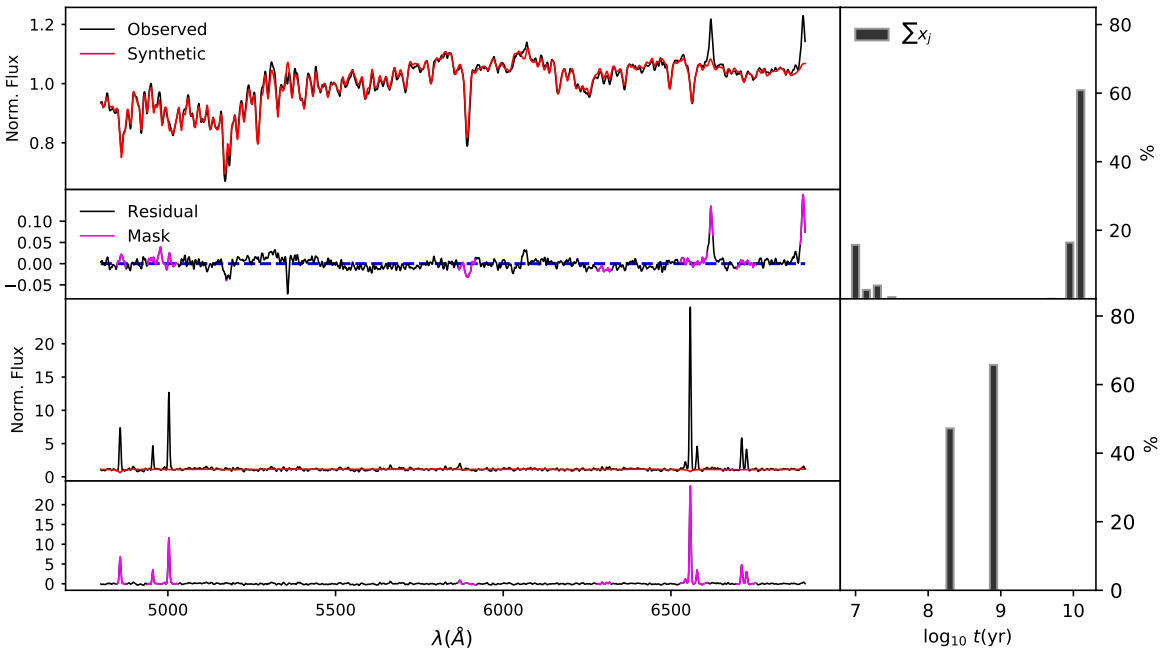

Figure 3. Synthesis results for the highest-SNR spaxel for Mrk 1172 and BCD-UFRGS-01. *Top left panel*: In black, the observed spectrum of Mrk 1172, where the flux is normalized using $F(\lambda_0)$. In red, the synthetic spectrum build from the best-fit stellar population synthesis. *Top middle panel:* Residual spectrum for Mrk 1172 in black, with the regions masked by sigma clipping method in magenta. At the bottom middle and bottom left panels, the same for BCD-UFRGS-01. *Top right panel*: Histogram presenting the luminosity-weighted percentual contribution of each stellar population for Mrk 1172 best fit and their ages, in logarithmic units. *Bottom right panel:* Same than top right panel, but for BCD-UFRGS-01.

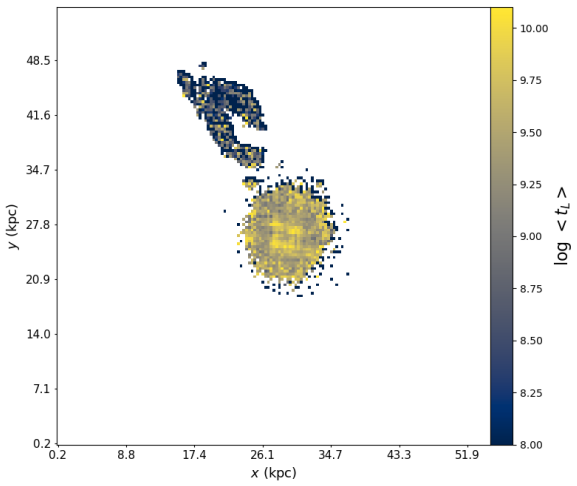

Figure 4. Map of the mean age weighted by luminosity in Gyr for Mrk 1172 and BCD-UFRGS-01 obtained via spatially resolved stellar population synthesis.

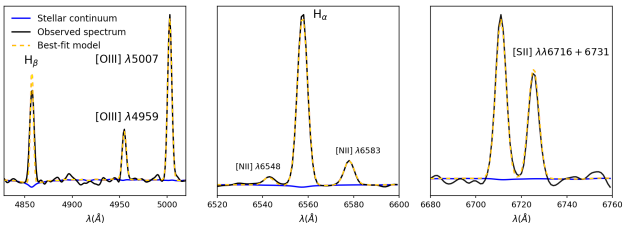

Figure 5. Emission lines in BCD-UFRGS-01 spectrum fitted using gaussian profiles with IFSCUBE. In black, the observed spectrum, in blue the continuum, and the dashed yellow line represents the model fit.

3.3 Extinction

We already corrected the observed spectra for galactic dust reddening using the Schlegel dust maps (Schlegel et al. 1998), but the effect still occurs in extragalactic scales, and applying this correction is crucial to obtain many of important properties concerning the gas component in BCD-UFRGS-01. Considering I_λ as the observed intensity for a given wavelength and I_{λ_0} as the intrinsic intensity, we have:

$$I_\lambda = I_{\lambda_0} \times 10^{-cf(\lambda)} \tag{2}$$

where c is an undetermined constant and $f(\lambda)$ is the extinction curve. The number of magnitudes of extinction A_λ is related to the lines intensity ratio by:

$$A_\lambda = -2.5 \log\left(\frac{I_\lambda}{I_{\lambda_0}}\right) \tag{3}$$

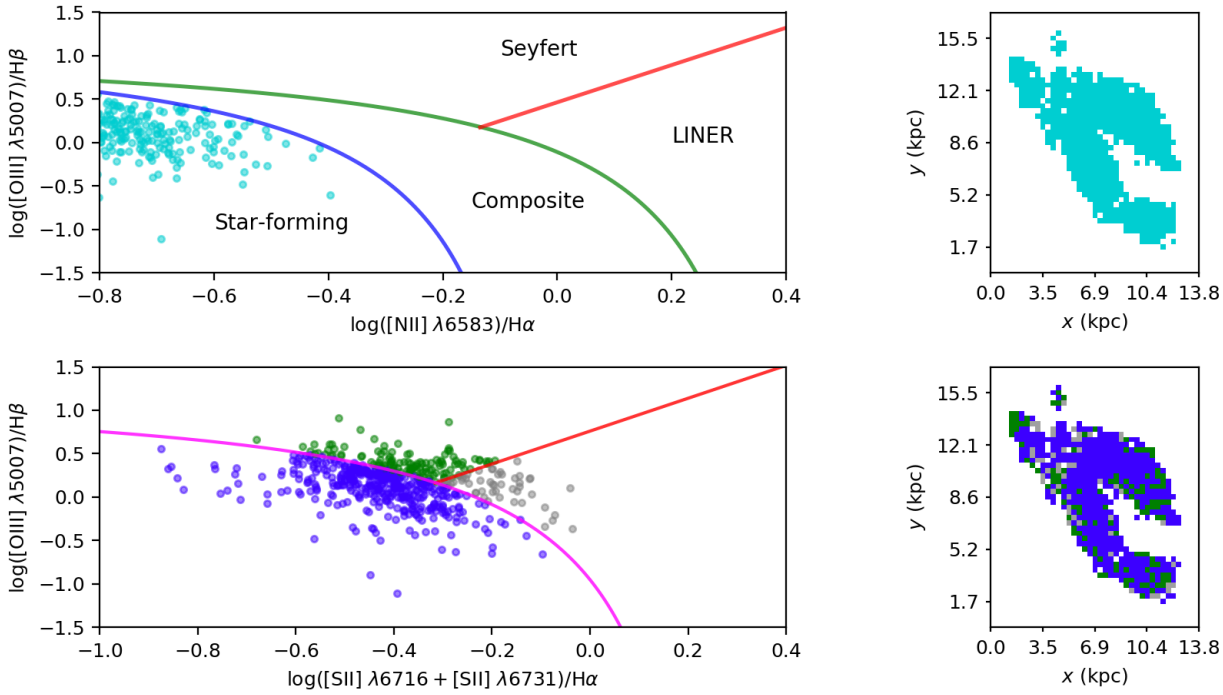

Figure 6. Spatially resolved diagnostic diagram for BCD-UFRGS-01. *Left top/bottom panel:* The circles represent the position of each single spaxel in the diagnostic diagram, where the solid lines represent the curves that define the excitation regions. *Right top/bottom panel*: BCD-UFRGS-01 with each spaxel colored corresponding to its position in the diagnostic diagram.

Since A_λ is related to A_V (reddening in V band) via reddening law, we assumed the case B of recombination, with an intrinsic intensity ratio of $H_\alpha/H_\beta = 2.87$, electronic temperature of 10000 K and and $R_V = 3.1$ (Osterbrock & Ferland 2006):

$$A_V = 7.23 \times \log\left[\frac{F(\mathrm{H}_\alpha)}{F(\mathrm{H}_\beta)}\right] - 3.31$$

where $F(\mathrm{H}_\alpha)$ and $F(\mathrm{H}_\beta)$ are the observed fluxes. The extinction map produced is shown in figure 7.

3.4 Star formation rate

From the diagnostic diagram one can see that BCD-UFRGS-01 is forming stars, so it is interesting to estimate its Star Formation Rate (SFR). We can calculate it using the recombination lines, like the Balmer recombination lines found in the spectra of BCD-UFRGS-01. Assuming case B of recombination, a Salpeter Initial Mass Function (IMF), we can use the expression below to estimate the instantaneous SFR of BCD-UFRGS-01 (Kennicutt Jr 1998):

$$\mathrm{SFR}(M_\odot\ \mathrm{yr}^{-1}) = 7.9 \times 10^{-42} L(H_\alpha)\ (\mathrm{erg\ s}^{-1}) \quad (4)$$

The luminosity $L(H_\alpha)$ can be obtained directly from the flux of H_α emission line, where we subtract the synthetic stellar population flux, by using:

$$L(H_\alpha) = 4\pi F(H_\alpha)\ d^2 \quad (5)$$

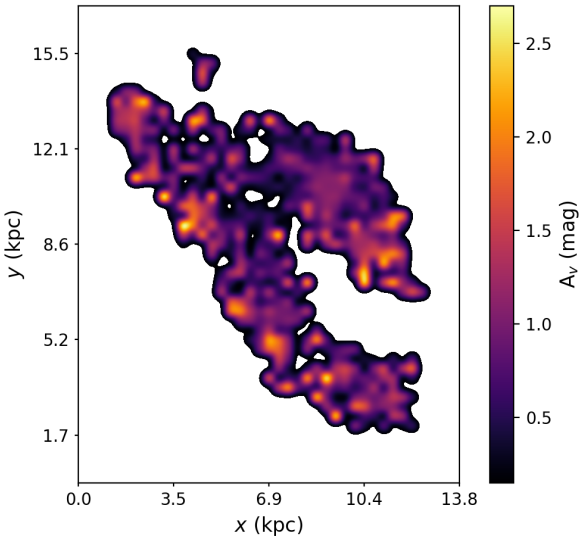

Figure 7. The BCD-UFRGS-01 extinction map. Lighter regions represent higher light extinction, while darker regions represent lower extinction. In white, the masked points, excluded form the plot. The colour bar shows the range of extinction values measured in the region in magnitude units.

where d is the distance of the galaxy, which can be obtained in literature or by taking $d = z(c/H_0)$. We calculated the distance of BCD-UFRGS-01 using the measured

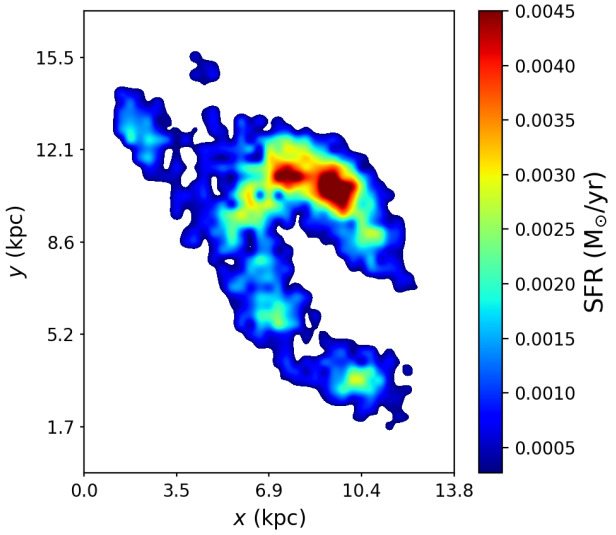

Figure 8. The BCD-UFRGS-01 SFR distribution map. Regions with high SFR appear in red, while regions without significant star formation appear in blue. The colour bar indicates the values of SFR associated to each colour in units of $M_\odot$/yr.

$z = 0.04025 \pm 0.00003$ and have obtained a $L(H_\alpha)$ value to be used in equation 4 for each spaxel, resulting in a SFR map that illustrates the SFR distribution, shown in figure 8. The blue regions in the map represent less significant star formation, while the yellow and red regions are forming stars more intensely, according to the colour bar. Integrating the SFR over all spaxels results in a total SFR of 0.71 $M_\odot$ yr^{-1} and a ΣSFR of 1.4 $\times 10^{-2}$ $M_\odot$ yr^{-1} kpc^{-2}, which was obtained by dividing the SFR by the area of each spaxel.

We can use the information acquired with the stellar population synthesis to estimate the current stellar mass $M_\star$[2]:

$$M_\star(M_\odot) = 4\pi d^2 \times \mathrm{Mcor_{tot}} \times 10^{-20} \times (3.826 \times 10^{33})^{-1} \quad (6)$$

where $\mathrm{Mcor_{tot}}$ is a STARLIGHT output parameter related to the current mass of stars in units of Å s^3 cm^{-2} g^{-1}. We can apply equation 6 to each spaxel of our datacube to obtain the total stellar mass for both Mrk 1172 and BCD-UFRGS-01. We obtain $M_\star \sim 1.76 \times 10^{11} M_\odot$ for Mrk 1172 and $M_\star \sim 4.06 \times 10^9 M_\odot$ for BCD-UFRGS-01. Similarly, we can estimate how many solar masses have been processed into stars through the lifetime of the system by using[2]:

$$M_\star^{\mathrm{ini}}\ (M_\odot) = 4\pi d^2 \times \mathrm{Mini_{tot}} \times 10^{-20} \times (3.826 \times 10^{33})^{-1} \quad (7)$$

where $\mathrm{Mini_{tot}}$ is another STARLIGHT output parameter that gives the mass that was once in stars, differing from $\mathrm{Mcor_{tot}}$ because the stars can lose mass to the ISM because of Sne, winds and other phenomena[2]. Applying equation 7 to all valid spaxels, we obtain $M_\star^{\mathrm{ini}} \sim 1.26 \times 10^{11} M_\odot$ for Mrk 1172 and $M_\star^{\mathrm{ini}} \sim 3.00 \times 10^9 M_\odot$ for BCD-UFRGS-01.

[2] `https://www.minerva.ufsc.brstarlight/files/papers/Manual_StCv04.pdf`

3.5 Ionized gas mass

Following the steps detailed in Nascimento et al. (2019) and Osterbrock & Ferland (2006), we can calculate the mass of the ionised gas by using the expression:

$$\mathrm{M} = n_e m_p V f \quad (8)$$

where n_e is the electron density of the gas, m_p is the mass of the proton, V is the volume of the ionised region and f is the filling factor, which tries to correct the fact that the ionised region does not entirely occupy the volume V. Using the emissivity of the H_β emission line (j_{H_β}), we can calculate the total luminosity of this line:

$$\mathrm{L}(H_\beta) = \int\int j_{H_\beta} \mathrm{d}\Omega \mathrm{dV} \quad (9)$$

We know (Osterbrock & Ferland 2006) that for recombination case B (assuming low-density limit), assuming T = 10^4 K we have:

$$\frac{4\pi j_{H_\beta}}{n_e n_p} = 1.24 \times 10^{-25}\ \frac{\mathrm{erg\ cm^3}}{\mathrm{s}}$$

where n_e and n_p are the electronic density and the density of protons, respectively. Using this result into the integral in equation 9 we obtain L(H_β) in units of erg s^{-1}:

$$\mathrm{L}(H_\beta) = 1.23 \times 10^{-25}\ n_e n_p V f$$

Assuming the gas to be completely ionised ($n_e = n_p = n$) we can isolate Vf from the expression above and use it in equation 8. Considering $n_e = 1.0$ cm^{-3}, which is the lower-limit density measurable using [S II] doublet, we obtain the mass of the ionised gas:

$$M(M_\odot) = 6.837 \times 10^{-34} L(H_\beta) \quad (10)$$

where $L(H_\beta)$ is the luminosity of H_β emission line, in units of ergs.s^{-1}. Since we used $n_e = 1.0$ cm^{-3}, the mass resulting from equation 10 should be interpreted as a lower-limit mass. We apply equation 10 to BCD-UFRGS-01, where H_β emission line is strong for the majority of the spaxels in the region, by using the reddening corrected $F(H_\beta)$ to calculate $L(H_\beta)$ for each spaxel in BCD-UFRGS-01. Integrating over the whole region correspondent to BCD-UFRGS-01, we have obtained $M = 3.5 \times 10^6 M_\odot$ for the ionised gas mass.

3.6 Abundances

We aim to characterise BCD-UFRGS-01 with respect to its gas abundance, for the elements that are present in the spectra wavelength range, namely H,N,O and S using the measured emission lines. For an emission line excited collisionally, as the case of N,O and S, we can calculate its intensity using:

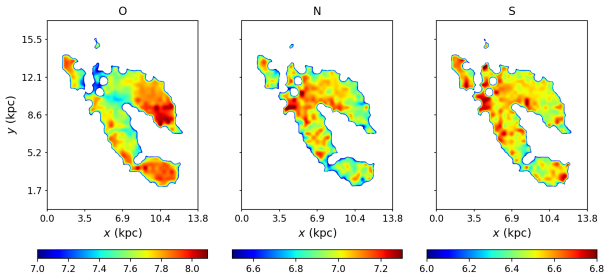

Figure 9. Abundance maps for the collisionally excited ions identified in BCD-UFRGS-01 spectra, namely O,N and S, respectively. Abundances are given in $\log_{10}N(X^i)$ with $H = 12$.

$$I_{\lambda_{l,m}} = \frac{1}{4\pi}\int N(X^i) n_e h(\nu_m - \nu_l)\ q_{l,m}(T_e)\ b dS \tag{11}$$

where $N(X^i)$ is the abundance of element X, and i is the element's degree of ionisation. The term $h(\nu_m - \nu_l)$ is the energy difference between atomic levels m and l, $q_{l,m}(T_e)$ is the collisional excitation rate, which depends on the electronic temperature of the gas T_e, and b is a factor that measures the deviation of the system from the thermodynamical equilibrium ($b = 1$ for an equilibrium state). The differential element dS is related to the path travelled by light in the observer line-of-sight. Considering n_e and $N(X^i)$ constant along the observer line-of-sight, we integrate the argument in equation 11 to obtain a new expression, dependent on S. To eliminate this dependency we can divide $I_{\lambda_{l,m}}$ by I_{H_β} and express the relative abundance in function of both intensities:

$$\frac{N(X^i)}{N(H)} = \frac{I_{l,m}}{I_{H_\beta}}\ \frac{h(\nu_m - \nu_l)\ q_{l,m}(T_e) b}{j_{H_\beta}} \tag{12}$$

To estimate the ionic abundances using equation 12 we use PYNEB python package[3], where we need to normalize the measured emission line fluxes to have $F(H_\beta) = 100$. The results are shown in figure 9, where the abundance values for O,N and S are represented in $\log_{10}N(X^i) + 12$ units (Claas 1951; Peimbert et al. 1992). In the case of BCD-UFRGS-01, we have the mean Oxygen, Nitrogen and Sulfur abundances: $N(O^{++}) = 7.71$, $N(N^+) = 6.91$ and $N(S^+) = 6.56$.

3.7 Kinematics

There are many intriguing aspects of BCD-UFRGS-01, i.e., its irregular shape, its proximity to Mrk 1172 and its physical properties that may indicate this gas may be falling towards Mrk 1172. Thus it is important to explore the kinematics of this gas to reveal some extra information about the motion of BCD-UFRGS-01. We can obtain the radial velocity v of the gas for the identified emission lines in BCD-UFRGS-01 spectra directly from IFSCUBE single gaussian fit, as well as the σ parameter, to be interpreted as the turbulence of the gas. In the fit process, we fit the doublets in the same kinematic group, meaning that the resulting velocity values will be the same for the same ion. In figure 10 we show both radial velocity and sigma maps for H_α, [O III]λ5007, [N II]λ6548 and [S II]λ6731 emission lines.

First we observe, specially in the maps of radial velocity, that the gradient seen is more smooth in the case of H_α emission line maps. This is due to the fact that in spaxels near the edge of BCD-UFRGS-01 the SNR is low and the measurement of emission lines other than H_α has high uncertainty at these points. Even so, all velocity maps exhibit the same kinematical trend for the motion of the gas, where it seems to be rotating in counterclockwise direction around an axis that crosses the image diagonally. A better visualisation of this axis can be seen in figures 12 and 11, represented by the $v = 0$ solid line. The turbulence of the gas, in its turn, presents no clear trend, and is uniformly distributed along BCD-UFRGS-01 structure.

4 DISCUSSION

From the stellar population analysis it is clear that Mrk 1172 and BCD-UFRGS-01 do not share similar SFHs, since the ETG is dominated by and old stellar population with no signs of ionised gas. Mrk 1172 has less than 20 % of its light contribution originated from stars formed in the past $10^8 \sim 10^9$ years, meanwhile BCD-UFRGS-01 presents a rich emission line spectrum with its stellar emission dominated by very young stellar populations ($t < 10^9$, see figures 4 and 3). It is worthwhile to mention that although figure 3 brings information about individual spaxels, it is representative for all the spaxels of each system, and arguments based on this figure can be extended then to the entire systems.

We also wish to understand the mechanism responsible for the gas excitation, evidenced by the strong emission lines observed in BCD-UFRGS-01 spectrum. Since Mrk 1172 has an inactive Black Hole (BH) in its central regions, BCD-UFRGS-01 could be ionised by the hard radiation originated from the BH, i.e., it could be an AGN echo like the prototypical *Hanny's voorwerp* near IC 2497 (Lintott et al. 2009; Rampadarath et al. 2010; Keel et al. 2012). However, from the BPT diagnostic diagrams shown in figure 6 it is clear that the gas within BCD-UFRGS-01 is excited by young hot stars rather than by a hard radiation field. Despite this, the presence of such energetic field is observed in several BCDGs, where the nature of its source remains unexplained, although several mechanisms have been proposed, i.e., massive main-sequence stars (Schaerer & de Koter 1997), Wolf-Rayet stars (Schaerer & Vacca 1998; Schaerer & Stasinska 1999), primordial zero-metallicity stars (Schaerer 2003), high-mass X-ray binaries (Garnett et al. 1991) and fast radiative shocks (Dopita & Sutherland 1996). Unfortunately, due to the limitation in our spectral range we are not able to visualise emission lines such as He λ4686 and [Ne IV] that could indicate the presence of a powerful ionisation source. Even without the spectral limitation we probably would not be able to detect those lines, since they generally are too faint, about 5% of H_β flux in the case of He λ4686 and 2% in the case of [Ne V] $\lambda\lambda 3346 + 3426$ (Thuan & Martin 1981), and BCD-UFRGS-01 is considerably faint. Consulting shock models from Allen et al. (2008) we concluded that fast ra-

[3] `http://research.iac.es/proyecto/PyNeb//`

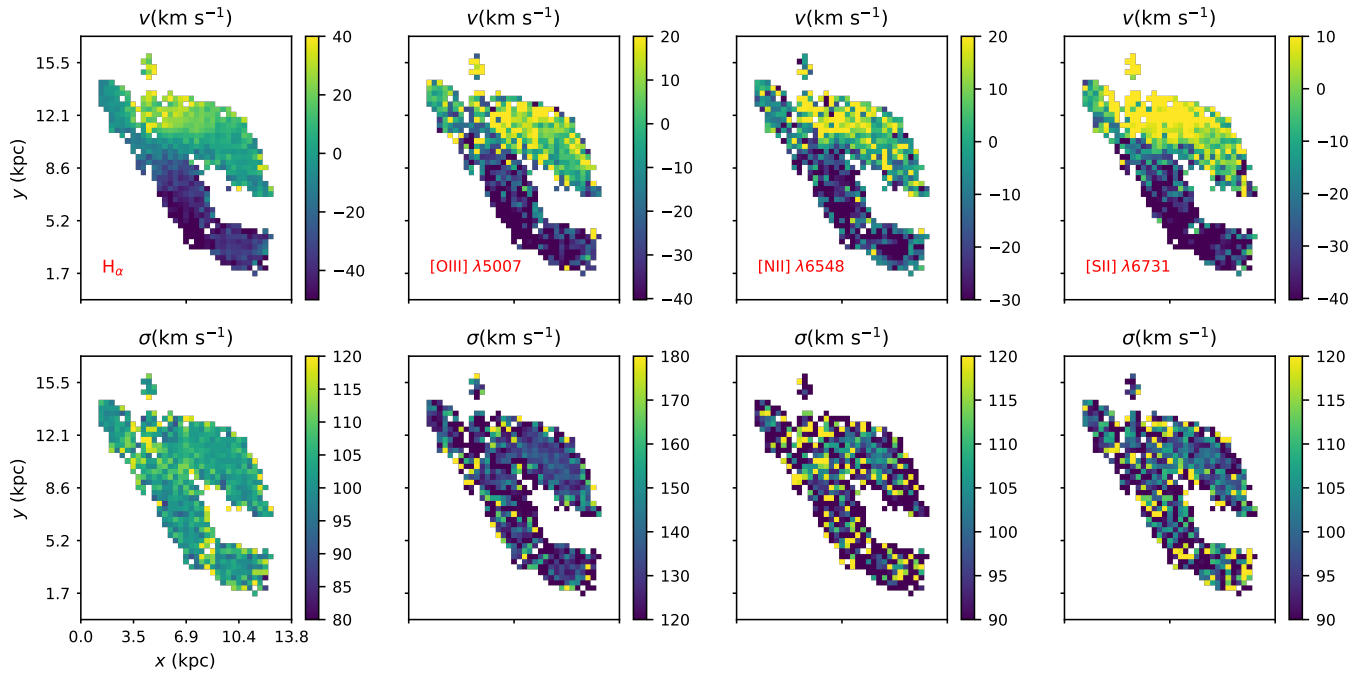

Figure 10. Kinematic maps for H_α, [O III]λ 5007, [N II]λ 6548 and [S II]λ 6731 emission lines. In the upper panel, radial velocity maps, and in the lower panel, the turbulence of the gas. Both parameters are obtained from a single gaussian used to fit the observed emission lines using IFSCUBE.

diative shocks are not the main mechanism involved in the ionisation of the gas.

It is clear then that BCD-UFRGS-01 is actively forming stars, although the efficiency of the process is unknown. The young stars that are ionizing the gas seem to be located in few clumpy knots along the structure of BCD-UFRGS-01, better traced by the SFR maps in figure 8. This structure also becomes visible when looking at the H_α collapsed image in figure 1 and in the continuum H_α emission in figure 2, and are typical structures formed in regions with active star formation. Since the mean A_V is moderately low (~ 0.9, as seen in the previous section), BCD-UFRGS-01 seems to be composed more of gas and stars than dust, though its presence shall not be neglected. By using the synthesis result we calculated the SFR using equation 4, obtaining a SFR of 0.71 $M_\odot$ yr^{-1}, which is close to the total SFR of 0.44 $M_\odot$ yr^{-1} found for H II regions in M31 (Azimlu et al. 2011). We also obtained the spatial distribution of SFR for BCD-UFRGS-01 ($\sum$SFR), resulting in 1.4×10^{-2} $M_\odot yr^{-1} kpc^{-2}$. In table 4 we present a comparison between the measured SFR of BCD-UFRGS-01 with BCDGs from the literature (Van Zee et al. 1998). But why do we compare this galaxy with known BCDGs rather than other class of objects?

As shown previously, we also calculated the mass of the ionised gas in BCD-UFRGS-01 using H_β emission line, resulting in a mass of $3.5 \times 10^6 M_\odot$, and a stellar mass of $4.06 \times 10^9 M_\odot$. In the case of Mrk 1172 we could not estimate the mass of ionised gas because of the lack of prominent emission lines, but we estimate a stellar mass of $1.76 \times 10^{11} M_\odot$, a typical value for massive ETGs and in agreement with other measures found in the literature (i.e, $8.91 \times 10^{10} M_\odot$, see Omand et al. (2014)). Meanwhile BCD-UFRGS-01 stellar mass is comparable with the SMC stellar mass of $6.5 \times 10^9 M_\odot$ (Bekki & Stanimirović 2009), and is order of magnitudes higher than the $\sim 10^5 M_\odot$ found for large emission nebula and H II regions, as N44 and the the Tarantula Nebula, for example (Tsuge et al. 2019; Bosch et al. 2009), indicating that the observed structure should not be taken as a simple H II region, but as a dwarf galaxy in interaction with Mrk 1172. However, the main reason for comparing BCD-UFRGS-01 with BCDGs rather than any other class of objects comes from the abundance measurements.

To estimate the fraction of heavy elements in the H II regions within BCD-UFRGS-01 we used the Oxygen abundance. Using this, we have found a mean Oxygen abundance of 7.71 for the spaxels shown in figure 9, where all spaxels within the region lie in the range $6.43 < \log(O/H) + 12 < 8.29$. Few of these spaxels may not have trustworthy values of Oxygen abundance, since edge spaxels present noisy H_β emission lines, hard to model correctly. However it is noticeable that the values of Oxygen abundance for all spaxels lie in the same metallicity range than the metal-poor BCDGs (adopting $\log(O/H) + 12 = 8.91$ for the sun), which lie among the most metal-poor galaxies in the Universe. In table 4 we compare this value with the Oxygen abundance measured for BCDGs in the literature. As we can see, BCD-UFRGS-01 is considerably metal deficient, presenting similar results with other BCGDs. Another characteristic of BCDGs is their magnitude in the B band. As cited previously, we lack the spectral range to measure the magnitude in B band using the spectrum of BCD-UFRGS-01. However we can use the

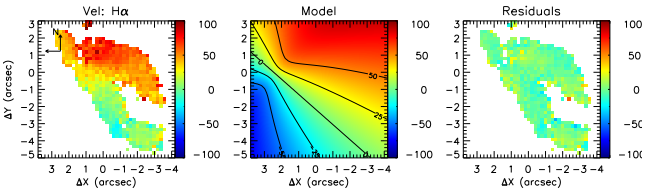

Figure 11. Dynamical model used, assuming circular orbits in the plane of a disk without constraints. The right panel the velocity map, in agreement with the kinematical map shown previously, is an indicative of the success of the chosen dynamical model. In the middle panel, the model indicating a counterclockwise rotation, with the dynamical axis and the rotation levels of the gas along the structure. In left panel, the residual map, uniformly distributed around zero.

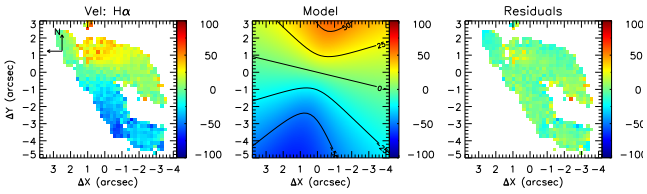

Figure 12. Same as figure 11, but now using the spaxel with higher stellar mass measured as the dynamical center of mass of the observed structure. Again, the fit is performed successfully.

available photometry data from SDSS in *ugriz* band system and convert it to B by using:

$$B - g = (0.349 \pm 0.009)\ (g - r) + (0.245 \pm 0.006) \quad (13)$$

The conversion equation above was obtained in Jordi et al. (2006) from comparing Stetson fields around Draco, NGC 2419 and NGC 7078 with their SDSS DR4 photometry and is best suited for metal-poor Population II stars, which is the case for the observed dwarf galaxy. There is another version of equation 13 which uses g and u rather than g and r, and applying the other version leads to the same result for B, but with much higher uncertainty, since u measurement magnitude has a considerably larger uncertainty than in the case of r band. Applying equation 13 we obtain $B = 21.00 \pm 0.37$, resulting in a absolute magnitude of $M_B \sim -15$ mag, which means the observed dwarf galaxy is very faint even in the blue and satisfies the criteria of $M_B > -18$, adopted as one of the main criteria to define BCDGs. We also know such objects should present $L(H_\alpha)$ luminosity lower than 5 $\times 10^7$ $L_\odot$. Measuring $L(H_\alpha)$ by using equation 5 we obtain $L(H_\alpha) \sim 2 \times 10^7$ $L_\odot$ for the integrated flux of the minor galaxy, below the lower limit introduced by Gallego et al. (1997). In table 4 we compare the measured M_B with other BCDGs (Van Zee et al. 1998).

A dynamical model can be used to investigate deeper the behaviour of the gas. We have used a model based on Bertola et al. (1991), assuming circular orbits in the plane of a disk. We tested two cases, one with all the parameters of the fit free of constraints and in the other case we used the spaxel which is the peak of the stellar mass distribution in BCD-UFRGS-01 as the position of the kinematic center. The first case is shown in figure 11 and the latter is presented in figure 12. Although simplistic, the behaviour seen in the upper panel of figure 10 is also reproduced by the dynamical model, in the left of both figures 11 and 12, despite the slight difference in the velocity values. We can also notice that in the residual map in the right uniformly distributed values around zero are observed, indicating that the fit predicts accurately the dynamical behaviour of the gas. The success of this fit may indicate that the observed region may actually be a low-metallicity disk galaxy that could be disrupted due to tidal forces.

5 SUMMARY AND CONCLUSIONS

We present here an extensive analysis of the physical and chemical properties of a new nebular emission line region, namely, BCD-UFRGS-01. It is located near the quiescent ETG Mrk 1172 in projection and was never reported in the literature, to the best of our knowledge. We measured the redshift of BCD-UFRGS-01 from its spectra and compared with the redshift of Mrk 1172. For BCD-UFRGS-01 we have obtained $z = 0.04025 \pm 0.00003$, or $d = 174 \pm 2$ Mpc while Mrk 1172 has a redshift of $z = 0.04115$, implying a distance of $d \sim 178$ Mpc (Chang et al. 2015). Below, we summarize the main conclusions of this work:

(i) Despite its low SNR in the continuum, the spectrum of BCD-UFRGS-01 presents strong emission lines, namely: H_α, H_β, [O III] $\lambda\lambda$4959+5007, [N II] $\lambda\lambda$6548+6583 and [S II] $\lambda\lambda$6716+6731. The stellar population synthesis reveals that Mrk 1172 is predominantly dominated by old stellar populations with $t \geq 10^{10}$ yrs, while BCD-UFRGS-01 shows the presence of a young stellar population with ages in the range of 10^7-10^8 yrs. An underlying stellar population with $t \sim 10^9$ yrs is also present, which we suggest that it might be related to the LSB component usually found for BCDGs.

(ii) From the stellar content of BCD-UFRGS-01 and Mrk 1172 we are able to estimate the stellar mass of both galaxies. We obtain $M_\star \sim 1.76 \times 10^{11} M_\odot$ for Mrk 1172, a value that lies close to a previous measurement found in the literature. This is relatively high value of mass, and considering that Mrk 1172 is classified as isolated (Argudo-Fernández et al. 2015), it is possible that many mergers events happened throughout the evolutionary history of this ETG. BCD-UFRGS-01 presents a stellar mass of $M_\star \sim 4.06 \times 10^9 M_\odot$, which is comparable to the mass of the SMC, ($M_\star = 6.5 \times 10^9 M_\odot$ Bekki & Stanimirović 2009) and to the BCDG Henize 2-10 ($M_\star = 3.7 \times 10^9 M_\odot$ Reines et al. 2011), for example.

(iii) In order to investigate the gas excitation mechanism, we perform a spatially resolved study making use of emission line diagnostic diagrams such as the BPT. Both diagrams indicate that the gas within BCD-UFRGS-01 is being photoionized by young massive hot stars rather than by an AGN power-law feature less continuum. In the edges of BCD-UFRGS-01 FoV the signal associated to the H_β emission line is low, and a few spaxels in these locations appear in the AGN region of the BPTs but we interpret them as spurious data. Shock models were also investigated, but they are negligible.

(iv) We have estimated $3.5 \times 10^6 M_\odot$ for the ionised gas

Galaxy	$\log(O/H)+12$	M_B	SFR ($M_\odot$ yr^{-1})
II Zw 40	8.13 ± 0.15	-16.2	1.2
UGC 4483	7.52 ± 0.03	-12.7	0.0031
UM 439	8.05 ± 0.15	-15.8	0.083
UM 461	7.74 ± 0.15	-14.4	0.071
UM 462	7.98 ± 0.15	-16.1	0.23
BCD-UFRGS-01	7.71	-15.3	0.71

mass. The values of mass and size ($\sim 14 \times 14$ kpc) of BCD-UFRGS-01 is orders of magnitude higher than massive H II regions and is more likely to be a dwarf galaxy than an giant H II region.

(v) We calculate maps for the ionic abundances of O, N and S for BCD-UFRGS-01. We have obtained an average $\log(O/H) + 12 = 7.71$ ($\sim 1/15\,Z_\odot$). This value characterises the environment of BCD-UFRGS-01 as metal-poor, and lies in the typical ranges of metallicity found for BCDGs.

(vi) Our measurements and observations strongly suggest that BCD-UFRGS-01 is actively forming stars. Thus it is important to quantify the total SFR. We use the reddening corrected H_α flux, to compute the instantaneous SFR. We obtain an integrated value of 0.71 $M_\odot\,\mathrm{yr}^{-1}$, which is high when compared to other BCDGs ($0.1 - 0.5\,M_\odot\,\mathrm{yr}^{-1}$, Van Zee et al. 1998; Remy-Ruyer et al. 2013; Lian et al. 2016). We also estimate a $\sum$SFR of 1.4×10^{-2} $M_\odot\,\mathrm{yr}^{-1}\,\mathrm{kpc}^{-2}$. It also presents clumpy knots that we have interpreted as active star-formation.

(vii) Radial velocity maps indicate that the gas seems to be rotating in the counter-clockwise direction along an axis that crosses BCD-UFRGS-01 diagonally. These velocity maps are well fitted with a disk model of Bertola et al. (1991), thus, indicating that the gas in BCD-UFRGS-01 is arranged on a disk structure.

(viii) We have found that BCD-UFRGS-01 has a $M_B = -15.3$ mag, a value close to other known BCDGs.

With the summarised results mentioned above we conclude that the faint nebular emission line region close in projection to Mrk 1172 is actually a gas rich low-metallicity dwarf galaxy, most likely a BCDG.

In H_α images bright knots are visible in BCD-UFRGS-01, where the highest fraction of its stellar content seems to be located. Analysis in these knots and how they are ionizing the surrounding gas may reveal more accurately the true nature of BCD-UFRGS-01 (Lassen et al, in preparation). Modelling the light profile of both galaxies is essential to improve our understanding about their detailed structure, which can reveal the Low-Surface Brightness component that is typical from BCDGs and may also trace mergers in the past history of both systems. The latter may help us to answer another important question, i.e., which are the origins of this low-metallicity gas and how this metal-poor environment affected the evolutionary processes of BCD-UFRGS-01? This is, however, behind the scope of this paper, and is left for a future publication (Lassen et. al, in preparation)

ACKNOWLEDGEMENTS

CAPES and CNPq. Visit to PUC Chile and ESO Jan/Feb 2018. Programa de Pós Graduação em Física.

REFERENCES

Allen M. G., Groves B. A., Dopita M. A., Sutherland R. S., Kewley L. J., 2008, The Astrophysical Journal Supplement Series, 178, 20
Amorin R. O., Munoz-Tunón C., Aguerri J. A. L., Cairós L. M., Caon N., 2007, Astronomy & Astrophysics, 467, 541
Argudo-Fernández M., et al., 2015, Astronomy & Astrophysics, 578, A110
Azimlu M., Marciniak R., Barmby P., 2011, The Astronomical Journal, 142, 139
Bacon R., et al., 2010, in Ground-based and Airborne Instrumentation for Astronomy III. p. 773508
Baldwin J. A., Phillips M. M., Terlevich R., 1981, Publications of the Astronomical Society of the Pacific, 93, 5
Bekki K., 2008, Monthly Notices of the Royal Astronomical Society: Letters, 388, L10
Bekki K., Stanimirović S., 2009, Monthly Notices of the Royal Astronomical Society, 395, 342
Bergvall N., Östlin G., 2002, Astronomy & Astrophysics, 390, 891
Bertola F., Bettoni D., Danziger J., Sadler E., Sparke L., de Zeeuw T., 1991, The Astrophysical Journal, 373, 369
Bosch G., Terlevich E., Terlevich R., 2009, The Astronomical Journal, 137, 3437
Cairós L. M., Caon N., Papaderos P., Noeske K., Vílchez J. M., Lorenzo B. G., Munoz-Tunón C., 2003, The Astrophysical Journal, 593, 312
Cardelli J. A., Clayton G. C., Mathis J. S., 1989, The Astrophysical Journal, 345, 245
Chang Y.-Y., van der Wel A., da Cunha E., Rix H.-W., 2015, The Astrophysical Journal Supplement Series, 219, 8
Cid Fernandes R., Mateus A., Sodré L., Stasińska G., Gomes J. M., 2005, Monthly Notices of the Royal Astronomical Society, 358, 363
Cid Fernandes R.and Pérez E., et al., 2013, Astronomy & Astrophysics, 557, A86
Cid Fernandes R., et al., 2014, Astronomy & Astrophysics, 561, A130
Claas W. J., 1951, Haarlem, J. Enschede, 1951.
De Paz A. G., Madore B., Pevunova O., 2003, The Astrophysical Journal Supplement Series, 147, 29
Dopita M. A., Sutherland R. S., 1996, The Astrophysical Journal Supplement Series, 102, 161
Gallego J., Zamorano J., Rego M., Vitores A., 1997, The Astrophysical Journal, 475, 502
Garnett D. R., Kennicutt Jr R. C., Chu Y.-H., Skillman E. D., 1991, The Astrophysical Journal, 373, 458
Hinshaw G., et al., 2013, The Astrophysical Journal Supplement Series, 208, 19
Izotov Y. I., Thuan T. X., 1999, The Astrophysical Journal, 511, 639
Jordi K., Grebel E. K., Ammon K., 2006, Astronomy & Astrophysics, 460, 339
Kauffmann G., et al., 2003, Monthly Notices of the Royal Astronomical Society, 346, 1055
Keel W. C., et al., 2012, The Astronomical Journal, 144, 66
Kennicutt Jr R. C., 1998, Annual Review of Astronomy and Astrophysics, 36, 189

Kepley A. A., Leroy A., Johnson K. E., Sandstrom K., Chen C.-H. R., 2016, AAS, 227, 136
Kewley L. J., Dopita M., Sutherland R., Heisler C., Trevena J., 2001, The Astrophysical Journal, 556, 121
Kunth D., Östlin G., 2000, The Astronomy and Astrophysics Review, 10, 1
Lebouteiller V., et al., 2017, Astronomy & Astrophysics, 602, A45
Lian J., Hu N., Fang G., Ye C., Kong X., 2016, The Astrophysical Journal, 819, 73
Lintott C. J., et al., 2009, Monthly Notices of the Royal Astronomical Society, 399, 129
Loose H.-H., Thuan T. X., 1986, The Astrophysical Journal, 309, 59
Mallmann N. D., et al., 2018, Monthly Notices of the Royal Astronomical Society, 478, 5491
Meurer G. R., Carignan C., Beaulieu S., Freeman K. C., 1996, arXiv preprint astro-ph/9601191
Nascimento J. C. d., et al., 2019, Monthly Notices of the Royal Astronomical Society, 486, 5075
Noeske K., Papaderos P., Cairós L., Fricke K., 2005, Astronomy & Astrophysics, 429, 115
O'Donnell J. E., 1994, The Astrophysical Journal, 422, 158
Oconnell R., Thuan T., Goldstein S., 1978, The Astrophysical Journal, 226, L11
Omand C. M., Balogh M. L., Poggianti B. M., 2014, Monthly Notices of the Royal Astronomical Society, 440, 843
Osterbrock D. E., Ferland G. J., 2006, Astrophysics Of Gas Nebulae and Active Galactic Nuclei. University science books
Papaderos P., Loose H.-H., Fricke K. a., Thuan T., 1996, Astronomy and Astrophysics, 314, 59
Papaderos P., Guseva N. G., Izotov Y. I., Fricke K. J., 2008, A&A, 491, 113
Peimbert M., Torres-Peimbert S., Ruiz M., 1992, Revista Mexicana de Astronomia y Astrofisica, 24, 155
Rampadarath H., et al., 2010, Astronomy & Astrophysics, 517, L8
Reines A. E., Sivakoff G. R., Johnson K. E., Brogan C. L., 2011, Nature, 470, 66
Remy-Ruyer A., Galametz M., Vaccari M., Madden S., 2013
Sargent W. L., Searle L., 1970, The Astrophysical Journal, 162, L155
Schaerer D., 2003, Astronomy & Astrophysics, 397, 527
Schaerer D., Stasinska G., 1999, arXiv preprint astro-ph/9903430
Schaerer D., Vacca W. D., 1998, The Astrophysical Journal, 497, 618
Schaerer D., de Koter A., 1997, Astronomy and Astrophysics, 322, 598
Schlegel D. J., Finkbeiner D. P., Davis M., 1998, The Astrophysical Journal, 500, 525
Shi F., Kong X., Li C., Cheng F., 2005, Astronomy & Astrophysics, 437, 849
Soto K. T., Lilly S. J., Bacon R., Richard J., Conseil S., 2016, Monthly Notices of the Royal Astronomical Society, 458, 3210
Thuan T. X., Izotov Y. I., 2005, The Astrophysical Journal Supplement Series, 161, 240
Thuan T., Martin G. E., 1981, The Astrophysical Journal, 247, 823
Tsuge K., et al., 2019, The Astrophysical Journal, 871, 44
Van Zee L., Skillman E. D., Salzer J. J., 1998, The Astronomical Journal, 116, 1186
Vazdekis A., Sánchez-Blázquez P., Falcón-Barroso J., Cenarro A., Beasley M., Cardiel N., Gorgas J., Peletier R., 2010, Monthly Notices of the Royal Astronomical Society, 404, 1639
Weilbacher P. M., Streicher O., Urrutia T., Jarno A., Pécontal-Rousset A., Bacon R., Böhm P., 2012, in Software and Cyberinfrastructure for Astronomy II. p. 84510B
Wu Y., Charmandaris V., Hao L., Brandl B., Bernard-Salas J., Spoon H., Houck J., 2006, The Astrophysical Journal, 639, 157
Zwicky F., 1970, Advances in Astronomy and Astrophysics, Vol. 7

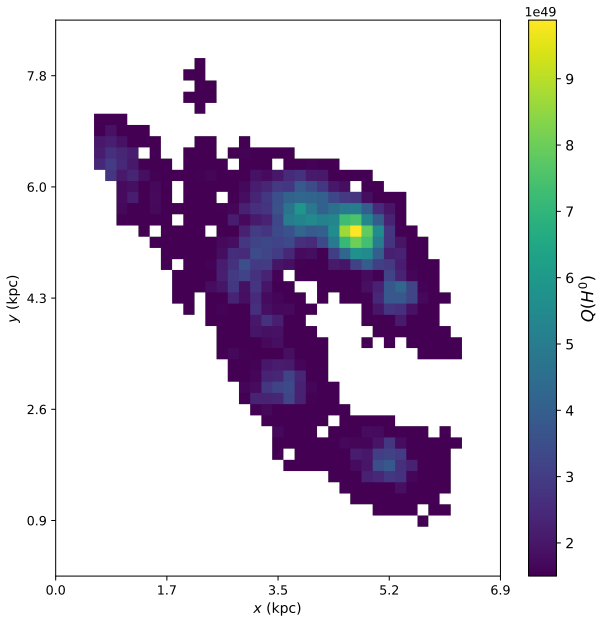

Figure A1. Map for the flux of ionizing photons for BCD-UFRGS-01. The gas is excited due to massive young stars, which seem to be concentrated in knots spread along the BCD-UFRGS-01 structure, which are also the regions with stronger SFR.

APPENDIX A: FLUX OF IONIZING PHOTONS

From Osterbrock & Ferland (2006) we have:

$$Q(H^0) \approx \frac{\alpha_B(H^0,T)}{\alpha^{\rm eff}_{\rm H_\beta}(H^0,T)} \frac{L(\rm H_\beta)}{h\nu_{\rm H_\beta}} \tag{A1}$$

where $Q(H^0)$ is the number of ionizing photons emitted by the stars ionizing the gas in BCD-UFRGS-01, $\alpha_B(H^0,T)$ is the recombination coefficient for all energy levels except for ground state, $\alpha^{\rm eff}_{\rm H_\beta}(H^0,T)$ is the effective recombination coefficient for $\rm H_\beta$ emission line and $h\nu_{\rm H_\beta}$ is the energy of a photon emitted in a $\rm H_\beta$ radiative transition. Since $\rm H_\alpha$ is the strongest line in the spectra of BCD-UFRGS-01, we may want to replace $L(\rm H_\beta)$ in equation A1 using the equation of reddening. Notice that this replacement also introduces the reddening correction for both lines. Using also equation 5, we have:

$$Q(H^0) \approx \frac{\alpha_B(H^0,T)}{\alpha^{\rm eff}_{\rm H_\beta}(H^0,T)} \frac{4\pi d^2}{h\nu_{\rm H_\beta} 10^{\frac{A_V+3.31}{7.23}}} F(\rm H_\alpha) \tag{A2}$$

which can be applied to each spaxel of BCD-UFRGS-01, in order to obtain a map for $Q(H^0)$, which can be visualized in figure A1.

This paper has been typeset from a TEX/LATEX file prepared by the author.

Chapter 4

Concluding remarks

Using data from the Multi Unit Spectroscopic Explorer (MUSE) we serendipitously found an emission line region within the FoV of the quiescent and massive ETG Mrk 1172. We measure the redshift of this nebular region and compare to values of redshifts found for Mrk 1172 in the literature ($z = 0.04115$ or $d = 178\,\mathrm{Mpc}$ for Mrk 1172 and $z = 0.04025 \pm 0.00003$ or $d = 174\,\mathrm{Mpc}$ for the nebular region). Although both galaxies seem to be too distant from each other ($\sim 4\,\mathrm{Mpc}$) to have considerable effects of gravitational interaction, in our redshift measurement we did not apply an corrections for peculiar velocities. Mrk 1172 has a massive halo, which possibly contains many satellite dwarf galaxies within it, as its SDSS image suggests, characterising a fossil group. In this case, a correction for peculiar velocities is needed, and this separation distance would be changed. Thus, we can not exclude the possibility of gravitational interaction between both galaxies, and further analysis of the environment is needed.

This galaxy in the FoV of Mrk 1172 appears in the GALEX catalogue (as GALEX J020536.7-081424) in the NUV and FUV wavelength range and photometrical properties in the optical on SDSS (as SDSS J020536.84-081424.7). However, we were not able to find the spectra of this object in previous studies in the literature, neither detailed studies about its properties.

Despite its low SNR in the continuum, the spectrum of BCD-UFRGS-01 presents strong emission lines, namely: Hα, Hβ, [O III] $\lambda\lambda$4959+5007, [N II] $\lambda\lambda$6548+6583 and [S II] $\lambda\lambda$6716+6731. These indicate the presence of ionised gas surrounding a few bright knots that become visible in Hα images, where we believe star formation is taking place. In order to investigate the stellar content of BCD-UFRGS-01 we perform a spatially resolved stellar population synthesis using the STARLIGHT code.

The best fit model reveals that Mrk 1172 is predominantly dominated by old stellar populations with $t \geq 10^{10}$ yrs, while BCD-UFRGS-01 shows the presence of a young stellar population with ages in the range of 10^7-10^8 yrs. An underlying stellar population with $t \sim 10^9$ yrs is also present, which we suggest that it might be related to the LSB component usually found for BCDGs.

In order to investigate the gas excitation mechanism, we perform a spatially resolved study making use of emission line diagnostic diagrams such as the BPT. Both diagrams indicate that the gas within BCD-UFRGS-01 is being photoionized by young massive hot stars rather than by an AGN power-law featureless continuum. In the edges of BCD-UFRGS-01 FoV the signal associated to the Hβ emission line is low, and a few spaxels in these locations appear in the AGN region of the BPTs but we interpret them as spurious data. Shock models were also investigated, but they are negligible.

Our measurements and observations strongly suggest that BCD-UFRGS-01 is actively forming stars. Thus it is important to quantify the total SFR. We use the reddening corrected Hα flux, to compute the instantaneous SFR. We obtain an integrated value of 0.71 $M_\odot\,\mathrm{yr}^{-1}$, which is high when compared to other BCDGs (0.1 – 0.5 $M_\odot\,\mathrm{yr}^{-1}$, Van Zee et al., 1998, Remy-Ruyer et al., 2013, Lian et al., 2016). We also estimate a $\sum$SFR of 1.4 $\times 10^{-2}$ $M_\odot\,\mathrm{yr}^{-1}\,\mathrm{kpc}^{-2}$.

Applying PYNEB we calculate the metallicity of each spaxel, resulting in an average value of $\log(O/H) + 12 = 7.71$. Adopting $\log(O/H) + 12 = 8.91$ for the Sun (Kunth & Östlin, 2000), we conclude that the average metallicity of the gas is approximately 1/15 $Z_\odot$, which lies within the typical metallicity range of BCDGs (1/3 $Z_\odot$ – 1/50 $Z_\odot$, Gil de Paz et al., 2003, and references therein). The uncertainty related to this measurement has strong dependency with T_e, which we were not able to determine, as discussed before. Thus, the uncertainty of this value is unknown, and we should apply an alternative method to estimate the abundance in this galaxy, in order to compare the values obtained. A possibility is to use the indirect method, as explained in details in Marino et al. (2013).

From the stellar content of BCD-UFRGS-01 and Mrk 1172 we are able to estimate the stellar mass of both galaxies. We obtain $M_\star \sim 1.76 \times 10^{11} M_\odot$ for Mrk 1172, a value that lies close to a previous measurement found in the literature. This is relatively high value of mass, and considering that Mrk 1172 is classified as isolated (Argudo-Fernández et al., 2015), it is possible that many mergers events happened throughout the evolutionary history of this ETG. BCD-UFRGS-01 presents a stellar mass of $M_\star \sim 4.06 \times 10^9 M_\odot$, which is comparable to the mass of the SMC,

($M_\star = 6.5 \times 10^9 \mathrm{M}_\odot$, Bekki & Stanimirović, 2009) and to the BCDG Henize 2-10 ($M_\star = 3.7 \times 10^9 \mathrm{M}_\odot$, Reines et al., 2011), for example. We also estimate a low-limit for the ionised gas mass of $M = 3.5 \times 10^6 M_\odot$. This value is higher than the mass of giant H II regions such as 30 Doradus and N44 nebulae ($4 \times 10^5\, M_\odot$ and $\sim 5 \times 10^5\, M_\odot$, respectively, Bosch et al., 2009, Tsuge et al., 2019). It is worth noting that [S II] $\lambda\lambda$6716+6731 emission lines, used to determine n_e, are saturated towards a low-density environment ($n_e \lesssim 1\,\mathrm{cm}^{-3}$), and therefore we assume $n_e = 1\,\mathrm{cm}^{-3}$ for the gas within BCD-UFRGS-01.

From the gaussians fitted to the emission lines we obtain the radial velocity of the gas, and the velocity dispersion σ. In the velocity dispersion maps we find no gradient, revealing that leaking gas and similar perturbations are unlikely to be significant in BCD-UFRGS-01. On the other hand, radial velocity maps present the same trend for all the observed emission lines. The gas seems to be rotating in the counter-clockwise direction along an axis that crosses BCD-UFRGS-01 diagonally. A dynamical model from Bertola et al. (1991) is used, where we assume circular orbits around the plane of a disk. This model reproduces the trend seen in the velocity maps, and the residual map is uniformly distributed around zero, indicating that the model is able to characterise the dynamics of BCD-UFRGS-01.

Since the spectra of BCD-UFRGS-01 do not cover the necessary wavelength range for us to integrate the flux and obtain the B-band magnitude of BCD-UFRGS-01 we use SDSS images and the conversion equation from Jordi et al. (2006) and derive an abstolute magnitude in the B-band of $M_B = -15.3$ mag. This value lies in the range of other known BCDGs (e.g., -13 $\sim$ -20 mag, Van Zee et al., 1998, Doublier et al., 1999, Remy-Ruyer et al., 2013), suggesting that BCD-UFRGS-01 is faint as the BCDGs.

From the above we conclude that BCD-UFRGS-01 is actively forming stars. We raise two possibilities to explain its nature: either (i) BCD-UFRGS-01 is a blue compact dwarf galaxy or (ii) a low metallicity disk galaxy with intense star formation. The former is our favoured scenario which we explore in more details below.

As in other BCDGs, BCD-UFRGS-01 shows many intense star-forming regions. The clumpy knots could be young massive star clusters like those found in the spatially resolved analysis of Haro 11 ($z = 0.02060$) (Menacho et al., 2019), which is shown in figure 4.1. In the work of Menacho et al. (2019), the analysis is made using data from MUSE and Hubble Space Telescope (HST), revealing inner structures of the irregular Haro 11, where its gaseous structure is composed of several young star

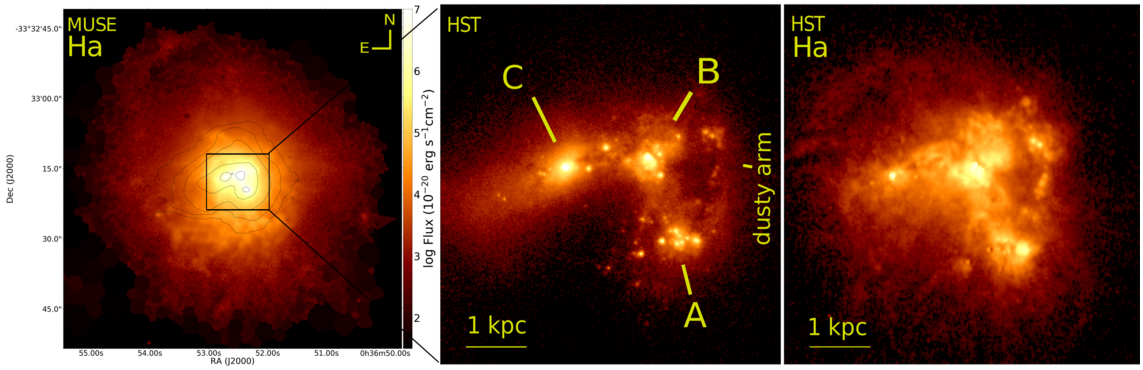

Figure 4.1: A spatially resolved analysis of Haro 11 using data from MUSE and from HST is performed in Menacho et al. (2019), revealing inner structures in the gas, such as large-scale bubbles and young massive star clusters. In left panel, the image of Haro 11 collapsed in Hα wavelength for MUSE FoV. In middle panel the central region inside the square shown in the first image, now for HST. The labels A, B and C indicate the location of the three main star clusters. In right panel, the image of HST now collapsed in Hα wavelength.

clusters and channels in the ISM tracing outflows and the creation of large-scale bubbles. BCD-UFRGS-01 resembles in many aspects Haro 11. However, this needs to be further investigated, and a separate analysis of the clumpy knots is recommended. Moreover, we must also separate the low surface brightness component from the other component.

Since we have estimates for the Oxygen abundance and stellar mass of BCD-UFRGS-01 we can investigate its position in the MZR. In figure 4.2 we plot all the relations shown previously in a combined figure, where the black dashed line is the low-end trend from Lian et al. (2016) (referred as L16), and the red balloon surrounding it represents the scatter of the sample of BCDGs seen in figure 1.4. In this plot the position of BCD-UFRGS-01 is represented by a red star, while the purple star represents the position of Haro 11, which has a stellar mass of $1.6 \times 10^{10}\, M_{\odot}$ (Menacho et al., 2019) and a metallicity of $\log(O/H) + 12 = 7.92$ (Masegosa et al., 1994, Raimann et al., 2000). Apart from being visually similar, both BCDGs lie close to each other in the MZR, where Haro 11 is more massive and metallic than BCD-UFRGS-01.

We thus conclude that the faint nebular emission line region near Mrk 1172 is actually a dwarf galaxy, most likely to be a BCDG. To proceed with the analysis of this system, further efforts in determining the light profile of our candidate BCDG may reveal traces of mergers and explicit the exponential profiles expected from the LSB component typically present in BCDGs. As seen in the Hα collapsed images of BCD-UFRGS-01 in figure 1.7, bright clumpy knots are noticeable. They

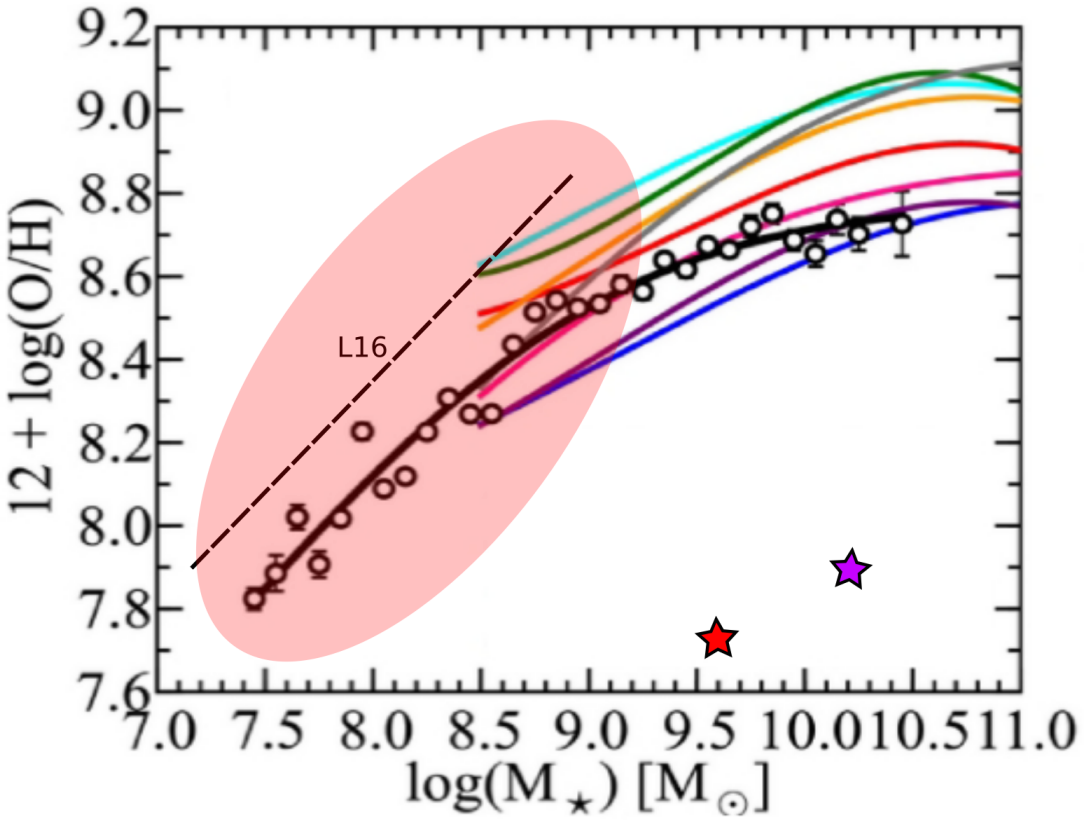

Figure 4.2: An adapted version of the MZR plot shown in Fig 1.3 from Andrews & Martini (2013), showing the position of BCD-UFRGS-01 represented by the red star at the bottom right part. The dashed black line, labelled as L16, is the trend found in the MZR for a sample of BCDGs analysed in Lian et al. (2016), which scatter around this line occupying the region represented by the red balloon. The purple star indicates the position of Haro 11 from Menacho et al. (2019), which lies relatively close to BCD-UFRGS-01.

represent the source of the flux that ionises the surrounding gas, and are probably young massive star clusters, resembling the star clusters found in Haro 11, shown in figure 4.1. A separate analysis on the bright clumpy knots in BCD-UFRGS-01 is also essential, since the measurements shown here are related to BCD-UFRGS-01 as a whole, while there seems to be a clear contrast between these knots and its surroundings. We are also interested in investigating deeper the dynamics of the system to further explore the origin of the observed metal-poor gas.

References

[1] ALLEN, DAVID A. Forbidden emission lines—i. In: EXERCISES IN ASTRONOMY, p. 251–254. Springer, 1987.

[2] ALLER, LAWRENCE HUGH. **Physics of thermal gaseous nebulae: Physical processes in gaseous nebulae**, v. 112: Springer Science & Business Media, 2012.

[3] AMORIN, RICARDO O, MUNOZ-TUNÓN, CASIANA, AGUERRI, J ALFONSO L, CAIRÓS, LUZ M, CAON, NICOLA. The stellar host in blue compact dwarf galaxies-the need for a two-dimensional fit. **Astronomy & Astrophysics**, v. 467, n. 2, p. 541–558, 2007.

[4] ANDERSON, LOREN D, BANIA, TM, BALSER, DANA S, CUNNINGHAM, V, WENGER, TV, JOHNSTONE, BM, ARMENTROUT, WP. The wise catalog of galactic h ii regions. **The Astrophysical Journal Supplement Series**, v. 212, n. 1, p. 1, 2014.

[5] ANDREWS, BRETT H, MARTINI, PAUL. The mass-metallicity relation with the direct method on stacked spectra of sdss galaxies. **The Astrophysical Journal**, v. 765, n. 2, p. 140, 2013.

[6] ANGLÉS-ALCÁZAR, DANIEL, FAUCHER-GIGUÈRE, CLAUDE-ANDRÉ, KEREŠ, DUŠAN, HOPKINS, PHILIP F, QUATAERT, ELIOT, MURRAY, NORMAN. The cosmic baryon cycle and galaxy mass assembly in the fire simulations. **Monthly Notices of the Royal Astronomical Society**, v. 470, n. 4, p. 4698–4719, 2017.

[7] ARGUDO-FERNÁNDEZ, M, VERLEY, S, BERGOND, G, PUERTAS, S DUARTE, CARMONA, E RAMOS, SABATER, J, LORENZO, M FERNÁNDEZ, ESPADA, D, SULENTIC, J, RUIZ, JE, OTHERS, . Cata-

logues of isolated galaxies, isolated pairs, and isolated triplets in the local universe. **Astronomy & Astrophysics**, v. 578, p. A110, 2015.

[8] BALDWIN, J. A., PHILLIPS, M. M., TERLEVICH, R. Classification parameters for the emission-line spectra of extragalactic objects. , v. 93, p. 5–19, February 1981.

[9] BARBUY, B, TREVISAN, J, ALMEIDA, ADE . Pfant: Stellar spectral synthesis code. **ascl**, p. ascl–1812, 2018.

[10] BEKKI, KENJI, STANIMIROVIĆ, SNEŽANA. The total mass and dark halo properties of the small magellanic cloud. **Monthly Notices of the Royal Astronomical Society**, v. 395, n. 1, p. 342–350, 2009.

[11] BERTOLA, FRANCESCO, BETTONI, DANIELA, DANZIGER, JOHN, SADLER, ELAINE, SPARKE, LINDA, ZEEUW, TIMDE . Testing the gravitational field in elliptical galaxies-ngc 5077. **The Astrophysical Journal**, v. 373, p. 369–390, 1991.

[12] BEZANSON, RACHEL, VAN DOKKUM, PIETER G, TAL, TOMER, MARCHESINI, DANILO, KRIEK, MARISKA, FRANX, MARIJN, COPPI, PAOLO. The relation between compact, quiescent high-redshift galaxies and massive nearby elliptical galaxies: evidence for hierarchical, inside-out growth. **The Astrophysical Journal**, v. 697, n. 2, p. 1290, 2009.

[13] BICA, E. Population synthesis in galactic nuclei using a library of star clusters. **Astronomy and Astrophysics**, v. 195, p. 76–92, 1988.

[14] BOSCH, GUILLERMO, TERLEVICH, ELENA, TERLEVICH, ROBERTO. Gemini/gmos search for massive binaries in the ionizing cluster of 30 dor. **The Astronomical Journal**, v. 137, n. 2, p. 3437, 2009.

[15] BOSELLI, ALESSANDRO. **A panchromatic view of galaxies**: John Wiley & Sons, 2012.

[16] BOURNAUD, FRÉDÉRIC, ELMEGREEN, BRUCE G, MARTIG, MARIE. The thick disks of spiral galaxies as relics from gas-rich, turbulent, clumpy disks at high redshift. **The Astrophysical Journal Letters**, v. 707, n. 1, p. L1, 2009.

[17] BRESSAN, ALESSANDRO, MARIGO, PAOLA, GIRARDI, LÉO, SALASNICH, BERNARDO, DAL CERO, CLAUDIA, RUBELE, STEFANO, NANNI, AMBRA. Parsec: stellar tracks and isochrones with the padova and trieste stellar evolution code. **Monthly Notices of the Royal Astronomical Society**, v. 427, n. 1, p. 127–145, 2012.

[18] BRUM, CARINE, DINIZ, MARLON R, RIFFEL, ROGEMAR A, RODRíGUEZ-ARDILA, ALBERTO, HO, LUIS C, RIFFEL, ROGÉRIO, MASON, RACHEL, MARTINS, LUCIMARA, PETRIC, ANDREEA, SÁNCHEZ-JANSSEN, RUBÉN. A close look at the dwarf agn of ngc 4395: optical and near-ir integral field spectroscopy. **Monthly Notices of the Royal Astronomical Society**, v. 486, n. 1, p. 691–707, 2019.

[19] CAIRÓS, LM, CAON, N, LORENZO, B GARCíA, KELZ, A, ROTH, M, PAPADEROS, P, STREICHER, O. Mapping luminous blue compact galaxies with virus-p-morphology, line ratios, and kinematics. **Astronomy & Astrophysics**, v. 547, p. A24, 2012.

[20] CARDELLI, JASON A, CLAYTON, GEOFFREY C, MATHIS, JOHN S. The relationship between infrared, optical, and ultraviolet extinction. **The Astrophysical Journal**, v. 345, p. 245–256, 1989.

[21] CHIAPPINI, CRISTINA. The formation and evolution of the milky way: The distribution of the chemical elements in our galaxy serves as a" fossil record" of its evolutionary history. **American Scientist**, v. 89, n. 6, p. 506–515, 2001.

[22] CHISHOLM, JOSEPH D, KINGSTONE, ALAN. Action video game players' visual search advantage extends to biologically relevant stimuli. **Acta psychologica**, v. 159, p. 93–99, 2015.

[23] CID FERNANDES, R, STASIŃSKA, G, MATEUS, A, VALE ASARI, N. A comprehensive classification of galaxies in the sloan digital sky survey: how to tell true from fake agn? **Monthly Notices of the Royal Astronomical Society**, v. 413, n. 3, p. 1687–1699, 2011.

[24] CID FERNANDES, ROBERTO, MATEUS, ABíLIO, SODRÉ, LAERTE, STASIŃSKA, GRAŻYNA, GOMES, JEAN M. Semi-empirical analysis of sloan digital sky survey galaxies–i. spectral synthesis method. **Monthly Notices of the Royal Astronomical Society**, v. 358, n. 2, p. 363–378, 2005.

[25] COELHO, PAULA RODRIGUES TEIXEIRA. A new library of theoretical stellar spectra with scaled-solar and α-enhanced mixtures. **Monthly Notices of the Royal Astronomical Society**, v. 440, n. 2, p. 1027–1043, 2014.

[26] CONROY, CHARLIE, GUNN, JAMES E, WHITE, MARTIN. The propagation of uncertainties in stellar population synthesis modeling. i. the relevance of uncertain aspects of stellar evolution and the initial mass function to the derived physical properties of galaxies. **The Astrophysical Journal**, v. 699, n. 1, p. 486, 2009.

[27] COOK, M, LAPI, A, GRANATO, GL. Two-phase galaxy formation. **Monthly Notices of the Royal Astronomical Society**, v. 397, n. 1, p. 534–547, 2009.

[28] CURTI, MIRKO, MANNUCCI, FILIPPO, CRESCI, GIOVANNI, MAIOLINO, ROBERTO. The mass–metallicity and the fundamental metallicity relation revisited on a fully t e-based abundance scale for galaxies. **Monthly Notices of the Royal Astronomical Society**, v. 491, n. 1, p. 944–964, 2020.

[29] DAVÉ, ROMEEL, OPPENHEIMER, BENJAMIN D, FINLATOR, KRISTIAN. Galaxy evolution in cosmological simulations with outflows–i. stellar masses and star formation rates. **Monthly Notices of the Royal Astronomical Society**, v. 415, n. 1, p. 11–31, 2011.

[30] DE LUCIA, GABRIELLA, BLAIZOT, JÉRÉMY. The hierarchical formation of the brightest cluster galaxies. **Monthly Notices of the Royal Astronomical Society**, v. 375, n. 1, p. 2–14, 2007.

[31] DENICOLÓ, GLENDA, TERLEVICH, ROBERTO, TERLEVICH, ELENA. New light on the search for low-metallicity galaxies—i. the n2 calibrator. **Monthly Notices of the Royal Astronomical Society**, v. 330, n. 1, p. 69–74, 2002.

[32] DIGBY, RUTH, NAVARRO, JULIO F, FATTAHI, AZADEH, SIMPSON, CHRISTINE M, OMAN, KYLE A, GOMEZ, FACUNDO A, FRENK, CARLOS S, GRAND, ROBERT JJ, PAKMOR, RUEDIGER. The star formation histories of dwarf galaxies in local group cosmological simulations. **Monthly Notices of the Royal Astronomical Society**, v. 485, n. 4, p. 5423–5437, 2019.

[33] DJORGOVSKI, S GEORGE. On the observability of primeval galaxies. In: COSMOLOGY AND LARGE-SCALE STRUCTURE IN THE UNIVERSE, v. 24, p. 73, 1992.

[34] DOTTORI, HORACIO A. Evolution of h ii regions. **Revista Mexicana de Astronomia y Astrofisica, vol. 14**, v. 14, p. 463–473, 1987.

[35] DOTTORI, HORACIO A, COPETTI, MARCUS VF. Statistical properties of h ii regions. **Revista Mexicana de Astronomia y Astrofisica, vol. 18**, v. 18, p. 115–119, 1989.

[36] DOUBLIER, V, CAULET, A, COMTE, G. Multi-spectral study of a new sample of blue compact dwarf galaxies-ii. b and r surface photometry of 22 southern objects. **Astronomy and Astrophysics Supplement Series**, v. 138, n. 2, p. 213–245, 1999.

[37] DUBOIS, YOHAN, PEIRANI, SÉBASTIEN, PICHON, CHRISTOPHE, DEVRIENDT, JULIEN, GAVAZZI, RAPHAËL, WELKER, CHARLOTTE, VOLONTERI, MARTA. The horizon-agn simulation: morphological diversity of galaxies promoted by agn feedback. **Monthly Notices of the Royal Astronomical Society**, v. 463, n. 4, p. 3948–3964, 2016.

[38] EFSTATHIOU, G, REES, MJ. High-redshift quasars in the cold dark matter cosmogony. **Monthly Notices of the Royal Astronomical Society**, v. 230, n. 1, p. 5P–11P, 1988.

[39] EGGEN, OJ, LYNDEN-BELL, D, SANDAGE, AR. Evidence from the motions of old stars that the galaxy collapsed. **The Astrophysical Journal**, v. 136, p. 748, 1962.

[40] ERB, DAWN K, SHAPLEY, ALICE E, PETTINI, MAX, STEIDEL, CHARLES C, REDDY, NAVEEN A, ADELBERGER, KURT L. The mass-metallicity relation at z 2. **The Astrophysical Journal**, v. 644, n. 2, p. 813, 2006.

[41] FANELLI, MICHAEL N, O'CONNELL, ROBERT W, THUAN, TRINH X. Spectral synthesis in the ultraviolet. ii-stellar populations and star formation in blue compact galaxies. **The Astrophysical Journal**, v. 334, p. 665–687, 1988.

[42] FENG, YU, MODI, CHIRAG. A fast algorithm for identifying friends-of-friends halos. **Astronomy and computing**, v. 20, p. 44–51, 2017.

[43] FERNANDES, CID, HECKMAN, T, SCHMITT, H, DELGADO, RM GONZÁLEZ, STORCHI-BERGMANN, T. Empirical diagnostics of the starburst-agn connection. **The Astrophysical Journal**, v. 558, n. 1, p. 81, 2001.

[44] FERNÁNDEZ, VITAL, TERLEVICH, ELENA, DíAZ, ANGELES I, TERLEVICH, ROBERTO, ROSALES-ORTEGA, FF. Primordial helium abundance determination using sulphur as metallicity tracer. **Monthly Notices of the Royal Astronomical Society**, v. 478, n. 4, p. 5301–5319, 2018.

[45] FERRARESE, LAURA, FORD, HOLLAND. Supermassive black holes in galactic nuclei: past, present and future research. **Space Science Reviews**, v. 116, n. 3-4, p. 523–624, 2005.

[46] FONTANOT, FABIO, DE LUCIA, GABRIELLA, MONACO, PIERLUIGI, SOMERVILLE, RACHEL S, SANTINI, PAOLA. The many manifestations of downsizing: hierarchical galaxy formation models confront observations. **Monthly Notices of the Royal Astronomical Society**, v. 397, n. 4, p. 1776–1790, 2009.

[47] FRENK, CARLOS S, WHITE, SIMON DM, DAVIS, MARC, EFSTATHIOU, GEORGE. The formation of dark halos in a universe dominated by cold dark matter. **The Astrophysical Journal**, v. 327, p. 507–525, 1988.

[48] GALLAGHER, ROBERT, MAIOLINO, ROBERTO, BELFIORE, FRANCESCO, DRORY, NIV, RIFFEL, ROGÉRIO, RIFFEL, R A. Widespread star formation inside galactic outflows. **Monthly Notices of the Royal Astronomical Society**, v. 485, n. 3, p. 3409–3429, 2019.

[49] GALLEGO, J, ZAMORANO, J, REGO, M, VITORES, AG. Spectroscopic properties and luminosity distribution of the universidad complutense de madrid survey galaxies. **The Astrophysical Journal**, v. 475, n. 2, p. 502, 1997.

[50] GARCíA-BENITO, RUBÉN, PÉREZ, ENRIQUE, DíAZ, ÁNGELES I, APELLÁNIZ, JESÚS MAíZ, CERVINO, MIGUEL. The 100 myr star formation history of ngc 5471 from cluster and resolved stellar photometry. **The Astronomical Journal**, v. 141, n. 4, p. 126, 2011.

[51] PAZ, ARMANDOGIL DE , MADORE, BF, PEVUNOVA, O. Palomar/las campanas imaging atlas of blue compact dwarf galaxies. i. images and integrated photometry. **Astrophysical journal supplement series**, v. 147, n. 1, p. 29–59, 2003.

[52] GORDON, MARK A, SOROCHENKO, ROMAN L. **Radio Recombination Lines: Their Physics and Astronomical Applications**, v. 282: Springer Science & Business Media, 2009.

[53] HALPERN, JP, STEINER, JE. Low-ionization active galactic nuclei-x-ray or shock heated? **The Astrophysical Journal**, v. 269, p. L37–L41, 1983.

[54] HARKO, TIBERIU. Gravitational collapse of bose-einstein condensate dark matter halos. **Physical Review D**, v. 89, n. 8, p. 084040, 2014.

[55] HIGGINBOTTOM, GAIL, CLAY, ROGER. Origins of standing stone astronomy in britain: new quantitative techniques for the study of archaeoastronomy. **Journal of Archaeological Science: Reports**, v. 9, p. 249–258, 2016.

[56] HODGE, PAUL W, KENNICUTT JR, RC. An atlas of h ii regions in 125 galaxies. **The Astronomical Journal**, v. 88, p. 296–328, 1983.

[57] HOPKINS, AM, SCHULTE-LADBECK, RE, DROZDOVSKY, IO. Star formation rates of local blue compact dwarf galaxies. i. 1.4 ghz and 60 micron luminosities. **The Astronomical Journal**, v. 124, n. 2, p. 862, 2002.

[58] HUBBLE, EDWIN P. Ngc 6822, a remote stellar system. **The Astrophysical Journal**, v. 62, 1925.

[59] HUNT, LK, HIRASHITA, H. The size-density relation of extragalactic h ii regions. **Astronomy & Astrophysics**, v. 507, n. 3, p. 1327–1343, 2009.

[60] HUNTER, DA, GALLAGHER III, JS. Star-forming properties and histories of dwarf irregular galaxies-down but not out. **The Astrophysical Journal Supplement Series**, v. 58, p. 533–560, 1985.

[61] IZOTOV, YU I, STASIŃSKA, G, MEYNET, G, GUSEVA, NG, THUAN, TX. The chemical composition of metal-poor emission-line galaxies in the data release 3 of the sloan digital sky survey. **Astronomy & Astrophysics**, v. 448, n. 3, p. 955–970, 2006.

[62] JANOWIECKI, STEVEN, SALZER, JOHN J, VAN ZEE, LIESE, ROSENBERG, JESSICA L, SKILLMAN, EVAN. Constraining the stellar populations and star formation histories of blue compact dwarf galaxies with sed fits. **The Astrophysical Journal**, v. 836, n. 1, p. 128, 2017.

[63] JORDI, KATRIN, GREBEL, EVA K, AMMON, KARIN. Empirical color transformations between sdss photometry and other photometric systems. **Astronomy & Astrophysics**, v. 460, n. 1, p. 339–347, 2006.

[64] JÓZSA, GIG, GARRETT, MA, OOSTERLOO, TA, RAMPADARATH, H, PARAGI, Z, ARKEL, HVAN , LINTOTT, C, KEEL, WILLIAM C, SCHAWINSKI, K, EDMONDSON, E. Revealing hanny's voorwerp: radio observations of ic 2497. **Astronomy & Astrophysics**, v. 500, n. 2, p. L33–L36, 2009.

[65] KAKKAD, D, GROVES, B, DOPITA, M, THOMAS, ADAM D, DAVIES, REBECCA L, MAINIERI, V, KHARB, PREETI, SCHARWÄCHTER, J, HAMPTON, EJ, HO, I-TING. Spatially resolved electron density in the narrow line region of z¡ 0.02 radio agns. **Astronomy & Astrophysics**, v. 618, p. A6, 2018.

[66] KAUFFMANN, GUINEVERE, HECKMAN, TIMOTHY M, TREMONTI, CHRISTY, BRINCHMANN, JARLE, CHARLOT, STÉPHANE, WHITE, SIMON DM, RIDGWAY, SUSAN E, BRINKMANN, JON, FUKUGITA, MASATAKA, HALL, PATRICK B, OTHERS, . The host galaxies of active galactic nuclei. **Monthly Notices of the Royal Astronomical Society**, v. 346, n. 4, p. 1055–1077, 2003.

[67] KEEL, WILLIAM C, BENNERT, VARDHA N, PANCOAST, ANNA, HARRIS, CHELSEA E, NIERENBERG, ANNA, CHOJNOWSKI, S DREW, MOISEEV, ALEXEI V, OPARIN, DMITRY V, LINTOTT, CHRIS J, SCHAWINSKI, KEVIN, OTHERS, . Agn photoionization of gas in companion galaxies as a probe of agn radiation in time and direction. **Monthly Notices of the Royal Astronomical Society**, v. 483, n. 4, p. 4847–4865, 2019.

[68] KEEL, WILLIAM C, LINTOTT, CHRIS J, SCHAWINSKI, KEVIN, BENNERT, VARDHA N, THOMAS, DANIEL, MANNING, ANNA, CHOJNOWSKI, S DREW, VAN ARKEL, HANNY, LYNN, STUART. The history and environment of a faded quasar: Hubble space telescope observations of hanny's voorwerp and ic 2497. **The Astronomical Journal**, v. 144, n. 2, p. 66, 2012.

[69] KEHRIG, C, VíLCHEZ, JM, SÁNCHEZ, SF, TELLES, E, PÉREZ-MONTERO, E, MARTíN-GORDÓN, D. The interplay between ionized gas and massive stars in the hii galaxy iizw70: integral field spectroscopy with pmas. **Astronomy & Astrophysics**, v. 477, n. 3, p. 813–822, 2008.

[70] KENNICUTT JR, ROBERT C. Star formation in galaxies along the hubble sequence. **Annual Review of Astronomy and Astrophysics**, v. 36, n. 1, p. 189–231, 1998.

[71] KEWLEY, LISA J, DOPITA, MA. Using strong lines to estimate abundances in extragalactic h ii regions and starburst galaxies. **The Astrophysical Journal Supplement Series**, v. 142, n. 1, p. 35, 2002.

[72] KEWLEY, LISA J, DOPITA, MA, SUTHERLAND, RS, HEISLER, CA, TREVENA, J. Theoretical modeling of starburst galaxies. **The Astrophysical Journal**, v. 556, n. 1, p. 121, 2001.

[73] KEWLEY, LISA J, DOPITA, MICHAEL A, LEITHERER, CLAUS, DAVÉ, ROMEEL, YUAN, TIANTIAN, ALLEN, MARK, GROVES, BRENT, SUTHERLAND, RALPH. Theoretical evolution of optical strong lines across cosmic time. **The Astrophysical Journal**, v. 774, n. 2, p. 100, 2013a.

[74] KEWLEY, LISA J, ELLISON, SARA L. Metallicity calibrations and the mass-metallicity relation for star-forming galaxies. **The Astrophysical Journal**, v. 681, n. 2, p. 1183, 2008.

[75] KEWLEY, LISA J, GROVES, BRENT, KAUFFMANN, GUINEVERE, HECKMAN, TIM. The host galaxies and classification of active galactic nuclei. **Monthly Notices of the Royal Astronomical Society**, v. 372, n. 3, p. 961–976, 2006.

[76] KEWLEY, LISA J, MAIER, CHRISTIAN, YABE, KIYOTO, OHTA, KOUJI, AKIYAMA, MASAYUKI, DOPITA, MICHAEL A, YUAN, TIANTIAN. The cosmic bpt diagram: confronting theory with observations. **The Astrophysical Journal Letters**, v. 774, n. 1, p. L10, 2013b.

[77] KEWLEY, LISA J, NICHOLLS, DAVID C, SUTHERLAND, RALPH S. Understanding galaxy evolution through emission lines. **Annual Review of Astronomy and Astrophysics**, v. 57, p. 511–570, 2019.

[78] KNAPEN, JH. Statistical properties of hii regions in the disc of m100. **Monthly Notices of the Royal Astronomical Society**, v. 297, n. 1, p. 255–264, 1998.

[79] KOBULNICKY, HENRY A, KEWLEY, LISA J. Metallicities of 0.3¡ z¡ 1.0 galaxies in the goods-north field. **The Astrophysical Journal**, v. 617, n. 1, p. 240, 2004.

[80] KONG, XU, CHENG, FZ, WEISS, A, CHARLOT, S. Spectroscopic study of blue compact galaxies-ii. spectral analysis and correlations. **Astronomy & Astrophysics**, v. 396, n. 2, p. 503–512, 2002.

[81] KORMENDY, JOHN, HO, LUIS C. Coevolution (or not) of supermassive black holes and host galaxies. **Annual Review of Astronomy and Astrophysics**, v. 51, p. 511–653, 2013.

[82] KUNTH, D, MAUROGORDATO, S, VIGROUX, L. Ccd observations of blue compact galaxies-a mixed bag of morphological types. **Astronomy and Astrophysics**, v. 204, p. 10–20, 1988.

[83] KUNTH, DANIEL, ÖSTLIN, GÖRAN. The most metal-poor galaxies. **The Astronomy and Astrophysics Review**, v. 10, n. 1-2, p. 1–79, 2000.

[84] KURUCZ, ROBERT L. Model atmospheres for population synthesis. In: THE STELLAR POPULATIONS OF GALAXIES, p. 225–232. Springer, 1992.

[85] LAOR, ARI. A note on the viability of gaseous ionization in active galaxies by fast shocks. **The Astrophysical Journal Letters**, v. 496, n. 2, p. L71, 1998.

[86] LAPI, ANDREA, CAVALIERE, A. Dark matter equilibria in galaxies and galaxy systems. **The Astrophysical Journal**, v. 692, n. 1, p. 174, 2009.

[87] LEBOUTEILLER, V, PÉQUIGNOT, D, CORMIER, D, MADDEN, S, PAKULL, MW, KUNTH, D, GALLIANO, F, CHEVANCE, M, HEAP, SR, LEE, M-Y, OTHERS, . Neutral gas heating by x-rays in primitive galaxies: Infrared observations of the blue compact dwarf i zw 18 with herschel. **Astronomy & Astrophysics**, v. 602, p. A45, 2017.

[88] LEJEUNE, TH, CUISINIER, F, BUSER, ROLAND. A standard stellar library for evolutionary synthesis-i. calibration of theoretical spectra. **Astronomy and Astrophysics Supplement Series**, v. 125, n. 2, p. 229–246, 1997.

[89] LEQUEUX, J, PEIMBERT, M, RAYO, JF, SERRANO, A, TORRES-PEIMBERT, S. Chemical composition and evolution of irregular and blue compact galaxies. **Astronomy and Astrophysics**, v. 80, p. 155–166, 1979.

[90] LI, YUN, MO, H. J., VAN DEN BOSCH, FRANK C., LIN, W. P. On the assembly history of dark matter haloes. , v. 379, n. 2, p. 689–701, August 2007.

[91] LIAN, JIANHUI, HU, NING, FANG, GUANWEN, YE, CHENGYUN, KONG, XU. The metallicity evolution of blue compact dwarf galaxies from the intermediate redshift to the local universe. **The Astrophysical Journal**, v. 819, n. 1, p. 73, 2016.

[92] LINTOTT, CHRIS J, SCHAWINSKI, KEVIN, KEEL, WILLIAM, VAN ARKEL, HANNY, BENNERT, NICOLA, EDMONDSON, EDWARD, THOMAS, DANIEL, SMITH, DANIEL JB, HERBERT, PETER D, JARVIS, MATT J, OTHERS, . Galaxy zoo:'hanny's voorwerp', a quasar light echo? **Monthly Notices of the Royal Astronomical Society**, v. 399, n. 1, p. 129–140, 2009.

[93] LONGAIR, MALCOLM S, EINASTO, JAAN. **The large scale structure of the universe**, v. 79: Springer Science & Business Media, 2013.

[94] LOOSE, HANS-HERMANN, THUAN, TRINH X. Surface brightness and color distributions in blue compact dwarf galaxies. i-haro 2, an extreme example of a star-forming young elliptical galaxy. **The Astrophysical Journal**, v. 309, p. 59–69, 1986.

[95] LU, YU, MO, HJ, KATZ, NEAL, WEINBERG, MARTIN D. On the origin of cold dark matter halo density profiles. **Monthly Notices of the Royal Astronomical Society**, v. 368, n. 4, p. 1931–1940, 2006.

[96] LURIDIANA, VALENTINA, MORISSET, CHRISTOPHE, SHAW, RICHARD A. Pyneb: a new tool for analyzing emission lines-i. code description and validation of results. **Astronomy & Astrophysics**, v. 573, p. A42, 2015.

[97] MARASTON, CLAUDIA. Evolutionary population synthesis: models, analysis of the ingredients and application to high-z galaxies. **Monthly Notices of the Royal Astronomical Society**, v. 362, n. 3, p. 799–825, 2005.

[98] MARASTON, CLAUDIA, STRÖMBÄCK, G. Stellar population models at high spectral resolution. **Monthly Notices of the Royal Astronomical Society**, v. 418, n. 4, p. 2785–2811, 2011.

[99] MARINO, RAFFAELLA ANNA, ROSALES-ORTEGA, FF, SÁNCHEZ, SF, DE PAZ, A GIL, VíLCHEZ, J, MIRALLES-CABALLERO, D, KEHRIG, C, PÉREZ-MONTERO, E, STANISHEV, V, IGLESIAS-PÁRAMO, J, OTHERS, . The o3n2 and n2 abundance indicators revisited: improved calibrations based on califa and te-based literature data. **Astronomy & Astrophysics**, v. 559, p. A114, 2013.

[100] MASEGOSA, JOSEFA, MOLES, MARIANO, CAMPOS-AGUILAR, ANA. Element abundances in h ii galaxies. **The Astrophysical Journal**, v. 420, p. 576–596, 1994.

[101] MCGAUGH, STACY S. H ii region abundances-model oxygen line ratios. **The Astrophysical Journal**, v. 380, p. 140–150, 1991.

[102] MENACHO, VERONICA, ÖSTLIN, GÖRAN, BIK, ADRIANUS, DELLA BRUNA, LORENZA, MELINDER, JENS, ADAMO, ANGELA, HAYES, MATTHEW, HERENZ, EC, BERGVALL, NILS. The impact of stellar feedback from velocity-dependent ionized gas maps–a muse view of haro 11. **Monthly Notices of the Royal Astronomical Society**, v. 487, n. 3, p. 3183–3198, 2019.

[103] MIHALAS, DIMITRI. Stellar atmospheres. **stat**, 1978.

[104] MO, HOUJUN, BOSCH, FRANKVAN DEN , WHITE, SIMON. **Galaxy formation and evolution**: Cambridge University Press, 2010.

[105] NASCIMENTO, JANAíNA C DO, STORCHI-BERGMANN, THAISA, MALLMANN, NíCOLAS D, RIFFEL, ROGÉRIO, ILHA, GABRIELE S, RIFFEL, ROGEMAR A, REMBOLD, SANDRO B, SCHIMOIA, JÁDERSON, COSTA, LUIZ NICOLACIDA , MAIA, MARCIO AG, OTHERS, . The first 62 agn observed with sdss-iv manga–iv. gas excitation and star formation rate distributions. **Monthly Notices of the Royal Astronomical Society**, v. 486, n. 4, p. 5075–5093, 2019.

[106] NEISTEIN, EYAL, VAN DEN BOSCH, FRANK C, DEKEL, AVISHAI. Natural downsizing in hierarchical galaxy formation. **Monthly Notices of the Royal Astronomical Society**, v. 372, n. 2, p. 933–948, 2006.

[107] NOESKE, KG, PAPADEROS, P, CAIRÓS, LM, FRICKE, KJ. New insights to the photometric structure of blue compact dwarf galaxies from deep near-infrared studies-ii. the sample of northern bcds. **Astronomy & Astrophysics**, v. 429, n. 1, p. 115–127, 2005.

[108] OEY, MS, PARKER, JEFFREY S, MIKLES, VALERIE J, ZHANG, XIAOLEI. H ii regions in spiral galaxies: Size distribution, luminosity function, and new isochrone diagnostics of density-wave kinematics. **The Astronomical Journal**, v. 126, n. 5, p. 2317, 2003.

[109] OSER, LUDWIG. **Formation and evolution of massive early-type galaxies**. 2012. Tese de Doutoramento – lmu.

[110] OSER, LUDWIG, OSTRIKER, JEREMIAH P, NAAB, THORSTEN, JOHANSSON, PETER H, BURKERT, ANDREAS. The two phases of galaxy formation. **The Astrophysical Journal**, v. 725, n. 2, p. 2312, 2010.

[111] OSTERBROCK, DONALD E, FERLAND, GARY J. **Astrophysics Of Gas Nebulae and Active Galactic Nuclei**: University science books, 2006.

[112] PAPADEROS, P, LOOSE, H-H, FRICKE, KJ AL, THUAN, TX. Optical structure and star formation in blue compact dwarf galaxies. ii. relations between photometric components and evolutionary implications. **Astronomy and Astrophysics**, v. 314, p. 59–72, 1996.

[113] PEARSON, MIKE PARKER. The sarsen stones of stonehenge. **Proceedings of the Geologists' Association**, v. 127, n. 3, p. 363–369, 2016.

[114] PETTINI, MAX, PAGEL, BERNARD EJ. [o iii]/[n ii] as an abundance indicator at high redshift. **Monthly Notices of the Royal Astronomical Society**, v. 348, n. 3, p. L59–L63, 2004.

[115] PILLEPICH, ANNALISA, MADAU, PIERO, MAYER, LUCIO. Building late-type spiral galaxies by in-situ and ex-situ star formation. **The Astrophysical Journal**, v. 799, n. 2, p. 184, 2015.

[116] PILYUGIN, LEONID S, VILCHEZ, JOSE M, THUAN, TRINH X. New improved calibration relations for the determination of electron temperatures and oxygen and nitrogen abundances in h ii regions. **The Astrophysical Journal**, v. 720, n. 2, p. 1738, 2010.

[117] PRADHAN, ANIL K, NAHAR, SULTANA N. **Atomic astrophysics and spectroscopy**: Cambridge University Press, 2011.

[118] PRITCHET, CJ. The search for primeval galaxies. **Publications of the Astronomical Society of the Pacific**, v. 106, n. 704, p. 1052, 1994.

[119] RADDICK, M JORDAN, BRACEY, GEORGIA, GAY, PAMELA L, LINTOTT, CHRIS J, CARDAMONE, CARIE, MURRAY, PHIL, SCHAWINSKI, KEVIN, SZALAY, ALEXANDER S, VANDENBERG, JAN. Galaxy zoo: Motivations of citizen scientists. **arXiv preprint arXiv:1303.6886**, 2013.

[120] RADDICK, M JORDAN, BRACEY, GEORGIA, GAY, PAMELA L, LINTOTT, CHRIS J, MURRAY, PHIL, SCHAWINSKI, KEVIN, SZALAY, ALEXANDER S, VANDENBERG, JAN. Galaxy zoo: Exploring the motivations of citizen science volunteers. **arXiv preprint arXiv:0909.2925**, 2009.

[121] RAIMANN, D, STORCHI-BERGMANN, THAISA, BICA, E, MELNICK, JORGE, SCHMITT, H. Gas properties of h ii and starburst galaxies: relation with the stellar population. **Monthly Notices of the Royal Astronomical Society**, v. 316, n. 3, p. 559–568, 2000.

[122] RAMPADARATH, HAYDEN, GARRETT, MA, JÓZSA, GIG, MUXLOW, T, OOSTERLOO, TA, PARAGI, Z, BESWICK, R, ARKEL, HVAN , KEEL, WILLIAM C, SCHAWINSKI, K. Hanny's voorwerp-evidence of agn activity and a nuclear starburst in the central regions of ic 2497. **Astronomy & Astrophysics**, v. 517, p. L8, 2010.

[123] REINES, AMY E, SIVAKOFF, GREGORY R, JOHNSON, KELSEY E, BROGAN, CRYSTAL L. An actively accreting massive black hole in the dwarf starburst galaxy henize 2-10. **Nature**, v. 470, n. 7332, p. 66–68, 2011.

[124] REMY-RUYER, A, GALAMETZ, M, VACCARI, MATTIA, MADDEN, SC. An overview of the dwarf galaxy survey. 2013.

[125] REYNOLDS, RJ, STERLING, NC, HAFFNER, LM, TUFTE, SL. Detection of [n ii] λ5755 emission from low-density ionized interstellar gas. **The Astrophysical Journal Letters**, v. 548, n. 2, p. L221, 2001.

[126] RIFFEL, ROGEMAR A, STORCHI-BERGMANN, THAISA, NAGAR, NEIL M. Near-infrared dust and line emission from the central region of mrk 1066: con-

straints from gemini nifs. **Monthly Notices of the Royal Astronomical Society**, v. 404, n. 1, p. 166–179, 2010.

[127] RODRIGUEZ-GOMEZ, VICENTE, PILLEPICH, ANNALISA, SALES, LAURA V, GENEL, SHY, VOGELSBERGER, MARK, ZHU, QIRONG, WELLONS, SARAH, NELSON, DYLAN, TORREY, PAUL, SPRINGEL, VOLKER, OTHERS, . The stellar mass assembly of galaxies in the illustris simulation: growth by mergers and the spatial distribution of accreted stars. **Monthly Notices of the Royal Astronomical Society**, v. 458, n. 3, p. 2371–2390, 2016.

[128] RUBIN, VERA C, FORD JR, W KENT. Rotation of the andromeda nebula from a spectroscopic survey of emission regions. **The Astrophysical Journal**, v. 159, p. 379, 1970.

[129] RYDEN, BARBARA, POGGE, RICHARD. **Interstellar and Intergalactic Medium**: The Ohio State University, 2015.

[130] SARTORI, LIA F, SCHAWINSKI, KEVIN, KOSS, MICHAEL J, RICCI, CLAUDIO, TREISTER, EZEQUIEL, STERN, DANIEL, LANSBURY, GEORGE, MAKSYM, W PETER, BALOKOVIĆ, MISLAV, GANDHI, POSHAK, OTHERS, . Joint nustar and chandra analysis of the obscured quasar in ic 2497-hanny's voorwerp system. **Monthly Notices of the Royal Astronomical Society**, v. 474, n. 2, p. 2444–2451, 2018.

[131] SCHAWINSKI, KEVIN, EVANS, DANIEL A, VIRANI, SHANIL, URRY, C MEGAN, KEEL, WILLIAM C, NATARAJAN, PRIYAMVADA, LINTOTT, CHRIS J, MANNING, ANNA, COPPI, PAOLO, KAVIRAJ, SUGATA, OTHERS, . The sudden death of the nearest quasar. **The Astrophysical Journal Letters**, v. 724, n. 1, p. L30, 2010.

[132] SCHAWINSKI, KEVIN, THOMAS, DANIEL, SARZI, MARC, MARASTON, CLAUDIA, KAVIRAJ, SUGATA, JOO, SEOK-JOO, YI, SUKYOUNG K, SILK, JOSEPH. Observational evidence for agn feedback in early-type galaxies. **Monthly Notices of the Royal Astronomical Society**, v. 382, n. 4, p. 1415–1431, 2007.

[133] SCHLEGEL, DAVID J, FINKBEINER, DOUGLAS P, DAVIS, MARC. Maps of dust infrared emission for use in estimation of reddening and cosmic microwave

background radiation foregrounds. **The Astrophysical Journal**, v. 500, n. 2, p. 525, 1998.

[134] SCHNEIDER, PETER. **Extragalactic astronomy and cosmology: an introduction**: Springer, 2014.

[135] SEARLE, LEONARD, SARGENT, WALLACE LW. Inferences from the composition of two dwarf blue galaxies. **The Astrophysical Journal**, v. 173, p. 25, 1972.

[136] SEARLE, LEONARD, ZINN, ROBERT. Compositions of halo clusters and the formation of the galactic halo. **The Astrophysical Journal**, v. 225, p. 357–379, 1978.

[137] SHI, FEI, KONG, X, LI, C, CHENG, FZ. Spectroscopic study of blue compact galaxies-v. oxygen abundance and the metallicity-luminosity relation. **Astronomy & Astrophysics**, v. 437, n. 3, p. 849–859, 2005.

[138] SIJACKI, DEBORA, SPRINGEL, VOLKER, DI MATTEO, TIZIANA, HERNQUIST, LARS. A unified model for agn feedback in cosmological simulations of structure formation. **Monthly Notices of the Royal Astronomical Society**, v. 380, n. 3, p. 877–900, 2007.

[139] SINGH, R, VEN, GVAN DE , JAHNKE, K, LYUBENOVA, M, FALCÓN-BARROSO, J, ALVES, J, FERNANDES, R CID, GALBANY, L, GARCíA-BENITO, R, HUSEMANN, B, OTHERS, . The nature of liner galaxies:-ubiquitous hot old stars and rare accreting black holes. **Astronomy & Astrophysics**, v. 558, p. A43, 2013.

[140] SOFUE, YOSHIAKI, RUBIN, VERA. Rotation curves of spiral galaxies. **Annual Review of Astronomy and Astrophysics**, v. 39, n. 1, p. 137–174, 2001.

[141] SOFUE, YOSHIAKI, TUTUI, Y, HONMA, M, TOMITA, A, TAKAMIYA, T, KODA, J, TAKEDA, Y. Central rotation curves of spiral galaxies. **The Astrophysical Journal**, v. 523, n. 1, p. 136, 1999.

[142] SOMERVILLE, RACHEL S, DAVÉ, ROMEEL. Physical models of galaxy formation in a cosmological framework. **Annual Review of Astronomy and Astrophysics**, v. 53, p. 51–113, 2015.

[143] STASIŃSKA, G. Biases in abundance derivations for metal-rich nebulae. **Astronomy & Astrophysics**, v. 434, n. 2, p. 507–520, 2005.

[144] STORCHI-BERGMANN, THAISA. The narrow line region in 3d: mapping agn feeding and feedback. **Proceedings of the International Astronomical Union**, v. 10, n. S309, p. 190–195, 2014.

[145] THUAN, TRINH X, IZOTOV, YURI I. High-ionization emission in metal-deficient blue compact dwarf galaxies. **The Astrophysical Journal Supplement Series**, v. 161, n. 2, p. 240, 2005.

[146] THUAN, TX, MARTIN, G EO. Blue compact dwarf galaxies. i-neutral hydrogen observations of 115 galaxies. **The Astrophysical Journal**, v. 247, p. 823–848, 1981.

[147] TREMONTI, CHRISTY A, HECKMAN, TIMOTHY M, KAUFFMANN, GUINEVERE, BRINCHMANN, JARLE, CHARLOT, STÉPHANE, WHITE, SIMON DM, SEIBERT, MARK, PENG, ERIC W, SCHLEGEL, DAVID J, UOMOTO, ALAN, OTHERS, . The origin of the mass-metallicity relation: insights from 53,000 star-forming galaxies in the sloan digital sky survey. **The Astrophysical Journal**, v. 613, n. 2, p. 898, 2004.

[148] TSUGE, KISETSU, SANO, HIDETOSHI, TACHIHARA, KENGO, YOZIN, CAMERON, BEKKI, KENJI, INOUE, TSUYOSHI, MIZUNO, NORIKAZU, KAWAMURA, AKIKO, ONISHI, TOSHIKAZU, FUKUI, YASUO. Formation of the active star-forming region lha 120-n 44 triggered by tidally driven colliding h i flows. **The Astrophysical Journal**, v. 871, n. 1, p. 44, 2019.

[149] VAN ZEE, LIESE, SKILLMAN, EVAN D, SALZER, JOHN J. Neutral gas distributions and kinematics of five blue compact dwarf galaxies. **The Astronomical Journal**, v. 116, n. 3, p. 1186, 1998.

[150] VAZDEKIS, A, COELHO, P, CASSISI, S, RICCIARDELLI, E, FALCÓN-BARROSO, J, SÁNCHEZ-BLÁZQUEZ, PATRICIA, BARBERA, F LA, BEASLEY, MA, PIETRINFERNI, A. Evolutionary stellar population synthesis with miles–ii. scaled-solar and α-enhanced models. **Monthly Notices of the Royal Astronomical Society**, v. 449, n. 2, p. 1177–1214, 2015.

[151] VAZDEKIS, A, RICCIARDELLI, E, CENARRO, AJ, RIVERO-GONZÁLEZ, JG, DíAZ-GARCíA, LA, FALCÓN-BARROSO, J. Miuscat: extended miles

spectral coverage–i. stellar population synthesis models. **Monthly Notices of the Royal Astronomical Society**, v. 424, n. 1, p. 157–171, 2012.

[152] VEILLEUX, SYLVAIN, OSTERBROCK, DONALD E. Spectral classification of emission-line galaxies. **The Astrophysical Journal Supplement Series**, v. 63, p. 295–310, 1987.

[153] WANG, KUAN, MAO, YAO-YUAN, ZENTNER, ANDREW R, LANGE, JOHANNES U, BOSCH, FRANK C, WECHSLER, RISA H. Concentrations of dark haloes emerge from their merger histories. **arXiv preprint arXiv:2004.13732**, 2020.

[154] WANG, W, LIU, X-W, ZHANG, Y, BARLOW, MJ. A reexamination of electron density diagnostics for ionized gaseous nebulae. **Astronomy & Astrophysics**, v. 427, n. 3, p. 873–886, 2004.

[155] WESTERA, P, LEJEUNE, T, BUSER, R, CUISINIER, FAGB, BRUZUAL, G. A standard stellar library for evolutionary synthesis-iii. metallicity calibration. **Astronomy & Astrophysics**, v. 381, n. 2, p. 524–538, 2002.

[156] WETZEL, ANDREW R, TINKER, JEREMY L, CONROY, CHARLIE. Galaxy evolution in groups and clusters: star formation rates, red sequence fractions and the persistent bimodality. **Monthly Notices of the Royal Astronomical Society**, v. 424, n. 1, p. 232–243, 2012.

[157] WHITE, SIMON DM, REES, MARTIN J. Core condensation in heavy halos: a two-stage theory for galaxy formation and clustering. **Monthly Notices of the Royal Astronomical Society**, v. 183, n. 3, p. 341–358, 1978.

[158] WOOD, DAVID B. Multicolor photoelectric photometry of galaxies. **The Astrophysical Journal**, v. 145, p. 36, 1966.

[159] YIN, JUN, JU, MENGTING, HAO, LEI, SHEN, SHIYIN, FENG, SHUAI. The hosts of blue compact dwarf galaxies in manga. **Proceedings of the International Astronomical Union**, v. 14, n. S344, p. 422–425, 2018.

[160] YOACHIM, PETER, DALCANTON, JULIANNE J. Structural parameters of thin and thick disks in edge-on disk galaxies. **The Astronomical Journal**, v. 131, n. 1, p. 226, 2006.

[161] ZARITSKY, DENNIS, KENNICUTT JR, ROBERT C, HUCHRA, JOHN P. H ii regions and the abundance properties of spiral galaxies. **The Astrophysical Journal**, v. 420, p. 87–109, 1994.

[162] ZHAO, YINGHE, GAO, YU, GU, QIUSHENG. A study on the chemical properties of blue compact dwarf galaxies. **The Astrophysical Journal**, v. 764, n. 1, p. 44, 2013.

[163] ZHAO, YINGHE, GU, QIUSHENG, GAO, YU. The stellar population and star formation properties of blue compact dwarf galaxies. **The Astronomical Journal**, v. 141, n. 2, p. 68, 2011.

[164] ZWICKY, FRITZ. Compact and dispersed cosmic matter, part ii. In: ADVANCES IN ASTRONOMY AND ASTROPHYSICS, v. 7, p. 227–283. Elsevier, 1970.